AgriLIFE RESEARCH & EXTENSION
Texas A&M System

TEXAS A&M UNIVERSITY

COLLEGE OF AGRICULTURE
AND LIFE SCIENCES

TR-392
2010

Lake Granbury and Lake Whitney Assessment Initiative

Final Report

Funding provided through the U.S. Department of Energy
DOE Award # DE-FG02-08ER64604

Principal Investigator and Recipient
B.L. Harris, Acting Director, Texas Water Resources Institute

Research Team Members
Daniel Roelke[1], James Grover[2], and Bryan Brooks[3]

[1]Texas AgriLife Research, Texas A&M University
[2]University of Texas – Arlington
[3]Baylor University

Project Management through
Texas Water Resources Institute, Texas A&M University System, College Station, Texas 77843-2118
http://lakegranbury.tamu.edu

October 2010

U.S. DEPARTMENT OF ENERGY

The University of Texas ARLINGTON

BAYLOR UNIVERSITY

Texas Water Resources Institute
make every drop count

TABLE OF CONTENTS

APPENDICES can be found on CD or at http://twri.tamu.edu/publications/report under TR-392

1. LIST OF FIGURES AND TABLES

1.1 FIGURES

1.2 TABLES

2. References to data in the Appendices

3. EXECUTIVE SUMMARY:

3.1 Research Approach

A team of Texas AgriLife Research, Baylor University and University of Texas at Arlington researchers studied the biology and ecology of *Prymnesium parvum* (golden algae) in Texas lakes using a three-fold approach that involved system-wide monitoring, experimentation at the microcosm and mesocosm scales, and mathematical modeling. The following are conclusions, to date, regarding this organism's ecology and potential strategies for mitigation of blooms by this organism.

3.2 Ecology of *P. parvum* in Texas lakes

Our in-lake monitoring revealed that golden algae are present throughout the year, even in lakes where blooms do not occur. Compilation of our field monitoring data with data collected by Texas Parks and Wildlife and Brazos River Authority (a period spanning a decade) revealed that inflow and salinity variables affect bloom formations. Thresholds for algae populations vary per lake, likely due to adaptations to local conditions, and also to variations in lake-basin morphometry, especially the presence of coves that may serve as hydraulic storage zones for *P. parvum* populations.

More specifically, our in-lake monitoring showed that the highly toxic bloom that occurred in Lake Granbury in the winter of 2006/2007 was eliminated by increased river inflow events. The bloom was flushed from the system. The lower salinities that resulted contributed to golden algae not blooming in the following years.

However, flushing is not an absolute requirement for bloom termination. In Lake Whitney, the highly toxic bloom that occurred that same winter was also stopped by high river inflow events. Flushing, however, did not terminate this bloom as the lake rose 10 feet but no water was released from the dam at this time. It was the influx of nutrients that stopped toxin production. This, coupled with the high rates of photodegradation for *P. parvum* toxins (which we determined in laboratory experiments), allowed other phytoplankton to out-compete golden algae.

Our laboratory experiments have shown that growth of golden algae can occur at salinities ~1-2 psu but only when temperatures are also low. This helps to explain why blooms are possible during winter months in Texas lakes.

Our in-lake experiments in Lake Whitney and Lake Waco, as well as our laboratory experiments, revealed that cyanobacteria, or some other bacteria capable of producing algicides, were able to prevent golden algae from blooming. Identification of this organism is a high priority as it may be a key to managing golden algae blooms.

Our numerical modeling results support the idea that cyanobacteria, through allelopathy, control the timing of golden algae blooms in Lake Granbury.

Our in-lake experiments in Lake Whitney and Lake Waco also revealed that as golden algae blooms develop, there are natural enemies (a species of rotifer, and a virus) that help slow the population growth. Again, better characterization of these organisms is a high priority as it may be key to managing golden algae blooms.

3.3 Potential management of *P. parvum* in Texas lakes

Manipulation of cove waters may be a key to mitigating *P. parvum* blooms. Should coves serve as a hot spot for bloom initiation, preventing bloom development in those areas could prevent large lake-scale blooms altogether. Should blooms develop elsewhere, manipulation of coves may still prove beneficial, as it may create refuge habitat for fish, thereby accelerating the recovery of fisheries after blooms have subsided.

Our laboratory and in-lake experiments and field monitoring have shown that nutrient additions will remove toxicity and prevent golden algae from blooming. In fact, other algae displace the golden algae after nutrient additions. Additions of ammonia are particularly effective, even at low doses (much lower than what is employed in fish hatchery ponds). Application of ammonia in limited areas of lakes, such as in coves, should be explored as a management option.

Our laboratory experiments and field monitoring also show that the potency of toxins produced by *P. parvum* is greatly reduced when water pH is lower, closer to neutral levels. Application of mild acid to limited areas of lakes (but not to a level where acidic conditions are created), such as in coves, should be explored as a management option.

Our field monitoring and mathematical modeling revealed that flushing/dilution at high enough levels could prevent *P. parvum* from forming blooms and/or terminate existing blooms. This technique could work using deeper waters within a lake to flush the surface waters of limited areas of the same lakes, such as in coves and should be explored as a management option. In this way, water releases from upstream reservoirs would not be necessary and there would be no addition of nutrients in the lake.

Biomanipulation of *P. parvum*, i.e., through taxon-specific algal pathogens and/or grazing by toxin-resistant zooplankton, has promise and should be explored in future research.

Finally, our laboratory and in-lake experiments have also shown that additions of barely straw extract (useful for controlling some nuisance algae) have no effect on golden algae blooms and should not be employed as a management technique.

4. PROJECT GOALS AND ACCOMPLISHMENTS:

4.1 Goals:

This research expanded the scope and extended the duration of previous research supported by a FY06 federal earmark and Texas Parks and Wildlife Department. In the expanded project our overarching objectives were two-fold: The first addressed the role of interactions between *P. parvum* and phytoplankton competitors through the mechanism of allelopathy as it relates to bloom initiation, persistence and termination. The second objective focused on the continued development of a predictive numerical model where competitive interactions, life history, the physicochemical environment, and lake dimensions were more accurately depicted.

4.2 Accomplishments:

We accomplished these objectives by:

Interactions between P. parvum *and plankton as it relates to bloom initiation, persistence and termination*

1. Conducting system-wide, year-round sampling at monthly intervals in Lakes Granbury and Whitney where parameters measured included multiple characterizations of water quality and plankton community composition. This effort included high-resolution spatial mapping of these lakes.

2. Performing multivariate statistical analysis of field data.

3. Performing controlled laboratory experiments using cultured competitors and grazers common to Lakes Granbury and Whitney, as well as cultured *P. parvum*, and investigating the potential roles of allelopathy from cyanobacteria in *P. parvum* bloom formation, persistence and termination.

Continued development of a predictive numerical model

4. Building phytoplankton competitors into our existing numerical model where interactions between species through allelopathy were represented.

5. Performing controlled laboratory experiments focused on the role of mixotrophy in *P. parvum* bloom formation and termination.

6. Building *P. parvum* mixotrophy effects into the numerical model.

7. Expanding a *P. parvum* population dynamics "box" model into a 1-dimensional, spatially explicit model more representative of a reservoir environment, thereby enabling the continued study of the factors influencing *P. parvum* bloom demographics.

5. SUMMARY OF PROJECT ACTIVITIES

5.1 System-wide, year-round sampling in Lakes Granbury and Whitney (1) and statistical analyses (2)

The field-monitoring component of this project was developed with the purpose of characterizing *P. parvum* bloom dynamics. Lakes Granbury and Whitney, reservoirs constructed on the main stem of the Brazos River, have experienced recent toxic blooms of *P. parvum* that have resulted in massive fish kills and concerns about general water quality. Both lakes are critical to this region as being primary water supplies, sources of revenue and recreational areas.

This project addressed these water quality issues by providing critical information about the relationships between *P. parvum*, salinity, nutrients and other water quality and food web parameters. In Lakes Granbury and Whitney, plankton, nutrient and water quality samples were collected at fixed-location stations, and high-resolution spatial maps were generated, using an on-board dataflow technology, of various plankton and water quality parameters. Linkages between the toxic *P. parvum* blooms and environmental conditions were examined. All the data from monitoring of Lakes Granbury and Whitney are included in the Appendices.

Our data record for Lake Granbury spans September 2006 through May 2010. For Lake Whitney, our data record spans September 2008 through August 2009. The September 2008 through August 2009 dates correspond to the work performed as a part of this contract. For our analysis, we added information collected from other projects focused on these lake systems, as well as monitoring data made available to us from Texas Parks and Wildlife and Brazos River Authority. The larger data set spans 10 years, i.e., 2000 to 2009. We also added a third lake to this analysis, Lake Possum Kingdom, which is also a reservoir constructed on the main stem of the Brazos River. The location of the lakes systems and locations of the sample stations for each lake are shown in Figures 5.1.1 and 5.1.2.

A

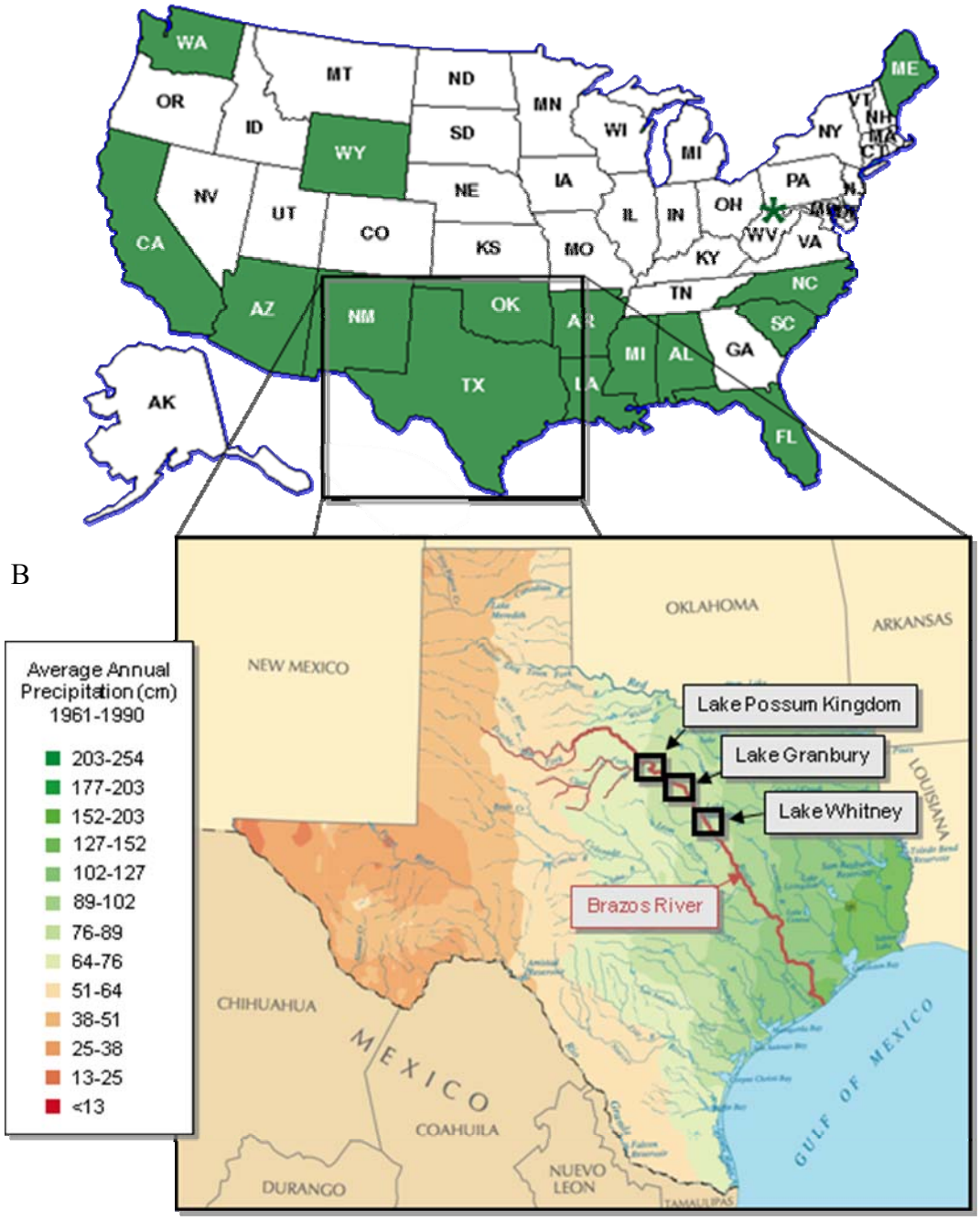

Fig. 5.1.1. States in the USA where *Prymnesium parvum* was confirmed (modified from Sager *et al*., 2008) where the '*' indicates the most recent northward spread of this invasive species (A), and the east-west precipitation gradient across Texas (B) (from The National Atlas of the United States of America, U.S. Department of the Interior and U.S. Geological Survey). The three lakes studied for this research included Lakes Possum Kingdom, Granbury and Whitney (Texas), situated along the Brazos River in an area receiving ~90 cm year^{-1} of rainfall.

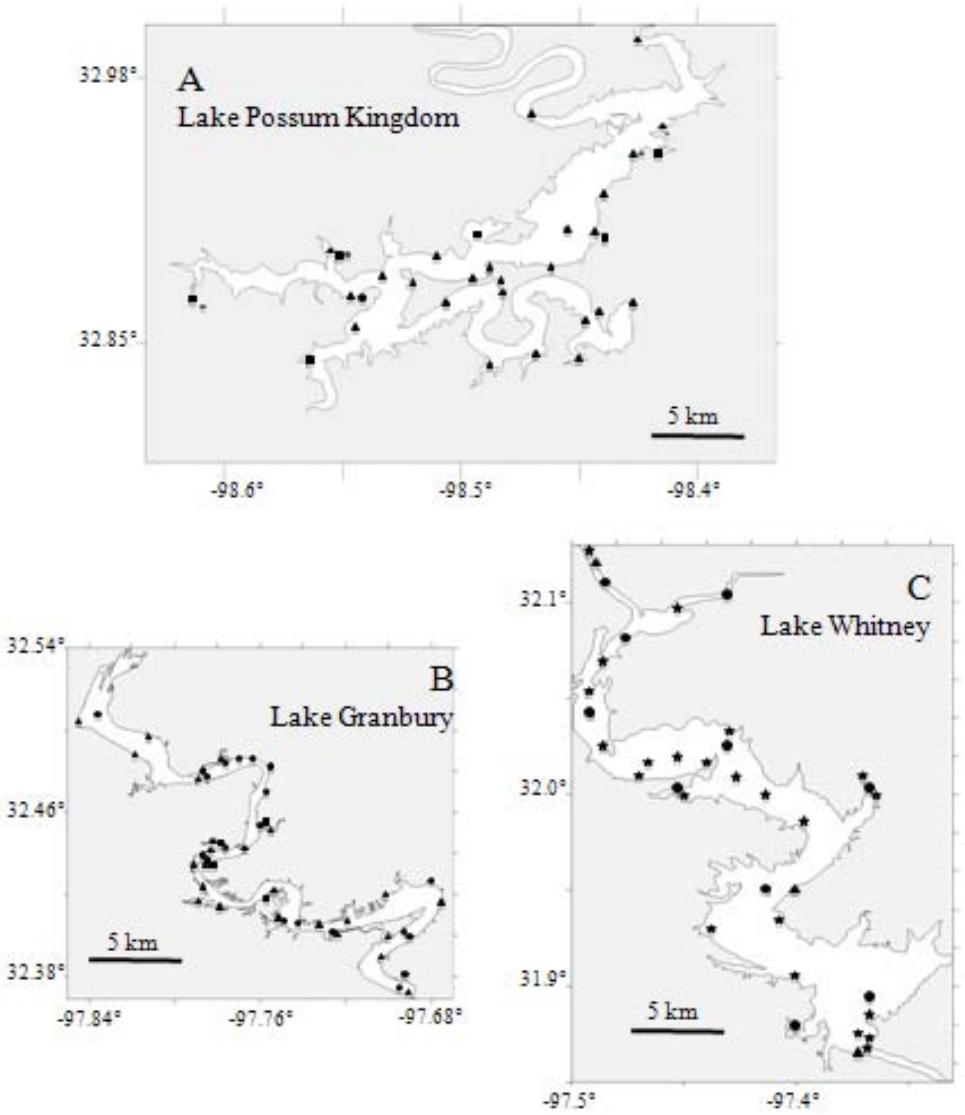

Fig. 5.1.2. Maps of Lakes Possum Kingdom (A), Granbury (B) and Whitney (C) showing the location of sampling stations. Circles (●) represent stations that were sampled monthly for periods spanning multiple years by Texas A&M University, stars (M) represent stations that were sampled weekly during periods of bloom and monthly otherwise for a period spanning two years (Texas Parks and Wildlife Department), and squares (■) and triangles (▲) represent stations that were sampled monthly or quarterly over periods spanning several years by Brazos River Authority and Texas Parks and Wildlife Department.

5.1.1 Sampling of fixed stations

During each monitoring trip we sampled fixed-location stations, which enabled us to characterize the seasonal succession pattern of plankton communities (phytoplankton and zooplankton) and determine seasonal changes in various water quality parameters (inorganic nutrients, toxicity, pH, temperature, dissolved oxygen, Secchi depth). We sampled 20 stations in Lake Granbury and 10 stations in Lake Whitney.

Estimates of total phytoplankton biomass and biomasses of higher taxa were achieved by measuring concentrations of phytopigments. Quantification of phytopigments followed Pinckney et al. (1998). Briefly, filters containing phytopigments were sonicated in 100% acetone (3 ml) for 30 seconds and then extracted in the dark for 20-24 h at -20° C. Extracts were filtered (0.2 µm) and injected (300 ul) into an HPLC system equipped with reverse-phase C_{18} columns in series (Rainin Microsorb-MV, 0.46 x 10 cm, 3mm, Vydac 201TP, 0.46 x 25cm, 5mm). A nonlinear binary gradient, adapted from Van Heukelem et al. (1994), was used for pigment separations. Solvent A consisted of 80% methanol and 20% ammonium acetate (0.5M adjusted to pH 7.2), and Solvent B was 80% methanol and 20% acetone. Absorption spectra and chromatograms were acquired using a Shimadzu SPD-M10av photodiode array detector, where pigment peaks were quantified at 440 nm.

Using the measured phytopigment concentrations, biomasses of higher phytoplankton taxa were estimated with CHEMTAX. CHEMTAX is a matrix factorization program that enables the user to estimate the abundances of higher taxonomic groups from concentrations of pigment biomarkers (Mackey et al. 1997, Wright et al. 1996). The program uses a steepest descent algorithm to determine the "best fit" of an unknown sample to an initial estimate of pigment ratios for targeted algal taxa. The taxa used in the analysis were cyanobacteria, euglenophytes, chlorophytes, prymnesiophytes, cryptophytes and diatoms, which were selected because of their prevalence in Lakes Granbury and Whitney.

Enumeration of *P. parvum* population density was performed using a settling technique (Utermöhl 1958). A 0.5-1 ml subsample was taken out of a well-mixed sample (preserved using glutaraldehyde, 3% v/v). Subsamples were settled for a 24 h period, and then counted using an inverted, phase-contrast, light-microscope (400x, Leica Microsystem Inc.). Depending on the density of material in the samples, a range of 15-50 randomly selected fields of view were counted per sample, which resulted in ~200 *P. parvum* cells counted per sample.

While examining the phytoplankton samples for *P. parvum* cells, we observed other phytoplankton species present and the condition of cells. Specifically, we looked for the presence of other harmful algal blooms (HAB) species common to Texas lakes (e.g., multiple cyanobacteria that will include *Microcystis*, *Anabaena* and *Cylindrospermopsis*), for signs of algal pathogens (e.g., remains of lysed cells and presence of parasitic fungi), and took note of the dominant taxonomic groups present in each sample.

Our sampling also included enumeration of zooplankton and bacteria. Zooplankton was collected using a 12-liter Schindler trap, concentrated to 50 ml and preserved in 2% buffered formalin. Subsamples, ~10 ml, were settled for a 24 h period, then counted using an inverted, phase-contrast, light-microscope (40x and 200x, Leica Microsystem Inc.). For each individual counted, geometric shapes were determined that best corresponded to the shape of the zooplankter and dimensions were measured that enabled calculation of the individual's biovolume (Wetzel and Likens 1991). Identification was to the taxonomic level of genus. For bacteria (Lake Granbury only), samples were preserved using paraformaldehyde and prepared for enumeration by adding a fluorescent DNA stain (Rigler 1966) to 1 mL of sample, then filtered through a 25 mm diameter black filter (Hobbie et al. 1977). Counts were performed using epifluorescent microscopy and our enumeration technique resulted in ~100 to ~300 cells counted per sample.

Samples for nutrient analyses were filtered through Whatman GF/F filters (pore size ~0.7 μm) and frozen for transport to the laboratory. Using autoanalyzer methodology (Armstrong and Sterns 1967, Harwood and Kuhn, 1970), analyses included nitrate (NO_3), nitrite (NO_2), ammonia (NH_4), and orthophosphate (PO_4).

Since toxins produced by *P. parvum* under various physiological states are not fully understood, standards for measuring concentrations of toxins are not available at this time; toxicity can be estimated using other methods. In previous studies, researchers commonly employed an *in vitro* hemolytic assay (Johannson and Granéli 1999, Barriero et al. 2005, Uronen et al. 2005) or non-standardized *in vivo* bioassays to assess biological effects of *P. parvum* cultures under nutrient limitation. In our previous research (see Roelke et al., 2007), ambient toxicity was evaluated rigorously using a standardized 24 h static acute toxicity assay with the fathead minnow (*P. promelas*) model and a standardized 10 day static renewal chronic toxicity test with a cladoceran (*D. magna*) model, generally following standardized aquatic toxicology methodology (US EPA 1994, 2002).

Samples were collected from Lakes Granbury and Whitney and transported to the laboratory where toxicity tests were initiated within 24 hrs. To evaluate toxicity relationships between treatment combinations, ambient samples were diluted using a 0.5 dilution series with reconstituted hard water (RHW), which was performed according to US EPA recommendations (US EPA 2002). This dilution approach is routinely used to evaluate water quality of surface waters because it allows for assessment of relative extracellular toxicity among samples if an undiluted ambient sample is acutely toxic.

For each *P. promelas* toxicity test sample, three replicate chambers with 7 organisms per chamber were used to assess toxicity at each dilution level. *D. magna* bioassays followed established US EPA protocols (US EPA 1994). RHW, was prepared according to standard methods (APHA 1998), and used as control treatment water for all toxicity assays. Alkalinity (mg/L as $CaCO_3$) and hardness (mg/L as $CaCO_3$) of RHW was measured potentiometrically and by colorimetric titration, respectively, before initiation of acute studies (APHA 1998). Specific conductance (μS/cm), pH and dissolved oxygen

(mg/L) of RHW was measured before toxicity testing. All toxicity tests were performed in climate controlled chambers at 25 ±1°C with a 16:8 hour light-dark cycle. Less than 48 h old fathead minnow larvae were fed newly hatched *Artemia nauplii* two hours before initiation of testing (US EPA 2002). *D. magna* were fed a Cerophyll®/green algae suspension daily, which was prepared according to methods reported previously (Brooks et al. 2004, Dzialowski et al. 2006). LC_{50} values for fathead minnow toxicity tests were estimated as percentage of ambient sample using Probit (Finney 1971) or Trimmed Spearman Karber (Hamilton et al. 1977) techniques, as appropriate.

Contour plots of fixed station data are provided in Appendices A and B for Lake Granbury. Data from the stations located in coves of Lake Granbury are provided in Appendix C. The data graphs are as follows:

Lake Granbury (deep water stations)
Figures A-1 through A-3 – Chlorophyll a, P. parvum, toxicity
Figures A-4 through A-8 – pH, temperature, salinity, Secchi depth, turbidity
Figures A-9 through A-13 – Cladoceran, copepod adult and nauplii, total rotifers, protozoan
Figures A-14 through A-15 – Phospahate, dissolved inorganic nitrogen
Figures A-16 through A-19 – Dissolved organic carbon, total bacteria, fecal coliform, E. coli
Figure A-20 - Cyanbacteria

Lake Granbury (shallow water stations)
Figures B-1 through B-3 – Chlorophyll a, P. parvum, toxicity
Figures B-4 through B-8 – pH, temperature, salinity, Secchi depth, turbidity
Figures B-9 through B-13 – Cladoceran, copepod adult and nauplii, total rotifers, protozoan
Figures B-14 through B-15 – Phospahate, dissolved inorganic nitrogen
Figures B-16 through B-19 – Dissolved organic carbon, total bacteria, fecal coliform, E. coli
Figure B-20 - Cyanobacteria

Lake Granbury (cove stations)
Figure C-1 – Description of cove stations
Figures C-2, 3 – Salinity, Temperature and Secchi depth
Figures C-4, 5 – NO3, NH4, and SRP
Figures C-6, 7 – P. parvum, Chlorophyll a, Zooplankton
Figures C-8, 9 – Fecal coliform, E. coli, Dissolved organic carbon
Figures C-10, 11 – Total bacteria

Contour plots of fixed station data are provided in Appendix D Lake Whitney. The contour plots are as follows:
Figures D-1 through D-3 – Chlorophyll a, P. parvum, toxicity
Figures D-4 through D-8 – pH, temperature, salinity, Secchi depth, turbidity
Figures D-9 through D-13 – Cladoceran, copepod adult and nauplii, total rotifers, protozoan
Figures D-14 through D-15 – Phosphate, dissolved inorganic nitrogen
Figure D-16 – Dissolved organic carbon

5.1.2 High-resolution spatial mapping

We measured spatial patterns of water quality in Lakes Granbury and Whitney at monthly intervals with Dataflow, a high-speed, flow-through measurement apparatus developed for mapping physicochemical parameters in shallow aquatic systems (Madden

and Day 1992). We used this integrated instrument system to concurrently measure chlorophyll *a*, dissolved organic matter, transparency, salinity, and temperature from a boat running closely spaced transects. Measurements were taken at 4-second intervals from ~20 cm below the surface. An integrated GPS was used to simultaneously plot sample positions, allowing geo-referencing of all measurements for each variable.

GPS and dataflow information were used to create highly detailed contour maps of water quality parameters in relation to physiographic features. We also collected discrete water samples from the flow-through system during our continuous sampling for laboratory analysis of multiple parameters that were used to calibrate the dataflow unit. In addition to these samples, we measured profiles of water quality parameters that include dissolved oxygen and temperature to determine the degree of stratification of the water column.

High-resolution spatial maps are provided in Appendix E for Lake Granbury. The maps are as follows:
Figures E-01 through E-26 – Chlorophyll *a*
Figures E-27 through E-53 – Salinity
Figures E-54 through E-80 – Temperature
Figures E-81 through E-104 – pH
Figures E-105 through E-131 – Turbidity
Figures E-132 through E-158 – Dissolved Organic Carbon

High-resolution spatial maps are provided in Appendix F for Lake Whitney. The maps are as follows:
Figures F-1 through F-10 – Chlorophyll *a*
Figures F-11 through F-20 – Salinity
Figures F-21 through F-30 – Temperature
Figures F-31 through F-40 – pH
Figures F-41 through F-50 – Turbidity
Figures F-51 through F-60 – Dissolved Organic Carbon

5.1.3 Other data collection

Daily discharges from the Brazos River were measured at the following upstream locations: South Bend, USGS Station Number 08088000 (Lake Possum Kingdom); Dennis, USGS Station Number 08090800 (Lake Granbury); and Glen Rose, USGS Station Number 08091000 (Lake Whitney). Salinities were measured during sampling using water quality multiprobes (Quanta, Hydrolab) and refractometers.

To better relate inflow magnitudes to the specific growth rate of *P. parvum*, we estimated daily system flushing rates during the time of peak flows. For this purpose, flushing rates of the system were estimated by dividing the daily inflow from the Brazos River by the lake volume.

5.1.4 Statistical analysis and simple model application

Correlations using linear-, exponential- and power-fit functions (Kaleidagraph, v.4.03), and multiple regression analysis (Matlab, v.7.5.0.338) were performed between *P. parvum* population density, inflow and salinity using the 10-year compiled data record of multiple lakes. We used correlation analyses to estimate the percent variability in *P. parvum* population density explained by either inflow or salinity (based on R^2), and the multiple regression analysis enabled us to simultaneously compare the relative roles of inflow and salinity as they affect *P. parvum* population density (based on the weighting coefficients). For inflows, we used 7-day, 10-day, 30-day and 365-day cumulative inflow prior to each sampling date. The 7-day cumulative inflows showed the best relationships. So, only those results are reported here.

For analysis of *P. parvum* and other water quality parameters over a shorter period (coinciding with a system-wide, fish killing bloom), non-metric multidimensional scaling (NMS) was used to explore multivariate relationships within the fixed-station data (PC-ORD v.5.1; McCune and Mefford, 1999). Matrices were based on normalized physical, chemical and biological variables. We employed the Sorensen (Bray-Curtis) dissimilarity metric to determine the dimensional distances among each sampling time at each fixed-station. A final solution of two dimensions was achieved based on the lowest stress obtained using a Monte-Carlo test after 250 iterations (repeated 10 times) in a cascade procedure and using a stability criterion of 0.0001 (McCune and Grace 2002). Final stress was calculated as 12.88. Joint vectors were then used to identify significant variables that mediate the temporal and spatial changes. Vectors were drawn as the hypotenuse of regression determination coefficients (r^2) between variables (see McCune and Grace 2002).

Based on our observations of the system-wide, fish killing bloom, hydraulic flushing played an important role as a mechanism influencing *P. parvum* population dynamics. To better evaluate its relative impact, we estimated in-lake specific growth rates for *P. parvum* using a mathematical model. The model (eq. 1) was based on laboratory experiments using a strain of *P. parvum* isolated from Texas waters where salinity, temperature and light were varied (Baker et al. 2007, 2009), and was used previously to investigate *P. parvum* population dynamics (Grover et al. 2010). The model was as follows:

$$\begin{aligned}\mu = {} & -3.531 + 0.02534(S - 1.833) - 0.06311(S - 1.833)^2 + 7.468e^{0.7*((T-20)/20)} \\ & - 3.414e^{1.4*((T-20)/20)} + 0.1697(S - 1.833)e^{0.7*((T-20)/20)} + 0.000611(E - 222) \\ & - 0.00000573(E - 222)^2\end{aligned} \qquad (5.1.4.1)$$

where μ was the specific growth rate (d^{-1}), S was salinity (psu), T was temperature (°C) and E was irradiance ($\mu mol \cdot m^{-2} \cdot s^{-1}$). These equations were formulated under experimental conditions where inorganic nutrients did not limit *P. parvum* specific growth rate.

For purposes of this research, we used the average underwater irradiance (I_{avg}) as a surrogate for E. This was approximated using the surface irradiance, a relationship between the light extinction coefficient and Secchi depth, and the average depth of Lake Granbury. Surface irradiance (at zero depth, I_0) was estimated using mathematical models that accounted for time of year and latitude, and assumed cloudless conditions and a fixed water reflectance (Kirk 1994, Wetzel 2001). The light extinction coefficient (k) was estimated as a function of Secchi depth ($1.7/z_{Secchi}$, Wetzel 2001). The average underwater irradiance was then approximated using:

$$I_{avg} = I_0(1 - e^{-kz})/(kz) \qquad (5.1.4.2)$$

where z (meters) was the average depth of Lake Granbury.

The calculated specific growth rate was used along with flushing losses to estimate the change in population density attributable to flushing during the period when the bloom was terminated using a simplified differential equation employed in previous studies (Roelke et al. 2003, Roelke and Eldridge 2008, 2009):

$$\frac{d\phi}{dt} = (\mu - d)\phi \qquad (5.1.4.3)$$

where ϕ was the *P. parvum* population density with an initial condition equal to the March sampling date (just prior to the flushing event), μ was the daily specific growth rate interpolated between the March and April samplings (based on equations 1 and 2), and d was the daily flushing rate for the period between March and April samplings calculated by dividing the daily inflow (USGS records) by the volume of naturally occurring well-mixed segments of the lake. Based on the dataflow maps for chlorophyll *a*, the length over which lake waters were well-mixed was determined to range between 1 and 6 km for the March and April samplings, respectively. By employing average lake depth and width dimensions, the volume of well-mixed segments was estimated.

5.1.5 Findings

5.1.5.1 Results from multiple lake comparison over 10-year period (2000-2009)

After the 1985 Pecos River event (James and De La Cruz, 1989) when *P. parvum* was first linked to a fish kill in this region, and multiple smaller-sized fish kills, in the Brazos River area and elsewhere, during the following decade (Southard *et al*., 2010), the first large-scale, fish-killing *P. parvum* blooms in Texas occurred in multiple systems along the Brazos River during the late fall 2000-early spring 2001. In the Brazos River Basin, the blooms first appeared in Lake Possum Kingdom, then in the state fish hatchery between Lakes Possum Kingdom and Granbury, next in Lake Granbury and eventually they reached Lake Whitney. This stretch of the Brazos River is ~120 km. Several fish

kills resulted from these *P. parvum* blooms (Southard *et al*., 2010), but observations of population densities and bloom spread downstream are largely anecdotal.

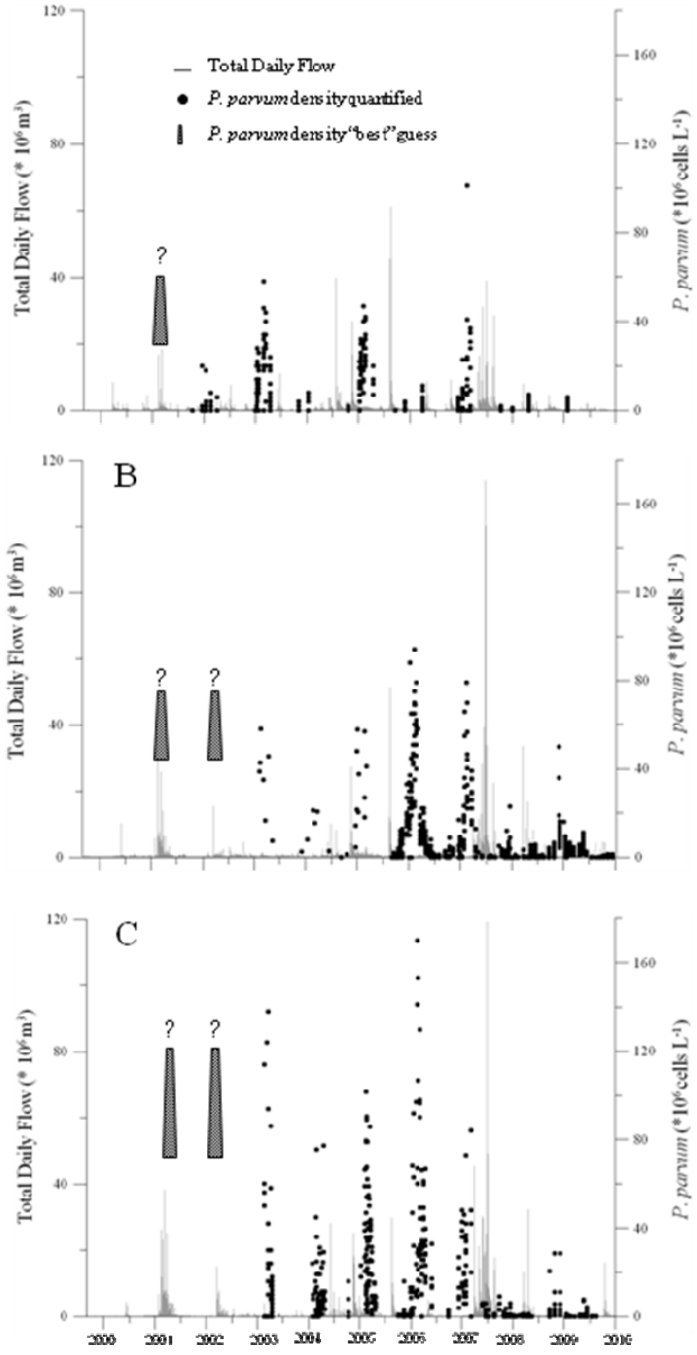

Fig. 5.1.5.1.1. Recurrent blooms of *Prymnesium parvum* and daily inflows for a period spanning 2000 through 2009 for Lakes Possum Kingdom (A), Granbury (B) and Whitney (C). During late 2000-early 2001 for Lake Possum Kingdom, and 2001-2002 for Lakes Granbury and Whitney, population densities were approximated from anecdotal information. Otherwise, population densities were quantified. Inflow data was obtained from U.S. Geological Survey.

In the years following the 2000-2001 blooms (when quantitative sampling commenced) until the early spring of 2007, fish-killing *P. parvum* blooms were recurrent winter phenomena in all three lake systems, lasting ~2 months (Figure 5.1.5.1.1). The timing of these blooms was no longer sequential, as it was during the 2000-2001 period, but instead concurrent. Bloom density maxima increased further down the watershed with maximum bloom densities of ~40-60 x 10^6 cells L^{-1} in Lake Possum Kingdom, ~80-100 x 10^6 cells L^{-1} in Lake Granbury, and ~140-170 x 10^6 cells L^{-1} in Lake Whitney. During these events, waters took on a golden color, surface foam was observed, and dead fish were seen throughout the affected lakes (Figure 5.1.5.1.2). After early-spring 2007, recurrent *P. parvum* population maxima still occurred during the late-fall through early-spring months. Maximum population densities were lower, however, typically reaching ~10 x 10^6 cells L^{-1} for Lake Possum Kingdom, ~20-60 x 10^6 cells L^{-1} for Lake Granbury, and ~10-30 x 10^6 cells L^{-1} for Lake Whitney. During this period, fish kills were smaller and localized within each lake.

Fig. 5.1.5.1.2. Features of fish-killing *Prymnesium parvum* blooms. During periods of high *P. parvum* population density waters take on a characteristic golden color (A). Usually when this color is apparent, waters are toxic to fish and large die-offs result (B,C) (Photographs courtesy of Brazos River Authority and Texas Parks and Wildlife Department).

As is typical for this region, rains and associated in-stream flows were highest during the early-spring through early-summer months (Figure 5.1.5.1.1). Lake inflows increased in magnitude further down the watershed, presumably because of the increased area of catchment. The spring of 2007 was the wettest period of this data record, with peak inflows attaining ~60 x 10^6 m^3 d^{-1} for Lake Possum Kingdom and ~120 x 10^6 m^3 d^{-1} for

Lakes Granbury and Whitney. Whole system flushing rates during peak inflows in the spring of 2007 were 0.08, 0.7 and 0.3 d^{-1} for Lakes Possum Kingdom, Granbury and Whitney. Dry years occurred earlier in the data record where inflows were barely discernable at times. For Lake Possum Kingdom, located highest in the watershed, 2008 and 2009 were also dry years. For Lakes Granbury and Whitney, 2009 was a dry year.

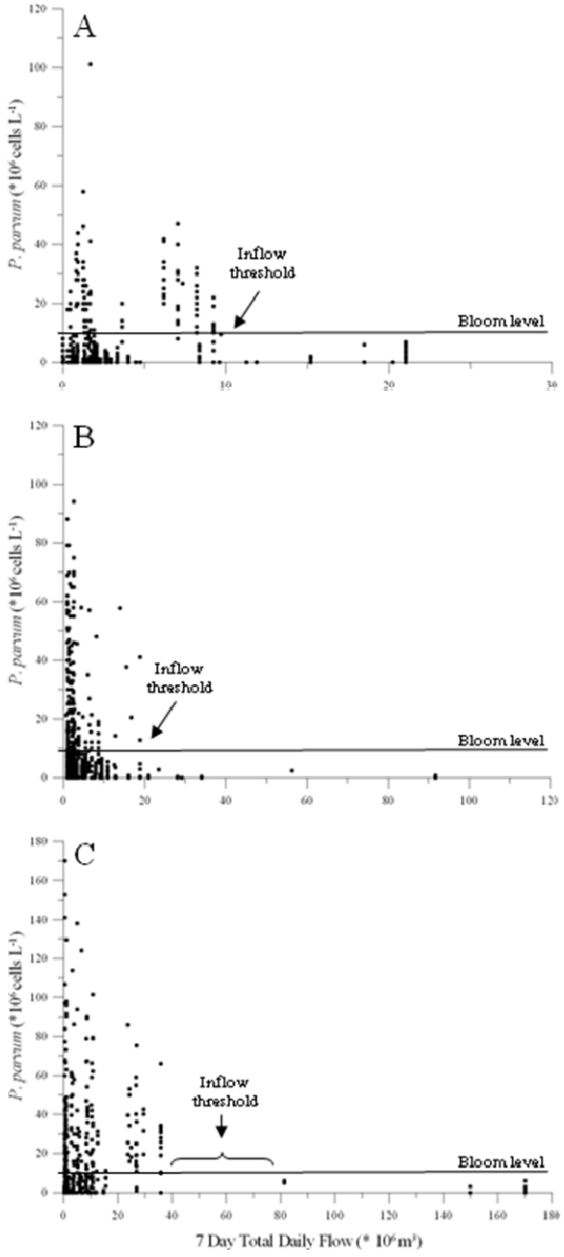

Fig. 5.1.5.1.3. *Prymnesium parvum* population density plotted against the cumulative inflow over the 7-day period prior to the date of sampling for Lakes Possum Kingdom (A), Granbury (B) and Whitney (C). Population densities greater than 10 x 10^6 cells L^{-1}, the defined bloom level, occurred when 7-day accumulated inflows were <10 x 10^6 m^3 for Lake Possum Kingdom, <20 x 10^6 m^3 for Lake Granbury and conservatively <40 x 10^6 m^3 for Lake Whitney. These bloom inflow-thresholds corresponded to system flushing rates of 0.01, 0.12 and 0.10 d^{-1}.

Cumulative inflow for the 7-day period prior to each sampling time showed that higher inflows resulted in lower population densities (Figure 5.1.5.1.3). Although more observations of *P. parvum* population density at higher inflows are needed, inflow bloom-thresholds (defined as 10 x 10^6 cells L^{-1}) were apparent, and they varied for each lake, i.e., ~10 x 10^6 m^3 d^{-1} for Lake Possum Kingdom (corresponding to a whole system flushing rate of 0.01 d^{-1}), ~20 x 10^6 m^3 d^{-1} (0.12 d^{-1}) for Lake Granbury, and ~40 x 10^6 m^3 d^{-1} (0.10 d^{-1}) for Lake Whitney. Inflow to these lakes exceeded thresholds during the spring and early-summer months. For Lake Possum Kingdom, this occurred during eight of the ten years analyzed. For Lakes Granbury and Whitney, this occurred in seven and six of the years, respectively. While an inflow threshold was observed, above which *P. parvum* populations did not accumulate, monotonic trends were not seen. Linear-, power- and exponential-functions used to correlate 7-day cumulative inflow and *P. parvum* population densities were poor. Using data pooled from all three lakes, models only explained 2%, 1% and 1% of the total variability (equations not shown). Similar findings were obtained when lakes were analyzed separately.

Reports of salinity during the 2000-2001 bloom period were as high as 4 psu in Lake Possum Kingdom (J. Glass, personal communication). Our records for salinity started in 2004 and typically showed annual maxima of ~2-3 psu for these three lakes prior to the early-spring of 2007 (Figure 5.1.5.1.4). After the wet season of 2007, annual maxima were typically ~1-2 psu. There appeared to be a salinity threshold below which *P. parvum* blooms did not occur. At salinities below ~1.5 psu for Lake Possum Kingdom and 0.5 psu for Lakes Granbury and Whitney, population densities of *P. parvum* were <10 x 10^6 cells L^{-1} (Figure 5.1.5.1.5). There was one exception in Lake Whitney where *P. parvum* population density exceeded bloom level at low salinity. When data from all three lakes was pooled, linear- (eq.4), power- (eq.5) and exponential-functions (eq.6) used to correlate salinity and *P. parvum* population densities explained 41%, 40% and 34% of the total variability in this data record. Model equations were:

$$[pop] = 12.11[sal] - 4.86 \quad (5.1.5.1.1)$$

$$[pop] = 1.84[sal]^{2.01} \quad (5.1.5.1.2)$$

$$[pop] = 0.21e^{1.93[sal]} \quad (5.1.5.1.3)$$

Similar findings were obtained when lakes were analyzed separately (not shown). The multiple linear regression (eq. 7) using the 7-day cumulative inflow and salinity indicated salinity more strongly influenced *P. parvum* population density than inflow, where the model was:

$$[pop]=0.02[inflow]+8.96[sal]-3.78 \quad (5.1.5.1.4)$$

However, this model only explained ~11% of the variance in *P. parvum* population density.

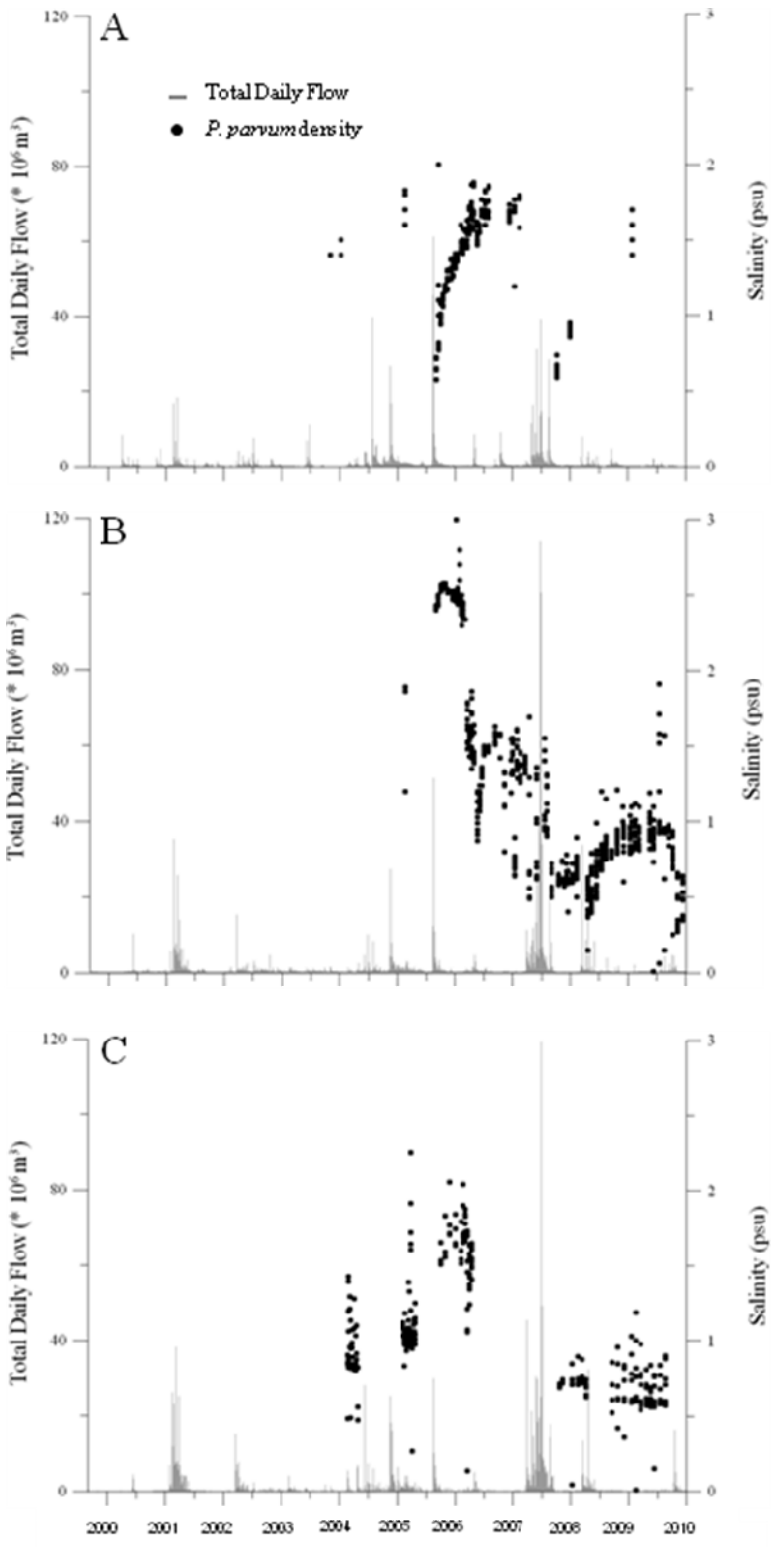

Fig. 5.1.5.1.4. Salinity and inflows for a period spanning 2000 through 2009 for Lakes Possum Kingdom (A), Granbury (B) and Whitney (C). Prior to the wet spring of 2007, annual salinity maxima typically ranged from 2-3. After this wet period, annual salinity maxima typically ranged between 1-2.

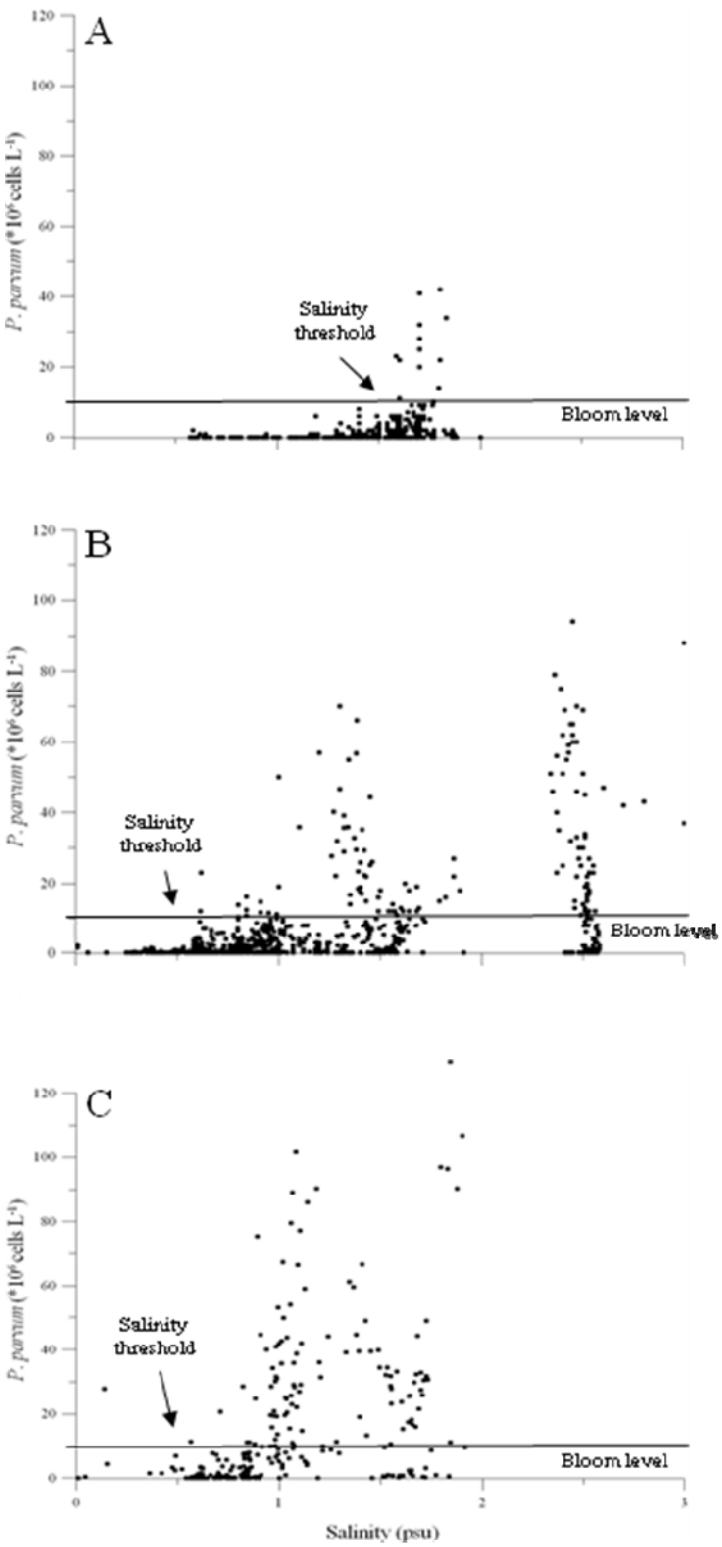

Fig. 5.1.5.1.5. *Prymnesium parvum* population density plotted against salinity for Lakes Possum Kingdom (A), Granbury (B) and Whitney (C). Population densities greater than 10 x 10^6 cells L^{-1}, the defined bloom level, occurred when salinities were > 1.5 for Lake Possum Kingdom, and >0.5 for Lakes Granbury and Whitney.

5.1.5.2 Discussion of multiple lake comparison over 10-year period (2000-2009)

Prymnesium parvum in Texas appears to be the result of invasion (Lutz-Carrillo *et al*., 2010). Our data suggest that invading *P. parvum* established quickly in lakes downstream from early bloom events. For example, fish-killing blooms appeared sequentially down the watershed after they were first noticed in late 2000-early 2001. However, between 2004 and 2007, fish-killing blooms were concurrent, suggesting that immigration of *P. parvum* from upstream sources was no longer necessary for bloom initiation. The apparent rapid spread of *P. parvum* across the southern USA, and now with fish-killing blooms in northern areas (e.g., West Virginia and Pennsylvania, USA), also suggests that this species is an effective invader.

Paradoxically, our documentation of this invasive species showed that the recurrent blooms occurred under conditions far removed from the growth optimum. Laboratory studies using a Texas strain of *P. parvum* (UTEX LL 2797) showed optimal reproductive growth rates of ~0.8 d^{-1} when salinity and temperature were 22 psu and 27°C (Baker *et al*., 2007, 2009). Using the equation from Baker *et al*. (2009) and winter temperatures of ~10°C, maximum reproductive growth rates were estimated to be ~0.1 d^{-1} for the period prior to early-spring 2007, when annual salinity maxima ranged from 2-3 psu. In other words, blooms occurred when reproductive growth was stressed by low salinity and temperature. In the absence of significant loss factors, such as grazing, these low reproductive growth rates can lead to blooms of high population density, as was demonstrated using a simplified biophysical model depicting *P. parvum* bloom dynamics in Lake Granbury (Roelke *et al*., 2010a). Production of grazing-inhibiting toxins would facilitate this condition, and appears to be the case for *P. parvum*, which produces greater amounts of grazing-inhibiting toxin when stressed (Uronen *et al*., 2005; Granéli and Salomon, 2010).

Prymnesium parvum blooms in these lakes were vulnerable to large inflow events because they occurred during a time of year when maximum reproductive growth rates were low. Thus, it is not surprising that *P. parvum* blooms only developed when inflows were below critical levels. In addition, blooms ceased when inflows exceeded these inflow bloom-thresholds during early-spring through early summer months. Estimated winter reproductive growth rates during bloom years (~0.1 d^{-1}) were similar to whole system flushing levels estimated at the inflow thresholds for Lakes Granbury and Whitney, 0.12 and 0.10 d^{-1}, respectively. This is consistent with observations from other systems where hydraulic flushing influenced plankton dynamics and the incidence of blooms (Jacoby *et al*., 2000; Moustaka-Gouni *et al*., 2006; Mitrovic *et al*., 2008; Roelke *et al*., 2010a). High inflows were not a requirement for bloom decline, however, as blooms ended with only modest inflows during years 2003, 2005 and 2006.

Inflow bloom-thresholds varied between lakes. Most notably, Lake Possum Kingdom required much less inflow to suppress *P. parvum* populations, where the corresponding system flushing rate was 0.01 d^{-1}. Flushing thresholds were an order of magnitude greater for Lakes Granbury and Whitney. Differing thresholds likely stemmed from morphometric variations between systems. For example, Lake Possum Kingdom is

larger in volume than Lakes Granbury and Whitney, and nearly twice as deep. However, it most likely does not mix well vertically, and flushing events may only affect surface waters. Consequently, the inflow required to flush a surface bloom from the system would be lower. Similarly, Lake Possum Kingdom is elongated and sinuous, and likely does not mix well longitudinally. Inflows needed to flush a smaller amount of surface water would also be lower than that required to flush the entire system.

Another factor concerning inflow bloom-thresholds pertains to cove presence and connectivity. In a lake north of our study area, *P. parvum* population densities were much higher in a disconnected cove compared to those of the open lake (Hambright et al. 2010). Coves might harbor seeding *P. parvum* populations and serve as hydraulic storage zones. Volume exchange rates between storage zones and open waters were shown to influence the magnitude of inflow required to flush blooms from a system (Reynolds, 1990; Grover *et al*., 2009, *In Press*). It is likely that dendritic lakes may require higher inflows to terminate *P. parvum* blooms, though analysis of cove connectivity in these lakes is beyond the scope of the present research.

High inflows need not terminate blooms through hydraulic flushing. For example, toxin production by the Texas strain of *P. parvum* is sensitive to nutrient pulses (Grover *et al*., 2007; Roelke *et al*., 2007a; Errera *et al*., 2008). In Lake Whitney, termination of a bloom was observed coinciding with an inflow event where the lake level rose, but no out-flow occurred. The *P. parvum* population declined 52%, where direct dilution accounted for ~30% of this decrease, and toxicity was completely removed (Schwierzke-Wade *et al*., *In Review*). Without the advantages imparted to *P. parvum* under stressful conditions (in this case, low nutrient concentrations), this bloom did not re-establish. It is likely that increased nutrient loading associated with inflows during 2003, 2005 and 2006 contributed to those bloom declines.

When comparing *P. parvum* population dynamics from the periods before and after the high inflow events of early-spring 2007, the incidence of blooms appeared sensitive to small variations in salinity. For example, only when annual salinity maxima reached 2-3 psu did system-wide blooms of high population density occur. These blooms were accompanied by extensive fish-kills (see Southard *et al*., 2010). When annual salinity maxima ranged from 1-2 psu, maximum *P. parvum* population densities were reduced to ~30% of previous levels, and fish kills were small and localized. The higher maximum reproductive growth rates estimated prior to the early-spring of 2007 likely contributed to the higher population densities at that time. Shifts in plankton community dynamics and structures that are sensitively dependent on environmental conditions were previously documented with bloom-forming flagellates and other nuisance taxa (Buskey *et al*., 1998; Roelke *et al*., 2007b; Shatwell *et al*., 2008).

Interestingly, salinity bloom-thresholds varied between lakes. Blooms occurred in Lake Possum Kingdom only when salinity was >1.5 psu and in Lakes Granbury and Whitney when salinity was >0.5 psu. Inorganic nutrient concentrations were similar between these lakes during the periods of bloom development (Roelke *et al*., 2007a, 2010a; Schwierzke *et al*., 2010), so differential nutrient concentrations did not likely affect thresholds. It

may be that plankton community sensitivity to salinity varied in these lakes. Due to its higher position in the watershed, the plankton population of Lake Possum Kingdom is likely exposed to greater natural salinity variations and consequently more tolerant to elevated salinity levels. It may be that less-stressed plankton communities are more resistant to *P. parvum* blooms, which in the case of Lake Possum Kingdom, might lead to a greater salinity bloom-threshold.

Relationships between *P. parvum* population density, inflow and salinity were not monotonic. Instead, large ranges in *P. parvum* population densities were observed when inflows were lower and salinities were higher. In other words, lower inflows and higher salinities alone did not indicate *P. parvum* population densities would be high. Other factors not accounted for during our study were likely important. These may include competition for resources (Baker *et al*., 2009), allelopathic effects from chemicals produced by *P. parvum* (Fistarol *et al*., 2003, 2005; Granéli and Johansson, 2003; Michaloudi *et al*., 2009), sensitivity of *P. parvum* to chemicals produced by other algae (Grover *et al*., 2010; Roelke *et al*., 2010b, James *et al*., *In Review*), use of alternative energy and nutrient sources through mixotrophy and saprophytic nourishment (Nygaard and Tobiesen, 1993; Skovgaard and Hansen, 2003; Lindehoff *et al*., 2009), grazing inhibition (Granéli and Johansson, 2003; Tillmann, 2003; Michaloudi *et al*., 2009; Brooks *et al*., 2010), and grazing by toxin-resistant taxa and infection by virus (Schwierzke *et al*., 2010). All of these processes influence *P. parvum* population dynamics to varying degrees and are not solely a function of inflow and salinity. So, it is not surprising that complex patterns and high variability in *P. parvum* population density were observed over the ranges of inflow and salinity recorded in this study.

Our synopsis of the multiple lake comparison over a 10-year period, then, is that *P. parvum* blooms (and annual population maxima for the period after early-spring 2007) were recurrent winter phenomena in this area of the south-central USA. Bloom initiation and development only occurred at a time of year when inflows were low, and large fish-killing blooms occurred only when salinity was higher. Bloom termination followed high inflow events, likely through direct flushing of cells and indirect physiological affects. This linkage between incidence of *P. parvum* blooms, inflows and salinity raises concern because sequestration of water continues to increase in this area with rising human population. Combined with variations in precipitation and evaporation predicted from climate change, flows in this area may decrease by 60% (Cai and McCarl, 2009). Though not the focus of climate change models, it is likely that increased evaporation rates associated with regional warming will also result in higher salinity. Consequently, both human population increase and climate change may lead to an increased incidence of *P. parvum* blooms.

5.1.5.3 Results from a focused analysis of a system-wide, fish-killing bloom in Lake Granbury (2006-2007)

For the period of study focusing on a system-wide, fish-killing bloom in Lake Granbury (2006-2007, see Figure 5.1.5.3.1), inflows into Lake Granbury were episodic, as is common in lakes of the south-central USA. From September 2006 through March 2007

inflows were barely discernable (Figure 5.1.5.3.2). In April 2007 the first large inflow event occurred with peak flows attaining 80 x 10^6 m^3 d^{-1}, corresponding to single-day hydraulic flushing peaks of 16 d^{-1} (if well-mixed patches are on the scale of 1 km) and 2.7 d^{-1} (if well-mixed patches are on the scale of 6 km). Episodic inflows of varying magnitude and duration persisted through June, where the largest inflow event reached ~120 x 10^6 m^3 d^{-1}.

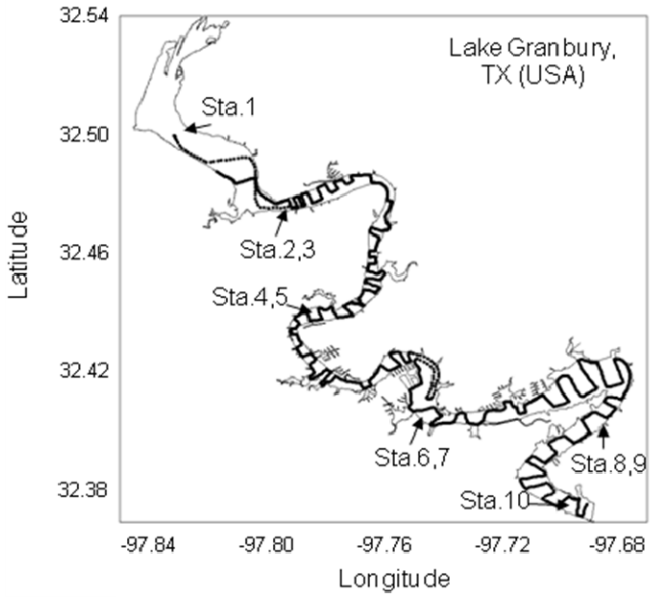

Fig. 5.1.5.3.1. Lake Granbury located in the south-central USA. This research coupled fixed station sampling with high-resolution spatial mapping (dark line indicates path of on-board data collection) that enabled detailed analysis of the plankton environment and system-wide characterizations of bloom dynamics.

According to our CHEMTAX pigment model, phytoplankton biomass peaked in March just prior to the first large inflow event of 2007, with highest biomass occurring towards the lower end of the lake (Figure 5.1.5.3.2a). Phytoplankton composition varied somewhat during the three months leading up to the biomass peak (January through March 2007). Prymnesiophytes were prevalent from January to February, comprising ~92% of the total phytoplankton biomass. During this same period other taxonomic groups changed little and were ~6% diatoms, ~1% green algae and ~0.5 % cyanobacteria. For the period between February and March the prevalence of prymnesiophytes declined to 87% of the total phytoplankton biomass. The prevalence of diatoms and cyanobacteria increased to 10% and 2% during this period.

Our direct cell counts of *P. parvum* were in agreement with our CHEMTAX predictions and indicated that the *P. parvum* bloom reached its highest population densities of ~40 x 10^6 cells $liter^{-1}$ in February with highest population densities occurring in the mid-reaches of the lake (91% of the phytoplankton biovolume). Cell densities >10 x 10^6 cells $liter^{-1}$ are considered bloom proportions based on historical observations in lakes of the south-central USA (TPWD 2003, Roelke et al. 2007, Schwierzke et al. 2010). Average *P. parvum* densities for the lake declined ~27% by March (Figure 5.1.5.3.2b), a larger

proportional decrease than predicted by the CHEMTAX model. Measurements of ambient toxicity to fish were consistent with observed population densities, with LC_{50} values as low as 4% observed in February in the mid reaches of the lake, with toxicity to fish decreasing (LC_{50} increasing) by March (Figure 5.1.5.3.2c). *P. parvum* population densities for the lake were obliterated after the first large inflow event to the lake, decreasing by 89% from the March to April sampling. In addition, waters were no longer toxic to fish.

Cyanobacteria were not abundant in Lake Granbury during the time of bloom development or termination. Cyanobacteria biomass was maximal during the months of July through September 2007 (Figure 5.1.5.3.2d) and in the lower reaches of the lake, accounting for ~7-8% of the total phytoplankton biomass according to CHEMTAX pigment estimates.

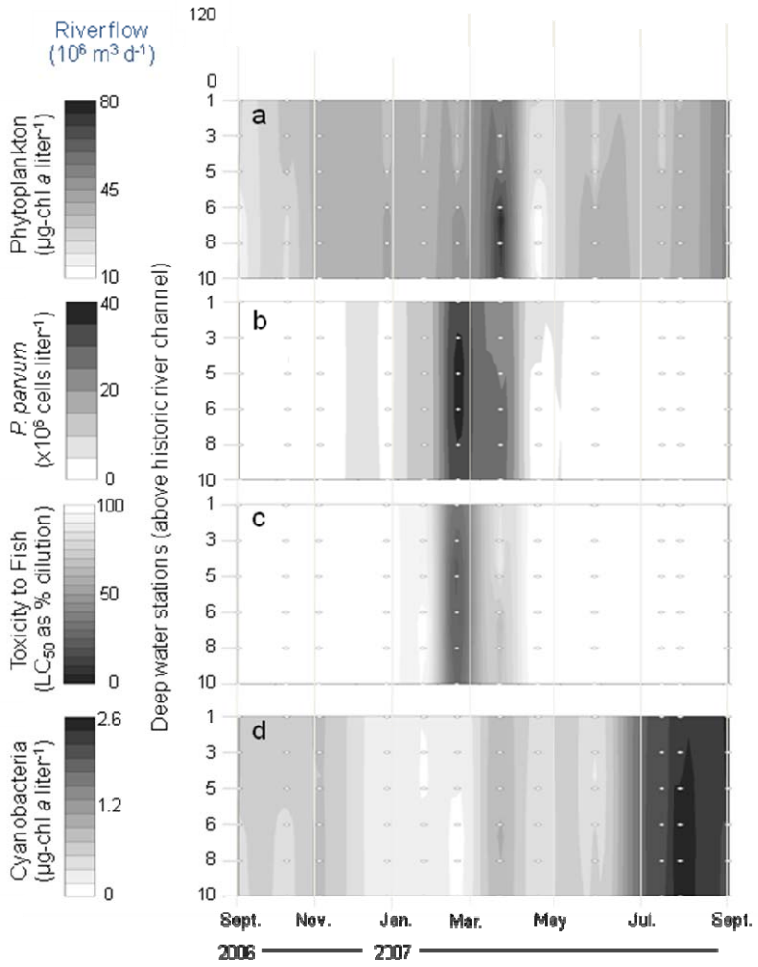

Fig. 5.1.5.3.2. Characterizations of the phytoplankton and ambient toxicity for a one-year period that spanned the formation and termination of a *P. parvum* bloom. The bloom developed during the fall months and peaked in winter, but following a high inflow event in April the bloom was greatly diminished, as evidenced by trends in chlorophyll *a* (a) and *P. parvum* population densities (b). Toxicity (c) was maximal during the peak of *P. parvum* population density, but ceased after this inflow event. Cyanobacteria (d), potential competitors through allelopathy, were prevalent only during the summer months.

Dataflow mapping revealed that the bloom was patchy throughout Lake Granbury with characteristic patches of ~1 km (Figure 5.1.5.3.3a, representative map during the bloom). The location of elevated chlorophyll *a* patches did not appear related to morphometric attributes such as shoreline development or depth. While we have microscopic and photopigment verification of the *P. parvum* bloom only from the fixed stations, visual observations indicated 'golden' colored water, foam lines and dead fish throughout the lake during January to March 2007. This suggests that the in-vivo fluorescence signal attributed to chlorophyll *a* from the Dataflow unit indicates the *P. parvum* bloom distribution. After the first inflow event in April 2007, phytoplankton biomass was greatly diminished and patchiness decreased, where characteristic patches were ~6 km (Figure 5.1.5.3.3b).

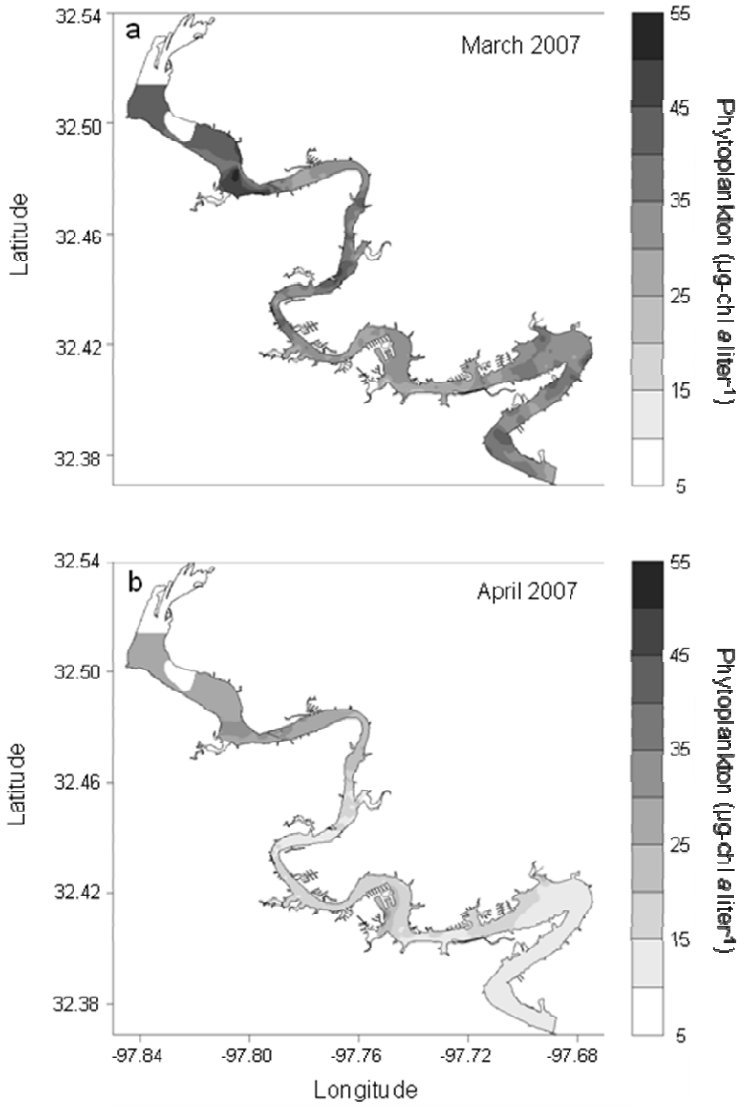

Fig. 5.1.5.3.3. System wide characterizations of phytoplankton biomass using high-resolution spatial mapping. During the winter months, biomass patterns suggest a system-wide, but patchy bloom of *P. parvum* (a). After the flushing event, phytoplankton densities were much lower and the distribution remained patchy (b).

As with many of the lakes in the south-central USA, Lake Granbury can sometimes be brackish. Prior to April 2007, when inflows were not significant, salinity was ~1.5 psu throughout Lake Granbury (Figure 5.1.5.3.4a). The lake remained at salinities >1 psu until after the first large inflow event in April 2007, at which time salinity dropped to ~0.5 psu. Temperature changes in the lake were seasonal, with minima of ~6°C in February 2007 and maxima of ~32°C in August 2007 (Figure 5.1.5.3.4b). While Secchi depth varied spatially and temporally, a prominent feature was relatively deep Secchi depths (~1 meter) coinciding with the *P. parvum* bloom, while a rapid decrease in light penetration (to ~0.5 meters) immediately followed the first large inflow event in April 2007 (Figure 5.1.5.3.4c). Similarly, pH was greatest (~8.8) during the period of bloom and decreased (to ~7.8) immediately following the first large inflow event in April (Figure 5.1.5.3.4d).

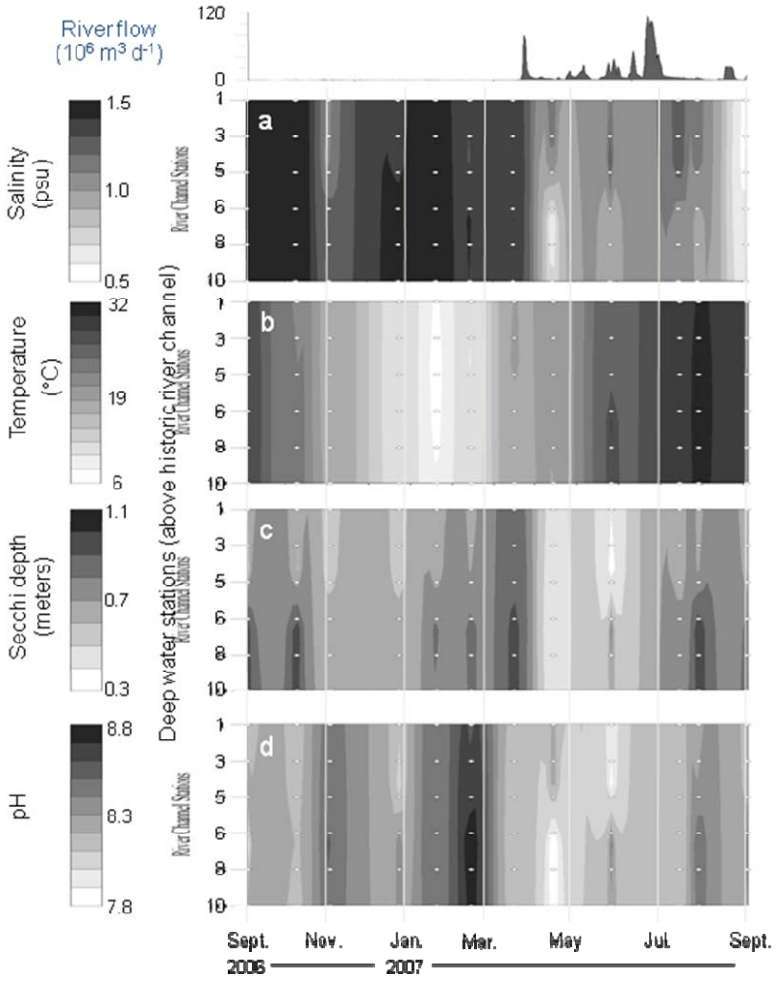

Fig. 5.1.5.3.4. Characterizations of the physicochemical environment for a one-year period that spanned the formation and termination of a *P. parvum* bloom. Salinity (a) was highest in the earlier part of the study period, but decreased following the April inflow event. Temperature (b) followed a typical seasonal cycle for north-hemisphere, sub-tropical climates. Irradiance, as approximated with Secchi depth (c), showed decreased with the spring inflow events. pH (d) was highest during the peak bloom period, and decreased following the April inflow event.

Dissolved inorganic nutrients also showed a strong relationship with inflow, and immediately following the first large inflow event in April 2007 both SRP and DIN reached their maxima of ~0.55 µM-P and ~24 µM-N (Figure 5.1.5.3.5). Highest nutrient concentrations were measured in the lower reaches of the lake at this time. During January through March 2007, when *P. parvum* population densities were greatest and then started to decline, the DIN:SRP was ~30 with SRP concentrations ~0.05 µM-P and DIN ~1.35 µM-N. Except for December 2006, nutrient concentrations during the bloom were similar to the months prior to the bloom. In December, SRP concentrations were at their lowest, ~0.03 µM-P, while DIN was ~3.55 µM-N (DIN:SRP ~122).

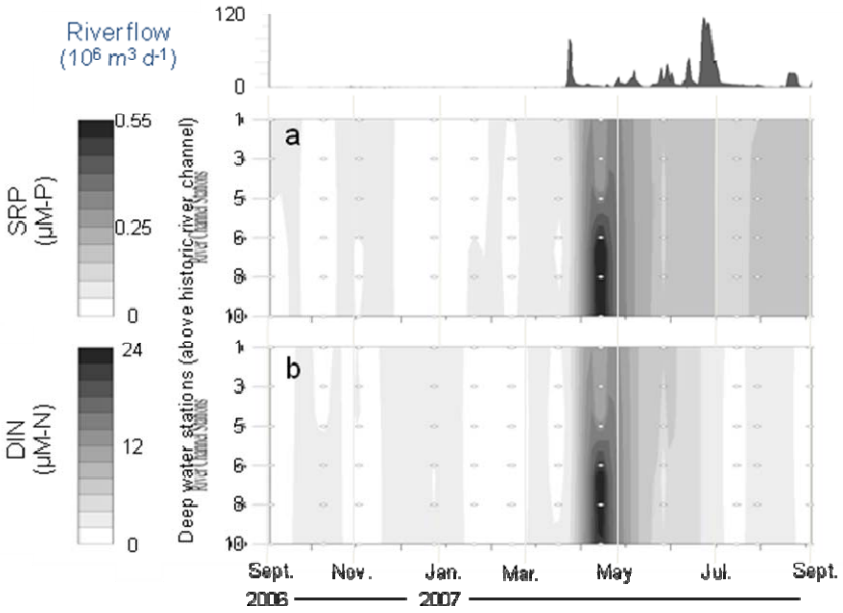

Fig. 5.1.5.3.5. Characterizations of inorganic nutrients for a one-year period that spanned the formation and termination of a *P. parvum* bloom. Soluble reactive phosphorus (a) and dissolved inorganic nitrogen (b) were low in the lake prior to the April inflow event, but were still at concentrations high enough to support P. parvum growth.

The multivariate NMS analyses also revealed strong temporal patterns in Lake Granbury (Figure 5.1.5.3.6). A prominent feature of the two-dimensional solution (71% and 22% of the variability in the data shown on axis 1 and 2, respectively) was the *P. parvum* bloom occurring in the winter months (January through March 2007). The maxima in copepod adults and rotifers that occurred during these months (data not shown), but not coincident with the *P. parvum* maximum, was also clearly shown. Other prominent features of the analysis showed the higher nutrient concentrations following the inflow events to Lake Granbury during the spring and early summer months (April through July 2007), a period when *P. parvum* cell densities were greatly reduced. Finally, the cladocera maximum in the spring (data not shown), and the cyanobacteria and ciliated protozoa maxima (data not shown) in the summer months, were prominent features of the analysis.

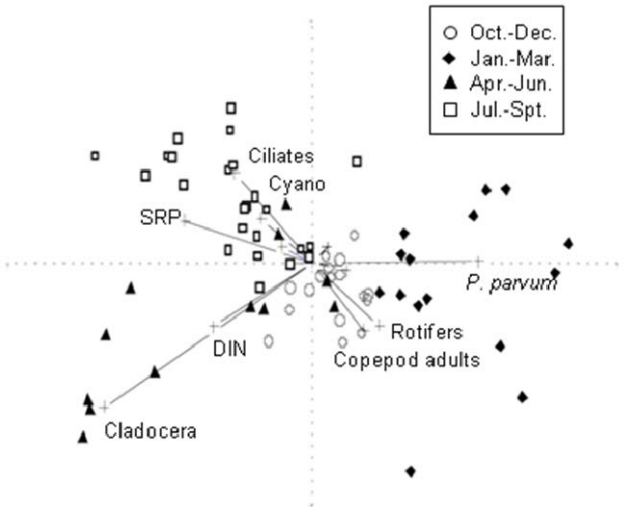

Fig. 5.1.5.3.6. Non-metric multidimensional analysis (71% and 22% of the variability shown on axes 1 and 2, respectively) reinforced field observations by showing the bloom of *P. parvum* to be associated with the winter months along with adult copepods and rotifers, the nutrient loading to be associated with the spring and early-summer inflow events, cladocera abundance to be associated with the spring months, and ciliates and cyanobacteria to be associated with the summer months. Each point in this graph represents a single sampling in space and time. That is, no averaging of data is shown.

The mathematical model used to predict the specific growth rate of *P. parvum* (eq. 1) indicated that growth rate of *P. parvum* was lowest at the time when cell densities were highest, i.e., January and February 2007 (Figure 5.1.5.3.7a). Interestingly, specific growth rate predictions increased for March 2007, at the time when *P. parvum* population densities were beginning to decline. The temperature terms in these models strongly affected predictions. As temperature increased during January to March, growth rate increased. In late summer (August and September 2007), temperatures above the modeled optimum for *P. parvum* led to predictions of decreased growth rate.

The size of well-mixed surface water patches varied. During March, after an extended period of low inflows, patches were on the scale of ~1 km. During April, after a large inflow event, the lake was better mixed and patches were on the scale of ~6 km. Patch size influences the estimate of hydraulic flushing. Because our frequency of sampling did not match the rate of hydraulic change, we evaluated hydraulic flushing for this period bounded by lower (6 km) and upper (1 km) bounds for flushing estimates. This analysis showed that hydraulic flushing was near non-existent prior to the first large inflow event in April, and that inflow pulses started in April and continued sporadically through the early summer months producing flushing losses higher than specific growth rates for *P. parvum* (Figure 5.1.5.3.7b).

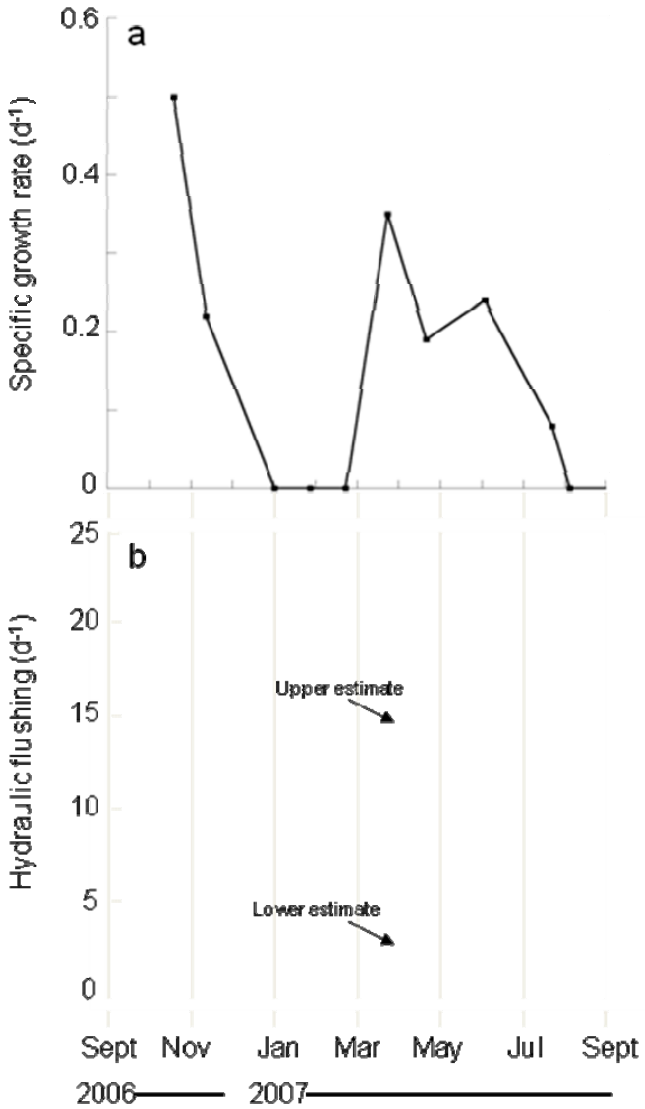

Fig. 5.1.5.3.7. Mathematical model (eq. 1) that predicts *P. parvum* growth rate as a function of salinity, temperature and light (a) revealed that periods of stress coincided with January and February (the period of peak bloom intensity) and late summer. Estimates of hydraulic flushing (b) showed that prior to the first large inflow event in April hydraulic flushing was negligible. When inflows commenced, however, they resulted in flushing losses greater than the specific growth rate of *P. parvum*. Lower and upper estimates of flushing were calculated based on well-mixed patches of 6 and 1 km, respectively.

Focusing on the period between March and April, when the first large inflow event occurred, average *P. parvum* population density in the lake decreased ~89%, as mentioned above. Modeled population reductions for this month-long period (based on equation 3) were 100% and 68% for the scenarios where well-mixed lake segments were 1 and 6 km (see Figure 5.1.5.3.3). The model, however, predicted that this decrease to the *P. parvum* bloom occurred over a period of only 4 days (Figure 5.1.5.3.8).

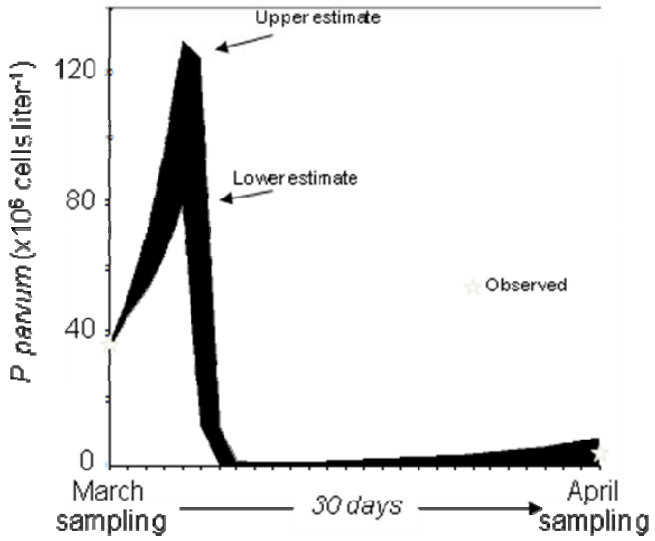

Fig. 5.1.5.3.8. Numerical model (equation 4) simulation that reproduced our monthly observation of the *P. parvum* bloom decline (open stars), showing that the actual bloom termination occurred over an estimated period of 4 days. Lower and upper estimates of population density were from simulations that employed well-mixed patches of 6 and 1 km, respectively.

5.1.5.4 Discussion of a system-wide, fish-killing bloom in Lake Granbury (2006-2007)

This more focused study is the first to document the dynamics of *P. parvum* across an entire lake and over an annual cycle, encompassing bloom formation, toxicity to fish, and bloom termination. Some of the patterns found here confirm current understanding of population dynamics and toxicity of this HAB species, while others raise questions.

Production of toxic chemicals by *P. parvum* increases when environmental conditions are stressful (Nygaard and Tobiesen 1993, Barreiro et al. 2005, Uronen et al. 2005, Roelke et al., 2007, Errera et al. 2008). Like other HAB species (Granéli and Hansen 2006, Turner 2006, Prakash et al. 2009), production of toxic chemicals might enable *P. parvum* to initiate blooms because it imparts a competitive advantage over other phytoplankton or inhibits grazers.

During the months prior to the *P. parvum* bloom in Lake Granbury (September through December 2006), it is unclear which environmental conditions might have been stressful. Salinity, temperature and light were favorable for *P. parvum* growth. Nutrient concentrations during those months did not seem strongly limiting. SRP reached its lowest concentrations in December 2006, when it was ~0.03 µM-P (DIN:SRP ~121). While this concentration might have limited growth of some phytoplankton species (Grover 1989, Grover et al. 1999, Reynolds 2006), it was not likely limiting to *P. parvum*, which has shown positive growth at SRP concentrations lower than this (Baker et al. 2009). Lack of stress, and generally favorable conditions suggest that the *P. parvum* bloom could have initiated from *in situ* growth in Lake Granbury, and that

allelopathic effects were not important at this early stage. Another possibility is that conditions favorable to bloom initiation occurred in a lake up-river of Lake Granbury, i.e., Lake Possum Kingdom (Roelke et al. 2007), and that the bloom developed due to mass effects (*sensu* Liebold and Miller 2004) resulting from large migrations of *P. parvum* cells into Lake Granbury.

In contrast to these early stages, environmental conditions were stressful to *P. parvum* during the periods of bloom development and peak population densities (January and February 2007). While nutrient concentrations did not appear to be strongly limiting, predicted growth rates based on temperature, salinity and light were near zero, primarily due to the low winter temperatures. Consistent with the notion that *P. parvum* cells are more toxic when stressed by suboptimal growth (Baker et al. 2007), the highest observed fish toxicities were during these winter months.

At this time, the *P. parvum* bloom was extensive throughout the entire system, a phenomenon observed for many other HAB species (e.g., Roelfsema et al. 2006, Chang et al. 2008, Oh et al. 2009). The bloom was also patchy, as some areas of the lake experienced elevated phytoplankton biomass while others experienced the bloom at lower densities. Blooms of *P. parvum* are typically characterized by near-complete dominance of this species, which has been observed during blooms in other lakes of the Brazos River (Roelke et al. 2007, Schwierzke et al. 2010) and elsewhere (Sunda et al. 2006, Sopanen et al. 2008, Michaloudi et al. 2009). This *P. parvum* bloom in Lake Granbury was also near-monospecific (~92% decreasing to 87% before the first flushing event), with diatoms, green algae and cyanobacteria comprising much of the remaining biomass.

The first large inflow event, which occurred in April 2007, obliterated the *P. parvum* bloom. Single day estimates of hydraulic flushing for Lake Granbury at this time ranged between 2.7 and 16 d^{-1}. These estimates of flushing loss were greater than the predicted growth rate of *P. parvum* based on conditions of salinity, temperature and light. Our modeled estimate of net population growth rate predicted population declines that agree quantitatively with the monthly observed declines, but also indicated that the actual bloom termination occurred over a much shorter period, i.e., 4 days. Hydraulic flushing as a mechanism affecting the biology and ecology of entire systems has long been recognized (Ketchum 1951, 1954), and as a bloom-terminating mechanism has been observed for other HABs, particularly blooms of cyanobacteria (Jacoby et al. 2000, Moustaka-Gouni et al. 2006).

In addition to the direct loss of cells through flushing, *P. parvum* likely ceased production of toxins with the rapid increase in nutrient concentrations (Roelke et al. 2007, Errera et al. 2008). Our sampling revealed the complete removal of ambient toxicity to fish with this inflow event. This removal of fish toxicity might have resulted from the cessation of toxin production coupled to degradation of the existing toxins, dilution of in-lake toxin concentrations by hydraulic flushing, or it might have resulted because the pH dropped to levels that altered the ionization state of toxins, rendering them harmless (Valenti et al. 2010). Regardless of the mechanism, removal of toxicity would have greatly diminished *P. parvum*'s ability to compete with other phytoplankton or inhibit zooplankton.

Interestingly, the bloom started to decline (based on direct cell counts) before hydraulic flushing affected the lake. It is unclear why. The predicted growth rate of *P. parvum* based on salinity, temperature and light increased from February to March 2007, mostly because of the temperature increase. Inorganic nutrients did not appear limiting to *P. parvum*. Copepod biomass increased (data not shown), suggesting increased grazing, but these biomass increases were only observed in the upper reaches of the lake, in contrast to the system-wide decrease in *P. parvum*. Factors unaccounted for in this study include pathogens of *P. parvum*. Viruses and algicidal bacteria are known to deleteriously affect other HABs (Kodama et al. 2006, Salomon and Imai 2006). Furthermore, *in-situ* experiments from Lake Whitney, positioned down-river from Lake Granbury, showed that viruses impacted population dynamics of *P. parvum* in later stages of bloom development (Schwierzke et al. 2010). While we did not sample viruses in this study, it may be that they influenced *P. parvum* population densities just prior to the impact of the first inflow event.

The post-flushing distribution of phytoplankton was patchy, but at much lower densities than prior to the flushing event of April 2007. Although conditions of temperature, salinity, and light were predicted to be favorable for *P. parvum* growth, the bloom did not re-establish. This was likely due to the subsequent hydraulic flushing events that occurred in the remaining spring months of 2007. Early during the following summer, when inflows were reduced, the bloom still did not re-establish. Environmental conditions were not as stressful as spring conditions, and thus toxins were likely not being produced, leaving *P. parvum* vulnerable to zooplankton grazers, such as the rotifers that dominated the zooplankton community at this time.

Eventually, conditions again became stressful for *P. parvum* growth as summer temperatures rose above its optimum. Yet there was no indication of toxin production by *P. parvum*, and *P. parvum* did not become abundant. At this time, however, cyanobacteria were present. There is indirect evidence that some cyanobacteria might have an allelopathic effect on *P. parvum* in Texas lakes (Grover et al. 2010, Roelke et al. 2010). Thus their presence during summer months of 2007 might have prevented *P. parvum* from accumulating biomass.

This study underscores the importance of hydraulic flushing as a mechanism terminating *P. parvum* blooms in lakes of the south-central USA. In the decades to come, it is likely that the magnitude of lake-flushing events will decrease as human populations expand and the number of water impoundments increases. The effects of decreased through-flow might be exacerbated by climate change as well, as precipitation patterns alter. It may be that the affects of reduced through-flows and likely persistence of blooms can be offset by management efforts aimed at altering other factors influential to *P. parvum* bloom dynamics. For example, blooms might be mitigated by localized fertilization in areas where blooms develop in attempts to prevent toxin production (Barkoh et al. 2003, Grover et al. 2007, Roelke et al. 2007, Errera et al. 2008), promoting growth of phytoplankton that can suppress *P. parvum* through allelopathy (Grover et al. 2010, Roelke et al. 2010), manipulations of pH to negate the potency of toxins (Valenti et al.

2010), or introduction of natural predators and pathogens (Schwierzke et al. 2010). There is much understanding still to be gained, however, before effective management of *P. parvum* in lakes of the south-central USA can be implemented.

5.2 Microcystin ecological hazard assessment and laboratory experiments of microcystin-LR allelopathy to *P. parvum*

5.2.1 Background and rationale

Recent studies on *P. parvum* in Texas reservoirs by our research team identified a possible allelopathic response of *P. parvum* to cyanobacterial allelochemicals (Grover et al., 2010; Roelke et al., 2010). Such observations provided the impetus for the present study in which we examined whether *P. parvum* growth can be inhibited by the cyanobacterial toxin microcystin-LR (MC-LR). Cyanobacterial blooms can be associated with various allelochemicals and toxins (Watson, 2003), including the widely studied microcystins, which are cyclic heptapeptide algal toxins produced by a number of species, including members of the genera *Microcystis*, *Anabaena*, *Nodularia*, *Nostoc* and *Oscillatoria* (Chorus and Bartram, 1999). Approximately 80 microcystin congeners have been identified (e.g., MC-LR, -RR, -LA, –YR; Antoniou, 2008). Each compound shares a common structure of 3-amino-9-methoxy-2, 6, 8-trimethyl-10-phenyldeca-4, 6-diene acid (ADDA) and five amino acids connected by peptide bonds. Generally, microcystins with non-polar amino acids at positions 2 and 4 are more toxic than those with polar amino acid because of the increased likelihood of partitioning to lipid tissues (Sivonen and Jones, 1999). For example, the non-polar leucine on MC-LR contributes to its high degree of toxicity (Kotak and Zurawell, 2007). However, despite having non-polar properties, MC-LR, like all microcystins, is soluble in water (de Maagd et al., 1999). Whereas this characteristic limits passive uptake to tissues, other transport mechanisms allow the toxin to enter organisms and exert toxicity. MC-LR is the microcystin variant with the most experimentally documented toxicity to aquatic species. Studies have shown MC-LR to adversely affect algae, macrophytes, zooplankton, and fish (Pflugmacher, 2002; Mitrovic, et al., 2005; DeMott et al., 1991; Reinikainen et al., 2002; Oberemm et al., 1997). Further, MC-LR can bioaccumulate, which is expected based on the estimated octanol-water partitioning coefficient of 2.16 (Ward and Codd, 1999). Grazers appear to be the most likely organisms to bioaccumulate and transfer microcystins to higher trophic levels (Kotak et al., 1996; Ferrao-Filho, 2002).

Lake Waco, Texas has a high density of cyanobacteria, including species that produce microcystin-LR. In a recent microcosm study by Roelke et al. (2010), a dose-dependent decline of *P. parvum* cell density was observed when organisms were exposed to varying proportions of filtered Lake Waco and Lake Whitney water: the higher the proportion of Lake Waco water, the lower the growth of *P. parvum*. Based on these experimental observations, Roelke et al. (2010) concluded that grazers, salinity, nutrients, and anthropogenic contaminants were not responsible for such responses. However, Roelke et al. (2010) could not rule out toxins or other allelochemicals produced by cyanobacteria or bacteria. Though MC-LR was not quantified during their study, because MC-LR had been measured in Lake Waco in the past (Brooks, unpublished data) and species that

produce MC-LR were abundant at the time of the Roelke et al. (2010) study, they proposed that allelochemicals produced by cyanobacteria may have inhibited growth of *P. parvum*.

In the present study, we specifically examined the influence of MC-LR on *P. parvum* growth. To support selection of experimental treatment levels of MC-LR, a probabilistic distribution of environmental exposure was developed and compared to adverse response thresholds of other aquatic organisms. An environmental exposure distribution (EED), a probability distribution of reported concentrations of a compound measured in the environment, was developed for MC-LR following an extensive literature review. EEDs, a technique commonly employed in probabilistic ecological hazard and risk assessment (PEHA; Solomon et al., 2000; Dobbins et al., 2008, 2009), provides an approach to estimate the probability of observing a concentration of an environmental contaminant at or below a selected value, which can then be interpolated from the log-normal probability of aquatic exposure concentrations.

5.2.2 Materials and methods

5.2.2.1 Probabilistic exposure and effects distributions

An extensive literature review was conducted to find reported environmental levels in surface waters for microcystins (Table 5.2.1) in order to develop a probabilistic EED. Measurements reported in the literature came from water bodies with microcystin-producers present or likely to be present; thus, there were few non-detect values. Because the data reviewed did not include water bodies without microcystin-producers present, which theoretically could yield an infinite number of non-detect values, zero values were not included in constructing the EED. Thus, this EED represents a distribution of microcystin levels when microcystin producers are likely to occur. The literature values were not limited to MC-LR because many detection methods used (e.g., enzyme linked immunosorbent assay or ELISA) are not variant specific. However, because the MC-LR variant is the most common form (Sivonen and Jones, 1999), it is likely that a majority of the unspecific measurements included this particular variant. The literature values used to construct the EED generally represented total microcystins (intra- plus extra- cellular), though several values were extracellular microcystin only. Values reported by Jacoby and Kann (2007), which were compiled from data submitted by lake managers, laboratories, state and federal agencies, and universities, were unspecified. The EED was created by ranking the data in increasing order and calculating a percent rank for each concentration using a Weibull formula:

$$j = (i * 100) / (n + 1), \quad (1)$$

where j is the percent rank, i is the rank assigned to the measured microcystin value after placing the values in increasing order (1 to n), and n is the number of measurements (Solomon et al., 2000). The concentrations were plotted on a log scale against their respective percent rank plotted on a Gaussian probability scale (SigmaPlot, v10.0, San Jose, CA, USA). A best-fit regression line was added (Solomon et al., 2000) whose equation was then used to calculate the 10, 25, 50, 75, and 90th centile values, which were selected to serve as nominal treatment levels (0, 0.0623, 0.807, 13.9, 239, and 3090 µg L^{-}

[1] MC-LR, respectively) in the experimental study described below. These centile values represent the probability of detecting a microcystin concentration at or below a corresponding concentration in a freshwater system.

Centile values from the EED were used to select nominal concentrations for MC-LR treatment levels; specific centile values from the distribution were selected after evaluating the peer-reviewed literature for MC-LR concentrations that elicit effects on various aquatic plants. For example, at a concentration as high as 10,000 µg L^{-1}, growth and peroxidase activity of a filamentous alga was not adversely affected (Mitrovic et al., 2005), but a submerged macrophyte was found to experience growth inhibition as low as 1.0 µg L^{-1} (Pflugmacher, 2002). Therefore, MC-LR treatment levels in the laboratory experiment spanned several orders of magnitude to potentially encompass a *P. parvum* growth response. Because invertebrate studies were most common, the probabilities of encountering various MC-LR in aquatic systems were compared to invertebrate threshold values (Table 5.2.2).

5.2.2.2 Prymnesium parvum *stock culture*

A stock culture of *P. parvum* was initiated from a strain obtained from The University of Texas at Austin Culture Collection of Algae (strain UTEX LB 2797) that was originally isolated from the Colorado River in Texas. The culture was maintained in a 20-L glass carboy filled with 10 L of 2.4 psu Artificial Seawater (ASW) (Berges et al., 2001) enriched with f/2 levels of vitamins, trace metals, and nutrients (Guillard, 1975). The carboy was maintained in an incubator (VWR Model 2015, West Chester, PA, USA) at 20˚C on a 12:12 light:dark cycle. The culture was swirled daily and allowed to grow until stationary phase, at which time these organisms were used to inoculate the experimental units at each treatment level. Cell density of the stock culture at the time of inoculation was approximately 2 x 10^5 cells mL^{-1}.

5.2.2.3 Experimental design

Experimental units consisted of five replicate culture tubes (25x200 mm) each containing 50 mL of test solution at one of six different nominal concentrations of MC-LR (0, 0.0623, 0.807, 13.9, 239, and 3090 µg L^{-1}, corresponding to the 10, 25, 50, 75, and 90th centiles, respectively). The highest test solution concentration was prepared by mixing approximately 1 mg of purified (≥95%) MC-LR (Alexis Biochemicals/Enzo Life Sciences, Inc., Farmingdale, NY, USA) into 308 mL of f/2 medium. The other four concentrations were prepared from a concentrated stock solution by diluting approximately 1 mg MC-LR into two liters of f/2 medium; f/2 medium was used as a diluent for all concentrations. A final set of five culture tubes consisted of the 500 µg L^{-1} stock solution with no algal addition, hereafter referred to as blanks, were used to examine MC-LR degradation during the study period. After all test solutions were made, each culture tube (except for blanks) was inoculated with 10,000 cells mL^{-1} of *P. parvum*.

After inserting foam plugs, all flasks were placed on slanted test tube racks in an incubator (VWR model 2015, West Chester, PA, USA) maintained at 20˚C on a 12:12

L:D cycle for 27 days. Culture tubes were swirled once in the morning and gently vortexed in the afternoon before taking a fluorescence reading, after which their positions were rotated within the incubator. *In vivo* fluorescence was determined with a Turner fluorometer model 10AU (Turner Designs, Sunnyvale, California, USA) and values were converted to cell density using a standard curve of cell counts determined microscopically using a hemacytometer (US EPA, 2002).

5.2.2.4 Analytical verification of MC-LR treatment levels

When the study was initiated, nominal MC-LR concentrations of each experimental unit were verified with ELISA with a range of detection of 0.1 to 5 µg L^{-1} (Abraxis, Steamwhistle, PA, USA). In addition, final MC-LR concentrations on day 27 were determined with ELISA for all treatment levels to quantify the amount of toxin remaining at the end of the study. Any concentration that would or was expected to fall beyond the method limit of detection was diluted to the detection range of the ELISA.

5.2.2.5 Statistical analyses

Cell density of each treatment level was compared to the controls during each day of the study by a one way analysis of variance (ANOVA) and a Dunnett's test (JMP v6.1, SAS Institute, Cary, NC, USA) when a significant difference ($\alpha = 0.05$) was detected. In addition to determining cell densities, we also examined specific growth rates (μ, day^{-1}), which were calculated for days 2 through 7 for each replicate at each treatment level by regressing the natural log of the cell density against time. The first seven days of exposure were examined because this period corresponded to the microcosm study duration by Roelke et al. (2010). The exponential growth rate was then determined as the slope of the line of best fit. Mean exponential growth rate values were then determined for each treatment level and differences among treatment levels were determined by ANOVA.

5.2.3 Results

5.2.3.1 Microcystin exposure distribution

The EED (Figure 5.2.1) included 211 concentrations of microcystins reported in the peer-reviewed literature (Table 5.2.1). Most values were available from water bodies in the United States, but data also came from Canada, Finland, Australia, and Japan. The highest reported value used to develop the distribution was 12,176 µg L^{-1} microcystin from the Copco Reservoir in California, USA (Jacoby and Kann, 2007); 121 values were under 1 µg L^{-1}. Regression analysis of the exposure distribution resulted in the equation, $y = -0.6235x + 0.54588$ (r^2=0.94), though extremely high and low values may be underestimated by the linear regression approach employed here. The calculated 10, 25, 50, 75, and 90th centile values were 0.0623, 0.807, 13.9, 239, and 3,090 µg L^{-1} of microcystin, respectively. A wide range of adverse acute invertebrate mortality values were identified from the literature (Table 5.2.2). For example, a mayfly nymph (*Hexagenia* sp.) was the most sensitive (96 hr LC_{50} = 49 µg L^{-1}; Smith et al., 2008) and

Daphnia pulicaria was the least sensitive species (48 hr LC_{50} = 21,400 µg L^{-1}; DeMott et al., 1991) to MC-LR. Another cladoceran, *Daphnia hyalina*, had an intermediate 48 hr LC_{50} value of 11,600 µg L^{-1} MC-LR (DeMott et al., 1991). Using the EED of MC-LR in the study, it is possible to predict the probability of encountering MC-LR concentrations corresponding to such adverse acute thresholds (Table 5.2.3).

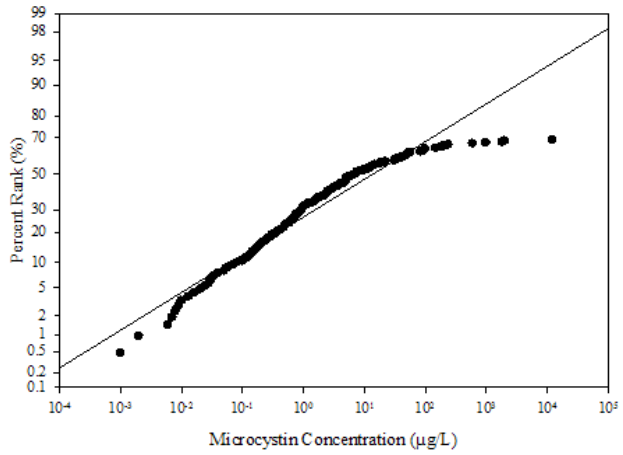

Figure 5.2.1. Probabilistic exposure distribution of microcystin in freshwater ecosystems based on 211 concentrations from the peer-reviewed literature (y = -0.6235x + 0.54588, r^2 = 0.94).

5.2.3.2 Analytical verification of MC-LR concentrations

Measured MC-LR treatment levels were 102 to 154% of the nominal concentrations; therefore, the measured values were used for all statistical analyses (Table 5.2.4). Measured initial concentrations approximated the 12th, 25th, 52nd, 76th, 91st centiles; all values were up to approximately two centiles higher than those chosen for nominal concentrations based on the EED. On the final day of the study (day 27), MC-LR remaining in the experimental units was determined (Table 5.2.4). Degradation was observed in all but the second lowest concentration (0.8 µg L^{-1}); however, this minor inconsistency approached measurement at the lower range of the ELISA limit of detection. Overall, 53 to 84 % of initial MC-LR remained in the experimental units at the termination of the experiment.

Table 5.2.1. Reported microcystin concentrations used to develop an environmental exposure distribution.

Reference	[MC] µg L^{-1}	Location	Reference	[MC] µg L^{-1}	Location
McDermott,		Wisconsin, US	Graham and	0.8	Missouri/ Iowa, US
1995	200	Suamico River	Jones, 2007	7	Missouri/ Iowa, US
	180	Green Bay			
	1.7	Green Bay	Fristachi *et al*.,	0.007	US/ Canada
	1.2	Quarry Park Lake	2007; Carmichael,	0.053	US/ Canada
	0.7	Long Lake #1	2001	0.013	US/ Canada
	19	Long Lake #2		0.007	US/ Canada
	0.3	Becker Lake		0.04	US/ Canada
	3.8	Round Lake		147.1	US/ Canada
	2.4	Boot Lake		4.7	US/ Canada
	22	Beaver Dam Lake #2		0.03	US/ Canada
	8	Beaver Dam access stream			
	2	Long Lake	Kotak and		Canada
	6.8	Kettle Moraine Lake	Zurawell, 2007	2.48	Little Beaver Lake
	0.5	Green Lake		11.2	Little Beaver Lake
	17	Green Lake Dam		1.5	Nakamun Lake
	50	Lake Weyauwega		1	Driedmeat Lake
	12.4	Mirror Lake			
	7.4	Shadow Lake	Murphy *et al*.		Canada
			2003	0.17	Hamilton Harbor, Lake Ontario
	11.2	White Lake	.	0.19	Hamilton Harbor, Lake Ontario
	5	Hartman Lake		0.01	Hamilton Harbor, Lake Ontario
	1	Fox River-Omro Park		0.01	Hamilton Harbor, Lake Ontario
	52	Lake Butte de Mortes		0.02	Hamilton Harbor, Lake Ontario
	3	Wolf River		0.06	Hamilton Harbor, Lake Ontario
	51	Lake Winnebago #1		33.1	Hamilton Harbor, Lake Ontario
	56	Lake Winnebago #2		0.25	Hamilton Harbor, Lake Ontario
				5.03	Hamilton Harbor, Lake Ontario
Jacoby and		Pacific Northwest, US		0.96	Hamilton Harbor, Lake Ontario
Kann, 2007	12176	Copco Reservoir, CA		0.47	Hamilton Harbor, Lake Ontario
	2032	Iron Gate Reservoir, CA		238.8	Hamilton Harbor, Lake Ontario
	46.73	Klamath River, CA		202.2	Hamilton Harbor, Lake Ontario
	0.7	Tenmile Lakes, OR		0.98	Hamilton Harbor, Lake Ontario
	1.61	Tenmile Lakes, OR		0.24	Hamilton Harbor, Lake Ontario

Table 5.2.1. Continued

Jacoby and Kann, 2007	0.19	Crane Prarie, OR	Murphy *et al.* 2003	0.024	Lake Erie
	4.92	Crane Prarie, OR		0.035	Lake Erie
	0.68	Lava Lake, OR		0.142	Lake Erie
	0.009	Paulina Lake, OR		0.302	Lake Erie
	84	Paulina Lake, OR		0.016	Lake Erie
	2.9	Wickiup Reservior, OR		0.009	Lake Erie
	2.54	Diamond Lake, OR		0.008	Lake Erie
	0.36	Suttle Lake, OR		0.001	Lake Erie
	0.51	Suttle Lake, OR		0.006	Lake Erie
	0.19	Lake Selmac, OR		0.002	Lake Erie
	13.5	Lake Selmac, OR		0.371	Lake Erie
	0.03	Odell Lake, OR		0.407	Lake Erie
	5.01	Odell Lake, OR		0.2	Lake Erie
	10	Odell Lake, OR		0.028	Lake Erie
	600	Upper Klamath (Agency) Lake , OR		0.031	Lake Erie
	14.6	Owyhee Reservoir, OR		0.009	Lake Erie
	18.5	Vancouver Lake, WA		0.008	Lake Erie
	0.91	Vancouver Lake, WA		0.009	Lake Erie
	7	Vancouver Lake, WA			
	9.5	Vancouver Lake, WA			
	0.25	Lake Garrett (Hicks), WA	Young *et al.*, 2006		Aland, Finland
	0.85	Lake Garrett (Hicks), WA		0.070	Hogbolstad
	0.26	Lake Garrett (Hicks), WA		1.400	Godby trask
	0.75	Lake Garrett (Hicks), WA		12.100	Prasttrasket
	0.74	Lake Garrett (Hicks), WA		0.130	Basttjarnan
	0.68	Lake Garrett (Hicks), WA		0.260	Brantsbole trask
	0.86	Lake Garrett (Hicks), WA		6.400	Nato Hemviken
	1	Green Lake, WA		0.200	Gloskars trask
	32	Green Lake, WA		0.250	Gloskars trask
	3	Green Lake, WA		0.760	Brantsbole trask
	100	Green Lake, WA		0.620	Brantsbole trask
	0.17	Green Lake, WA		0.670	Brantsbole trask
	2.2	Green Lake, WA		1.000	Stromma trask
	1	Lake Sammamish, WA		0.700	Kaldersfjarden
	43	Lake Sammamish, WA		2.300	Lembote Bytrask
	0.13	Lake Sammamish, WA		6.000	Lembote Bytrask
	0.17	Lake Sammamish, WA		5.400	Vargata trask

Table 5.2.1. Continued

Jacoby and Kann, 2007	0.16	Lake Sammamish, WA
	0.1	Lake Sammamish, WA
	0.14	Lake Union, WA
	0.15	Lake Union, WA
	0.12	Lake Union, WA
	0.14	Lake Union, WA
	0.18	Lake Washington, WA
	0.62	Lake Washington, WA
	0.68	Lake Washington, WA
	1.15	Lake Washington, WA
	4	Kitsap Lake, WA
	13	Steilacoom Lake, WA
	0.8	Waughop Lake, WA
	0.13	Moran State Park Lake, WA
	0.5	Lake Cassidy, WA
	3	Lake Cassidy, WA
	0.5	Ketchum Lake, WA
	3	Ketchum Lake, WA
	2.73	Lake Lawrence, WA
	0.99	McIntosh Lake, WA
	0.54	McIntosh Lake, WA
	0.51	McIntosh Lake, WA
	1.52	McIntosh Lake, WA
	0.54	McIntosh Lake, WA
	0.48	McIntosh Lake, WA
Touchette et al., 2007		North Carolina, US
	0.3	Kerr Scott
	0.13	Tuckertown
	0.11	Oak Hollow
	0.2	Jordan
	0.24	Falls
	0.15	Narrows
	0.28	Lake Rhodhiss
	0.15	Michie
	0.1	High Rock
	0.35	Tillery
	0.14	High Point Lake
Williams *et al.*, 2007		Florida, US
	0.05	Harris Chain of Lakes
	0.5	Harris Chain of Lakes
	3.6	Harris Chain of Lakes
	0.01	St. Johns River
	0.6	St. Johns River
	31	St. Johns River
	0.1	Lake Okeechobee
	0.1	Lake Okeechobee
	95	Lake Okeechobee

Young *et al.*, 2006	4.600	Vargata trask
	5.100	Godby trask
	0.100	Norra Langsjon, Saltvik
	0.940	Overby insjo
	0.240	Sodra Slemmern
	0.610	Hogskar
	0.160	Lillfjarden
	1.640	Katthavet
	3.100	Prasttrasket
	0.440	Hagn trask
	42.300	Vargata trask
	36.800	Vargata trask
	7.540	Prasttrasket
	3.100	Brantsbole trask
	0.210	Brantsbole trask
Jones and Orr, 1994		Temora, Australia
	990	Lake Centenary
	1830	Lake Centenary
Harada and Tsuji, 1998		Japan
	0.02	Lake Sagami
	0.04	Lake Sagami
	0.05	Lake Sagami
	0.6	Lake Sagami
	0.04	Lake Tsukui
	0.08	Lake Tsukui
	3.18	Lake Tsukui
	0.14	Lake Tsukui
	52	Lake Tsukui
	3.9	Lake Tsukui
	2.5	Lake Tsukui
	0.05	Lake Tsukui
	1.78	Lake Tsukui
	0.24	Lake Tsukui
	0.04	Lake Tsukui
	1.07	Lake Tsukui
Harada and Tsuji, 1998	93.8	Lake Tsukui
	0.08	Lake Tsukui
	0.02	Lake Tsukui

Table 5.2.2. Select acute median lethal concentration values for freshwater invertebrates exposed to microcystin-LR.

Reference	Organism	Statistic	Endpoint	Concentration ($\mu g\ L^{-1}$)
Smith *et al.*, 2008	*Hexagenia* spp. hatchling nymph	96 hr LC_{50}	mortality	49
Reinikainen *et al.*, 2002	*Eurytemora affinis*	48 hr LC_{50}	mortality	274
DeMott *et al.*, 1991	*Diaptomus birgei*	48 hr LC_{50}	mortality	450
Metcalf *et al.*, 2002	*Artemia salina*	72 hr LC_{50}	mortality	850
DeMott *et al.*, 1991	*Diaptomus birgei*	48 hr LC_{50}	mortality	1,000
DeMott *et al.*, 1991	*Daphnia pulex*	48 hr LC_{50}	mortality	9,600
DeMott *et al.*, 1991	*Daphnia hyalina*	48 hr LC_{50}	mortality	11,600
Kiviranta *et al.*, 1992	*Aedes aegypti*	48 hr LC_{50}	mortality	14,900
Chen *et al.*, 2005	*Daphnia magna*	48 hr LC_{50}	mortality	20,300
DeMott *et al.*, 1991	*Daphnia pulicaria*	48 hr LC_{50}	mortality	21,400

Table 5.2.3. Calculated centile values for probabilistic environmental exposure distribution (EED) for microcystins.

	Microcystin Concentration ($\mu g\ L^{-1}$)
Centile	EED
1%	0.0008
5%	0.01
10%	0.062
25%	0.807
50%	13.9
75%	239
90%	3,090
95%	14,303
99%	253,433

Table 5.2.4. Nominal microcystin-LR concentrations and mean measured values (n = 5) for *Prymnesium parvum* treatment levels on study days 0 and 27.

Day 0 Nominal Concentration (µg L^{-1})	Day 0 Measured Concentration (µg L^{-1})	Measured Percent of Nominal (%)	Day 27 Measured Concentration (µg L^{-1})	Day 27 Measured Percent of Day 0 (%)
0	0	0	0	0
0.0623	0.09	140	0.05	57
0.807	0.8	102	1.1	128
13.9	16.6	119	14.0	84
239.0	278.6	117	211.5	76
3090.0	4392.8	142	2589.4	59
500.0	768.7	154	410.3	53

Table 5.2.5. Mean exponential growth rate (n = 5; ± standard deviation) of *Prymnesium parvum* exposed to microcystin-LR treatment levels over a 7 d period.

MC-LR Concentration (µg L^{-1})	Exponential Growth Rate (divisions day^{-1})
0	0.700 (0.099)
0.09	0.678 (0.109)
0.8	0.945 (0.265)
16.6	0.939 (0.403)
278.6	0.903 (0.417)
4392.8	0.868 (0.416)

5.2.3.3 Prymnesium parvum *growth*

From day 17 until the end of the study on day 27, *P. parvum* density in the lowest MC-LR treatment level (0.09 µg L^{-1}) significantly increased *P. parvum* cell density ($p < 0.05$) relative to controls (with day 24 as an exception; Figure 5.2.2). However, on day 6-8, 13-14, and 22-23 (approximately one quarter of the duration of the study), the highest MC-LR treatment level (4,392.8 µg L^{-1}) significantly decreased *P. parvum* cell density relative to controls ($p < 0.05$; Figure 5.2.2). There was a significant ($p < 0.05$) decrease in cell density by the 16.6 µg L^{-1} treatment on day 13 only. Cell densities in all other treatments were not significantly different from the controls throughout the study period ($p > 0.05$). Specific growth rate was similar in all treatments for most of the test duration. Specific growth rate was the highest in the first five days, decreased until around 15 days, then leveled off through day 27 (Figure 5.2.3). Analysis of exponential growth rate (Table 5.2.5; Figure 5.2.3) from days two to seven showed that there was no significant difference of exponential growth rate among the treatment levels ($p>0.05$).

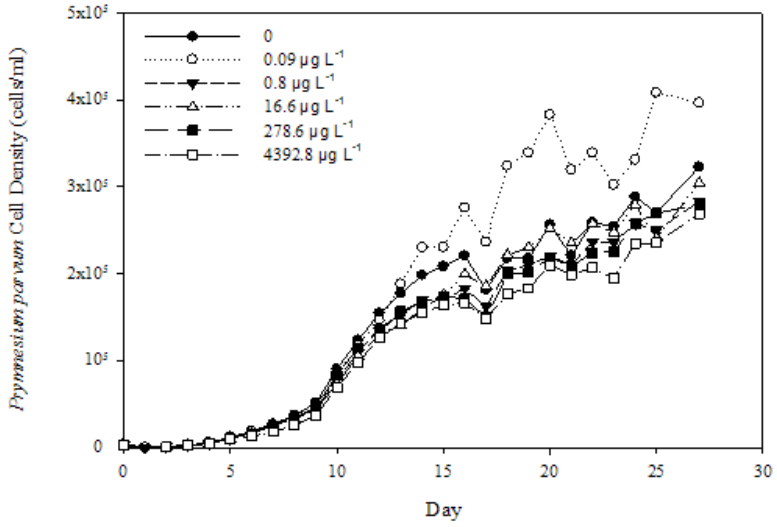

Figure 5.2.2. Mean (n=5) *Prymnesium parvum* cell density (cells mL^{-1}) responses to five microcystin-LR concentrations and a control over a 27 d study period.

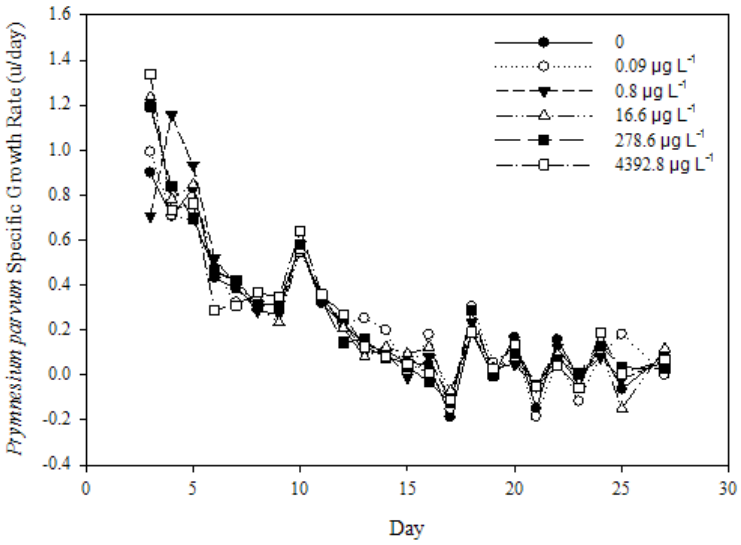

Figure 5.2.3. Specific growth rate of *Prymnesium parvum* during a 27 d exposure to five microcystin-LR concentrations and a control.

5.2.4 Discussion of cyanobacterial allelopathy

Roelke et al. (2010) observed a concentration dependent inhibition of *P. parvum* growth over a 7 day study by filtered water from a reservoir in which microcystin producing cyanobacteria contributed to the phytoplankton community. Because inhibition was observed when the cyanobacterial cells were removed by filtration, Roelke et al. (2010) suggested that dissolved compounds from cyanobacteria may have been responsible for growth inhibition. Further, two cyanobacteria, *Microcystis* sp. and *Anabaena* sp, present in Lake Waco during the Roelke et al. study (2010) are known to produce MC-LR (Lopez et al., 2008). Following from this suggestion, an objective of the present study was to examine the influence of microcystin-LR on *P. parvum* growth. In this study, exponential growth rate of *P. parvum* was not significantly affected over the first 7 d of the experiment (Table 5.2.5). However, based on cell abundance, the highest treatment level of MC-LR (4,392.8 μg L^{-1}) was identified as the Lowest Observed Effect Concentration (LOEC) during approximately 25% of the 27 day study and 278.6 μg L^{-1} was the No Observed Effect Concentration (NOEC) for *P. parvum* growth inhibition.

Previous studies have observed adverse effects from MC-LR to different species of plants and algae. For example, Pflugmacher (2002) identified growth inhibition of submerged macrophyte *Ceratophyllum demersum* by 1.0 μg L^{-1} MC-LR over six weeks and oxygen inhibition to occur at MC-LR concentrations as low as 0.05 μg L^{-1}; complete death was observed at 5,000 μg L^{-1} after 24 hours. In contrast, Mitrovic et al. (2005) found that even at a concentration as high as 10,000 μg L^{-1}, growth and peroxidase activity of the filamentous alga *Chlodophora fracta* and growth of the aquatic macrophyte *Wolffia arrhiza* were not adversely affected over a 5 d study. Kearns and Hunter (2001) observed that 10 μg L^{-1} MC-LR paralyzed a motile green alga *Chlamydomonas reinhardtii* and caused them to sink more rapidly than the untreated cells. This observation is important because paralysis affects settling, even though the cells remain viable. In an aquatic system, settling could create a competitor-reduced zone in a lake water column that might allow for the proliferation of cyanobacteria. It also may possibly lead to higher rates of grazer predation because lack of motility would decrease the ability to avoid predators. Because *P. parvum* cells were fixed before enumeration, neither the present study nor Roelke et al. (2010) examined the motility of the *P. parvum* cells. Because cell density was the main endpoint assessed in this study, it is possible that a more sensitive effect, such as motility or oxygen production, was inhibited by the treatment levels employed here.

In the present study, significant ($p<0.05$) stimulation of *P. parvum* growth was identified at the lowest treatment level of 0.09 μg L^{-1} MC-LR. Possibly, *P. parvum* was able to detoxify the toxin. Such detoxification pathways were proposed by Ou et al. (2005) for another mixotrophic alga, a chrysomonad *Poteriochromonas* sp. Like *P. parvum* growth in this study, growth of *Poteriochromonas* sp. was found to be stimulated in the presence of MC-LR, though at higher concentrations ranging from 100 to 4,000 μg L^{-1}. Because the growth rate of *Poterioochromonas* sp. was four to five times higher than the control, the authors concluded that the toxins served as a growth stimulus (Ou et al. 2005); however, Ou et al. (2005) also observed that toxin-treated cells showed low cellular

viability, suggesting that growth enhancement by microcystins was not a normal process, which coincided with other reports of tumor-promoting function of microcystins in vitro. In addition, Ou et al. (2005) reported that glutathione, malondialdehyde, and superoxide dismutase (SOD) content increased within eight hours of exposure to MC-LR (500 μg L^{-1}). A high level of SOD activity indicated that SOD was involved in decreasing oxidative stress caused by MC-LR (Ou et al., 2005). Antioxidant activity could be a valuable endpoint in future studies to understand how *P. parvum* protects itself from MC-LR induced damage. In addition, *Poterioochromonas* sp. was able to detoxify MC-LR at concentrations of 1,050, 2,500, and 4,000 μg L^{-1} (Ou et al., 2005). In the present study, 16-47% MC-LR degradation was observed in experimental units over a 27-day study period (Table 5.2.4). It is possible that *P. parvum* absorbed and detoxified MC-LR, though not as efficiently as *Poterioochromonas* sp., which exhibited high degrees of detoxification within a few hours of exposure. Degradation of exposure levels in the present study could also have resulted from bacterial transformation (Jones and Orr, 1994).

When microcystin-producing cyanobacteria are present in an aquatic ecosystem, concentrations are reported to range from ≤1 to ≥12,176 μg L^{-1} MC (Table 5.2.1). Exposure distributions of environmental concentrations of chemicals, such as the EED developed in the present study, are useful approaches employed for probabilistic ecological hazard and risk assessment, particularly when environmental exposure and/or effects data are limited (Solomon et al., 2000). In fact, these approaches are well accepted by the scientific and regulatory communities (Posthuma et al., 2002). For example, species sensitivity distributions are used retrospectively in PEHA to support development of numeric ambient water quality criteria in the US (Stephan, 2006), prospectively examine environmental safety of chemicals in the European Union (Williams et al., 2009), and were recently applied to *P. parvum* (Brooks et al., 2010). Understanding the magnitude of hazard and risk associated with an environmental contaminant, including biotoxins, can support sound science-based management decisions in aquatic ecosystems, particularly when data are limited. The EED constructed here to select experimental treatment levels, spanned a wide range of concentrations (Figure 1). In the United States, there are currently no Federal water quality criteria or maximum contaminant levels for any harmful algal species or their associated toxins; however, MC-LR is also the only algal toxin that has a provisional guideline value of 1 μg L^{-1} established for drinking water by the World Health Organization (WHO) (Lopez et al., 2008). Further, Health Canada established a drinking water guideline of 1.5 μg L^{-1} of MC-LR (Kotak and Zurawell, 2007). For recreational water bodies, WHO has determined the relative probability of acute health effects for total microcystins to be low at <20,000 cyanbacterial cells/mL (<10 μg L^{-1} MC), moderate at 20,000-100,000 cyanobacterial cells mL^{-1} (10-20 μg L^{-1} MC), high at 100,000-10,000,000 cyanobacterial cells/mL (20-2,000 μg L^{-1} MC), and very high at >10,000,000 cyanobacterial cells mL^{-1} (>2,000 μg L^{-1};Chorus and Bartrum, 1999). In the EED of the current study (Figure 5.2.1), 43% of the values were at or above the recommended WHO provisional drinking water guideline value of 1 μg L^{-1} and approximately 18% of the values exceeded the low probability of acute health effects classification for recreational water bodies. An important limitation to this probabilistic

prediction is that only detected data from the peer-reviewed literature were included (Table 5.2.1). It may be reasonable to project that analytical measurements were performed in these studies when cyanobacterial blooms were occurring or believed to be possible in the freshwater systems examined. Thus, the outcome of the probabilistic assessment presented here is likely applicable to ecosystems experiencing cyanobacterial blooms with MC-producing organisms. Wide ranges of sensitivities to MC-LR have been demonstrated for different species of algae and plants. Invertebrates also exhibit comparative sensitivities to MC-LR ranging over several orders of magnitude (Table 5.2.2). Clearly more information is needed for organisms at various trophic levels to fully characterize MC-LR effects on aquatic ecosystems (Murphy, 2003). In the interim, PEHA approaches are useful for modeling aquatic responses to contaminants (Dobbins et al., 2008, 2009), including harmful algae toxins (Brooks et al., 2010). Specific centiles of an EED can then be used to related environmental concentrations of a chemical contaminant to aquatic thresholds of adverse responses (Solomon et al., 2000; Dobbins et al., 2008, 2009). Based on the EED for MC-LR developed in the present study, *Hexagenia* sp. are expected to experience acute mortality following aquatic exposure to MC-LR at or above 49 μg L^{-1} (96 hr LC_{50}; Smith et al., 2008), which is likely to be encountered approximately 48.5% of the time (Table 5.2.3). Conversely, acute mortality of cladocerans, reported to range between 9.6 and 21.4 mg L^{-1} MC-LR (DeMott et al., 1991), would predicted by the EED to be observed in freshwater ecosystems much less frequently. Future studies are needed to develop robust SSDs for MC-LR and other microcystin congeners, which in combination with the PEHA approach presented here could advance ecological risk assessment and management efforts for microcystins. This would be a valuable tool for aquatic ecosystems managers facing cyanobacterial blooms.

Several differences between the present study and microcosm study by Roelke et al. (2010) are important to note. The Roelke et al. (2010) study was performed in the field during October where environmental conditions varied, whereas this study was performed at 20^{o}C with a 12:12 light: dark cycle in a laboratory incubator. Recent studies by our group highlight the influence of light of photolabile *P. parvum* toxins (James et al., In Press); and the influence of *P. parvum* toxins on cyanobacteria or even its own life cycle are not known. Lake Waco water used in Roelke et al. (2010) was phosphorus limited, but the laboratory cultures exposed to MC-LR here were nutrient sufficient. When phosphorus is limited, algae can upregulate the enzyme alkaline phosphatase in order to hydrolyze organic phosphorus compounds (Hoppe, 2003). In humans, MC-LR acts as a protein phosphatase inhibitor (MacKintosh et al., 1990). Thus, if *P. parvum* were phosphorus limited in the Roelke et al. (2010) study, it may have been that the combination of nutrient stress and inability to utilize phosphatases caused the observed *P. parvum* growth inhibition. Roelke et al. (2010) used additional treatments that were nutrient enriched and observed varied results, including *P. parvum* growth inhibition, variable phytoplankton growth, and stimulation of zooplankton, which could have affected *P. parvum* biomass.

In the present study we provide novel evidence that MC-LR can inhibit *P. parvum* growth, though the thresholds of such inhibition are relatively high. LOEC and NOEC values for *P. parvum* growth inhibition by MC-LR corresponded to the 91st and 76th

centiles of the MC-LR EED, respectively (Figure 5.2.1). Thus, the concentration at which *P. parvum* growth inhibition was observed in this study may be predicted to be observed or exceeded only 9% of the time in the aquatic systems when cyanobacteria that produce microcystins are present, based on the statistical model and probabilistic approach employed. The present study does not discount MC-LR as an inhibitor of *P. parvum* in the Roelke *et al*. (2010) study, particularly because MC-LR was not measured in Lake Waco waters; however, findings of the present study suggests that other dissolved chemicals produced by cyanobacteria may also contribute to the observed inhibition of *P. parvum* growth. For example, allelochemicals produced by cyanobacteria include other cyanotoxins (e.g., anatoxin, cylindrospermopsin; Chorus and Bartram, 1999), methylisoborneol, geosmin, volatile sulfur compounds, and polyunsaturated fatty acids (PUFA; Watson, 2003; Watson et al., 2008). Additionally, an algicidal chemical produced by a different organism, such as a bacterium, could have caused the observed inhibition in the Roelke et al. (2010) experiments. Because cyanobacteria may effectively limit the magnitude of severe *P. parvum* blooms (Roelke et al., 2010), further studies are warranted to assess sublethal responses of *P. parvum*, such as oxygen production, alkaline phosphatase activity, and motility, following MC-LR exposure. In addition, examination of other toxins (e.g., saxitoxins), microcystin congeners (e.g., MC-RR) and allelochemicals (e.g., terpenoids, PUFAs) that can be produced by cyanobacterial species and even *P. parvum* could help identify other potential causes of growth inhibition seen in Roelke et al. (2010), and potential environmental management strategies for *P. parvum*.

5.3 Building phytoplankton competitors into numerical model

A prior grant from DOE supported the construction and initial parameterization and calibration of a suite of models simulating *P. parvum* dynamics. These models were designed to be forced with limnological observations from reservoirs in Texas where *P. parvum* blooms occur, and appropriate data from Lake Granbury were used as input data in model development and testing. One model was a single-species model representing only the population of *P. parvum*. Four other models were constructed, two with one competing population of algae parameterized as cyanobacteria and two with four competing populations, including cyanobacteria. One of the one-competitor and one of the four-competitor models included an allelopathic effect on *P. parvum* of cyanotoxin excreted by the cyanobacteria. None of the models adequately predicted the seasonal pattern of *P. parvum* dynamics observed in a year of data from Lake Granbury that included a large bloom in winter. Although development of these models was largely completed under a prior grant, the current grant supported preparation of a manuscript reporting on these models (Grover et al., 2010).

During the current grant some additional modifications were made to the one-competitor model with allelopathy. A dynamically coupled zooplankton population was added, grazing on both *P. parvum* and the cyanobacteria. The grazing of this zooplankton population on *P. parvum* was inhibited by a toxin excreted by *P. parvum*. This section of the report details the development and calibration of this extended model of *P. parvum*

and competing algae. The calibration uses the first year of data that our team obtained from Lake Granbury, which included a large bloom. We also report an initial test of validity done by attempting to predict the dynamics of *P. parvum* subsequent to our first year of data, using the necessary input data on limnological conditions over that time period.

5.3.1 Model formulation

Model PP1 from Grover et al. (2010) was modified to construct a basic model with *P. parvum*, a competitor population (cyanobacteria) and a grazer population. Governing equations were

$$\frac{dZ}{dt} = D\left(Z_{in} - Z\right) + \mu_Z Z - m_Z Z \qquad (5.3.1a)$$

$$\frac{dN_i}{dt} = D\left(N_{in} - N\right) + \mu_i N_i - Z\frac{\iota_i}{V_i}, \quad i = p, c \qquad (5.3.1b)$$

$$\frac{dR}{dt} = D\left(R_{in} - R\right) - \sum_i \mu_i N_i q_{R,i} + Z\sum_i \left(\frac{\iota_i q_{R,i}}{V_i} - \mu_Z q_{R,Z}\right), \quad i = p, c \qquad (5.3.1c)$$

$$\frac{dS}{dt} = D\left(S_{in} - S\right) - \sum_i \mu_i N_i q_{S,i} + Z\sum_i \left(\frac{\iota_i q_{S,i}}{V_i} - \mu_Z q_{S,Z}\right), \quad i = p, c \qquad (5.3.1c)$$

Here, Z is the population density of zooplankton grazers, measured as biovolume (μm^3 / liter) to be compatible with observations from our monitoring program and to take advantage of volume-based parameterization (Hansen et al., 1997). Algal cell densities (cells / liter) are N_i, for *P. parvum* (p) and a cyanobacterial competitor (c). Inorganic nutrient concentrations (µmol / liter) are R for phosphorus and S for nitrogen. Many of the functions and parameters follow the assumptions and notation of Grover et al. (2010): Algal growth (μ_i, day^{-1}) on each nutrient follows a Monod function whose maximal growth rate μ_{max} depends on light, temperature and salinity for *P. parvum*, and on light and temperature for cyanobacteria. Liebig's law of the minimum is applied to the potential phosphorus- and nitrogen-limited growth rates of algae. Algal stoichiometry is assumed to be fixed, and quotas $q_{R,i}$ and $q_{S,i}$ (µmol / cell) are used instead of yield coefficients. Algal mortality is assumed to consist only of hydraulic flushing and zooplankton grazing (sinking is neglected for these types of algae, as in Grover et al. 2010). Algal cell volumes (V_i, μm^3 / cell) are new parameters required to formulate grazer dynamics in biovolume terms. All constituents are delivered in the inflow, with the parameters Z_{in}, R_{in} and S_{in} being the inflow concentrations for zooplankton biovolume, phosphorus and nitrogen, respectively. For simplicity, the same inflow concentration N_{in} is assumed for both algal species. For zooplankton and algae, these inflows serve to stabilize the populations against extinction, and are set to small values that do not appreciably affect dynamics when the population is far from extinction.

The volume-specific zooplankton ingestion rate on algal species i is assumed to be a type III functional response in relation to algal biovolume whose maximal rate depends on temperature (T, °C):

$$\iota_i(N_p, N_c; T) = \frac{\iota_{\max}(T) w_i V_i^2 N_i^2}{K_Z^2 + \sum_j w_j V_j^2 N_j^2} \qquad (5.3.2)$$

where K_Z is the half-saturation constant for zooplankton ingestion. The parameters w_i are dimensionless preference coefficients, with a value of 1 indicating an ideal, preferred food and values between 0 and 1 indicating less preferred foods. The maximal ingestion rate $\iota_{\max}$ increases with temperature according to

$$\iota_{\max}(T) = \iota_{\max}(20) Q_{10}^{\left(\frac{T-20}{10}\right)} \qquad (5.3.3)$$

where $\iota_{\max}(20)$ is the maximal ingestion rate at 20°C and Q_{10} is the factor by which this rate increases for a temperature increase of 10°C.

The ingestion rate (eq. 5.3.3) of algal species i is computed with dimensions of (volume algae) (volume zooplankton · time)$^{-1}$. Accordingly, the associated per capita mortality rate for algal species i is the product of zooplankton density Z and ingestion rate, divided by algal volume density ($V_i N_i$):

$$\text{algal per capita mortality rate} = Z \frac{\iota_i}{V_i N_i}$$

Multiplication by N_i to calculate the population mortality rate leads to the loss terms in eq. (5.3.1b).

Zooplankton population growth can be limited by the ingestion of algal food volume (a proxy for algal carbon), or by nitrogen or phosphorus. Therefore, three potential growth rates are calculated, and Liebig's law of the minimum is applied to select the realized growth rate. The volume-limited growth rate assumes an assimilation efficiency of e_Z for volume (carbon):

$$\mu_Z^C = e_Z \sum_i \iota_i \qquad (5.3.4)$$

The phosphorus- and nitrogen-limited growth rates are calculated assuming for simplicity that all of these nutrients in the ingested algae is assimilated:

$$\mu_Z^R = \frac{1}{Q_R} \sum_i \frac{\iota_i q_{R,i}}{V_i} \quad \text{and} \quad \mu_Z^S = \frac{1}{Q_S} \sum_i \frac{\iota_i q_{S,i}}{V_i} \qquad (5.3.4a, b)$$

where Q_R and Q_S are the phosphorus and nitrogen quotas per unit zooplankton biovolume (μmol / μm^3). Finally, the realized zooplankton growth rate is calculated as

$$\mu_Z = \min\{\mu_Z^C, \mu_Z^N \mu_Z^P\} \qquad (5.3.5)$$

Regeneration of inorganic phosphorus and nitrogen associated with zooplankton grazing is calculated by mass balance, assumed release to dissolved form of all nutrient not used for zooplankton growth. Per unit zooplankton biovolume, the recycling rates are

$$\sum_i \frac{\iota_i q_{R,i}}{V_i} - \mu_Z Q_R \quad \text{and} \quad \sum_i \frac{\iota_i q_{S,i}}{V_i} - \mu_Z Q_S \qquad (5.3.6a, b)$$

When zooplankton growth is carbon-limited, both inorganic nutrients are recycled; when zooplankton growth is nitrogen-limited, only phosphorus is recycled; and when zooplankton growth is phosphorus-limited, only nitrogen is recycled.

Zooplankton mortality is assumed to be temperature-dependent, in a manner similar to maximal ingestion rate:

$$m_Z(T) = m_Z(20) Q_{10}^{\left(\frac{T-20}{10}\right)} \qquad (5.3.7)$$

To accommodate the possible allelopathic effects of cyanotoxins on *P. parvum*, following Grover et al. (2010), cyanotoxin dynamics are governed by

$$\frac{dC}{dt} = \mu_C N_C \varepsilon_C - k_C C \qquad (5.3.8)$$

where C is cyanotoxin concentration (μg / liter), ε_C is a toxin production coefficient (μg / cell), and k_C is a first-order degradation constant (day^{-1}). The cyanotoxin is assumed to inhibit the growth rate of *P. parvum*. The nutrient-dependent growth rate of this species is multiplied by a factor

$$\frac{K_C^\xi}{K_C^\xi + C^\xi}$$

where K_C is a parameter specifying the cyanotoxin concentration inhibiting growth by 50%, and the exponent ξ controls the nonlinearity of the inhibition response.

Dynamics of toxins produced by *P. parvum* were modeled assuming that production is proportional to the degree that growth is below optimal, and that degradation is first order:

$$\frac{dP}{dt} = \left(\mu_p^{\text{opt}} - \mu_p\right) N_p \varepsilon_P - k_P P \qquad (5.3.8)$$

where μ_p^{opt} is the growth rate of *P. parvum* under optimal conditions (saturating nutrients, favorable temperature, salinity and light), e_P is a production coefficient for *P. parvum* toxins, and k_P is a first-order degradation constant. It is assumed that *P. parvum* toxins reduce the ingestion and growth rates of zooplankton. Specifically, the ingestion rate of *P. parvum* is multiplied by the factor

$$\frac{K_P^\eta}{K_P^\eta + P^\eta}$$

where K_P is a parameter specifying the cyanotoxin concentration inhibiting growth by 50%, and the exponent η controls the nonlinearity of the inhibition response.

In general, all parameters carried over from the suite of models in Grover et a. (2010) were assigned the default (uncalibrated) values from that paper. The modified models are formulated in terms of quotas rather than yield coefficients, and the initial quota values were taken are reciprocals of the previous yields. In the JAWRA paper, models with cyanotoxin assumed a value of 1.0 for the exponent ξ governing inhibition of *P. parvum* growth, so that is the initial value here.

Values for new parameters introduced here were assigned assuming that rotifers (or other small bodied zooplankton with similar physiology) are the predominant zooplankton group, and relying on the review by Hansen et al. (1997). Following this publication, the Q_{10} for zooplankton ingestion and mortality rates was 2.8. Trophic efficiency on a volume basis, e_Z, was set to 0.3. The half-saturation constant of the zooplankton functional response was set to 1.5×10^9 μm^3 / liter. Cell volumes for *P. parvum* and cyanobacteria (V_i) were set to 300 and 35 μm^3, respectively. The former is the approximate volume of *P. parvum* cells observed in cultures (J.P. Grover, personal observation), and the latter is the average cell volume of cyanobacteria observed in a study of Texas reservoirs (Grover and Chrzanowski, 2004). To derive the nutrient quotas per unit zooplankton volume, it was assumed that carbon content was 0.11 g C / cm^3 (Hansen et al., 1997). Data on stoichiometry of rotifers are rare, so values for small-bodied cladocera (also relatively common in Texas lakes) were used (Sterner and Elser 2002). Given the assumed carbon content, a C:P ratio of 150 and a N:P ratio of 20, the zooplankton quotas become $Q_R = 0.061 \times 10^{-9}$ μmol P / mm^3 and $Q_S = 1.2 \times 10^{-9}$ μmol N / mm^3.

Given very uncertain knowledge of the toxins produced by *P. parvum*, at best reasonable guesses can be made about parameters governing their dynamics. Assigning values of $\varepsilon_P = 1.0 \times 10^{-8}$ μg / cell and $k_P = 0.5$ day^{-1} predicts toxin concentrations on the order of μg / liter (Grover et al., 2010). Effects of *P. parvum* toxins on zooplankton ingestion and growth have frequently been observed (Brooks et al., 2010), so setting the parameter K_P to 0.5 μg / liter will make such effects likely in the model. However, such toxic effects

are not ubiquitous, suggesting possible nonlinearity in the response of zooplankton, so the initial value for the exponent η was 2.0.

The zooplankton mortality rate at 20°C was initially set to an arbitrary low value, 0.05 day^{-1}, to ensure that zooplankton would grow to levels affecting algal dynamics. The default value for the inflowing algal concentration (N_{in}) was set to 100 cells / ml. For *P. parvum*, the biovolume equivalent is 30×10^6 mm^3 / liter. The inflowing zooplankton concentration (Z_{in}) was set to $1/30^{th}$ of this value, 1.0×10^6 mm^3 / liter.

5.3.2 Initial results

With the initially assigned parameters, the model was run using one year of limnological observations from Lake Granbury as input data (Grover et al. 2010) until the predicted dynamics stabilized to an annual cycle. In this model, both cyanobacteria and *P. parvum* produce toxins. The cyanotoxins are allelopathic and reduce the growth rate of *P. parvum*; the *P. parvum* toxins inhibit the ingestion and growth rates of zooplankton. Dominance of cyanobacteria is predicted, with no blooms of *P. parvum* (Fig. 5.3.1). Cyanotoxin concentrations are predicted to be much higher than those of *P. parvum* toxins. Accordingly, allelopathic effects on *P. parvum* are predicted to be strong, but the inhibition of grazers by *P. parvum* toxins is predicted to be weak.

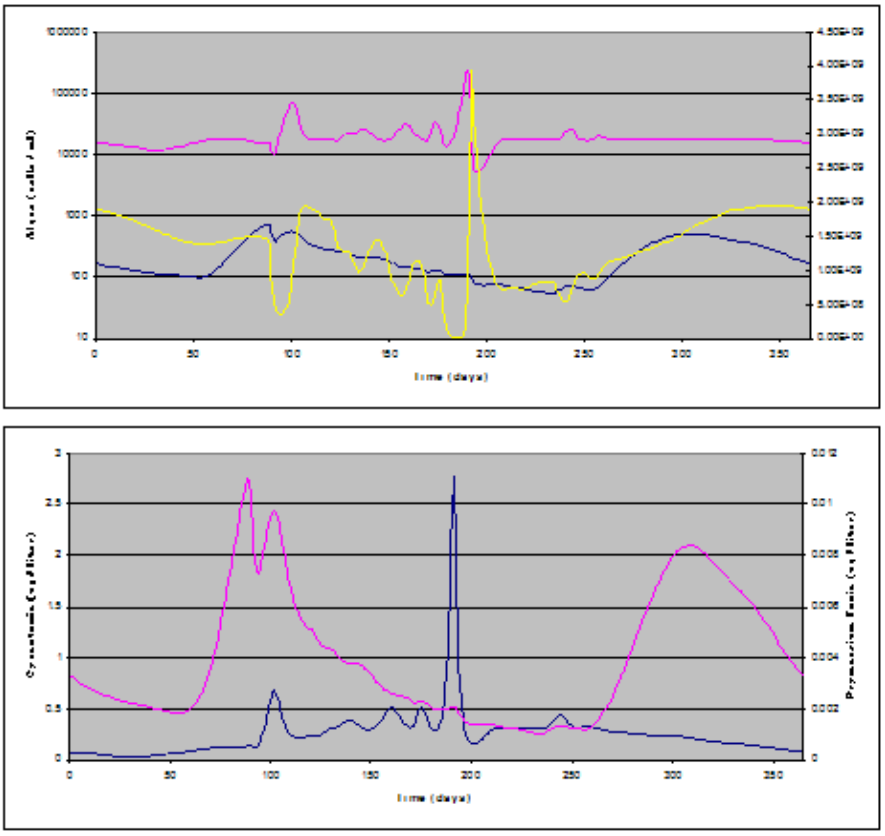

Figure 5.3.1

5.3.3 Sensitivity analysis and calibration

All model parameters were varied through 50 values, in a range 0.3× to 3× the initial value, excluding those parameters defining the maximal growth rates of algae and their responses to temperature. Because these parts of the models are based on extensive ecophysiological measurements, they were taken as better supported than values of other parameters, which are not as extensively measured or which have larger inherent variability. For each parameter value, 5 years of dynamics were simulated and errors in the predicted dynamics for the last year were evaluated with 6 metrics. The first metric (M_1) measured the relative error in the predicted maximum density of *P. parvum*:

$$M_1 = \left| \frac{\max N_p - \max \hat{N}_p}{\max \hat{N}_p} \right|$$

where N_p is the observed population density of *P. parvum* and $\hat{N}_p$ is the population density predicted by the model. The second metric measured relative error in the predicted minimum density of *P. parvum*:

$$M_2 = \left| \frac{\min N_p - \min \hat{N}_p}{\min \hat{N}_p} \right|$$

The third metric measured relative error in the predicted average of the natural log of density of *P. parvum* during winter (the first three months of the year):

$$M_3 = \left| \frac{\left\langle \ln N_p \right\rangle_{1-3} - \left\langle \ln \hat{N}_p \right\rangle_{1-3}}{\left\langle \ln \hat{N}_p \right\rangle_{1-3}} \right|$$

where the notation $\langle\ \rangle_{1-3}$ indicates time average for the first three months. The fourth metric measured relative error in the predicted average of the natural log of density of *P. parvum* during spring (the second three months of the year):

$$M_4 = \left| \frac{\left\langle \ln N_p \right\rangle_{4-6} - \left\langle \ln \hat{N}_p \right\rangle_{4-6}}{\left\langle \ln \hat{N}_p \right\rangle_{4-6}} \right|$$

where the notation $\langle\ \rangle_{4-6}$ indicates time average for the second three months. The fifth metric measured relative error in the predicted average of the natural log of density of *P. parvum* during summer (the third three months of the year):

$$M_5 = \left| \frac{\left\langle \ln N_p \right\rangle_{7-9} - \left\langle \ln \hat{N}_p \right\rangle_{7-9}}{\left\langle \ln \hat{N}_p \right\rangle_{7-9}} \right|$$

where the notation $\langle\ \rangle_{7-9}$ indicates time average for the third three months. The sixth metric measured relative error in the predicted average of the natural log of density of *P. parvum* during autumn (the fourth three months of the year):

$$M_6 = \left| \frac{\left\langle \ln N_p \right\rangle_{10-12} - \left\langle \ln \hat{N}_p \right\rangle_{10-12}}{\left\langle \ln \hat{N}_p \right\rangle_{10-12}} \right|$$

where the notation $\langle\ \rangle_{10-12}$ indicates time average for the fourth three months.

All six metrics were plotted against the 50 tested values for each parameter. Parameters were screened to identify those with large effects on error metrics, and for which changes might reduce error. Parameter adjustments were then made based on considerations described below for each model. At each step of this calibration, the sensitivity analysis was redone and further parameter adjustments made until it was judged that further improvement could not be achieved.

For the initially assigned parameters, values of these error metrics were:

Metric	Value
M_1	5282%
M_2	163%
M_3	96%
M_4	18%
M_5	34%
M_6	38%

The large errors reflect the substantial under-prediction of *P. parvum* density made by the uncalibrated model. These errors result in part from a substantial over-prediction of zooplankton biomass (about 10×). The sensitivity analysis suggested that several parameters describing the zooplankton-algae interaction could be adjusted to reduce errors, with the largest reductions coming from raising the half-saturation constant for zooplankton ingestion K_Z from 1.5×10^9 μm^3 / liter to 4.5×10^9 μm^3 / liter, the highest value tested.

The large errors reflect the substantial under-prediction of *P. parvum* density made by the uncalibrated model. These errors result in part from a substantial over-prediction of zooplankton biomass (about 10×). The sensitivity analysis suggested that several parameters describing the zooplankton-algae interaction could be adjusted to reduce errors (Fig. 5.3.2), with the largest reductions coming from raising the half-saturation

constant for zooplankton ingestion K_Z from 1.5 × 10^9 μm^3 / liter to 4.5 × 10^9 μm^3 / liter, the highest value tested.

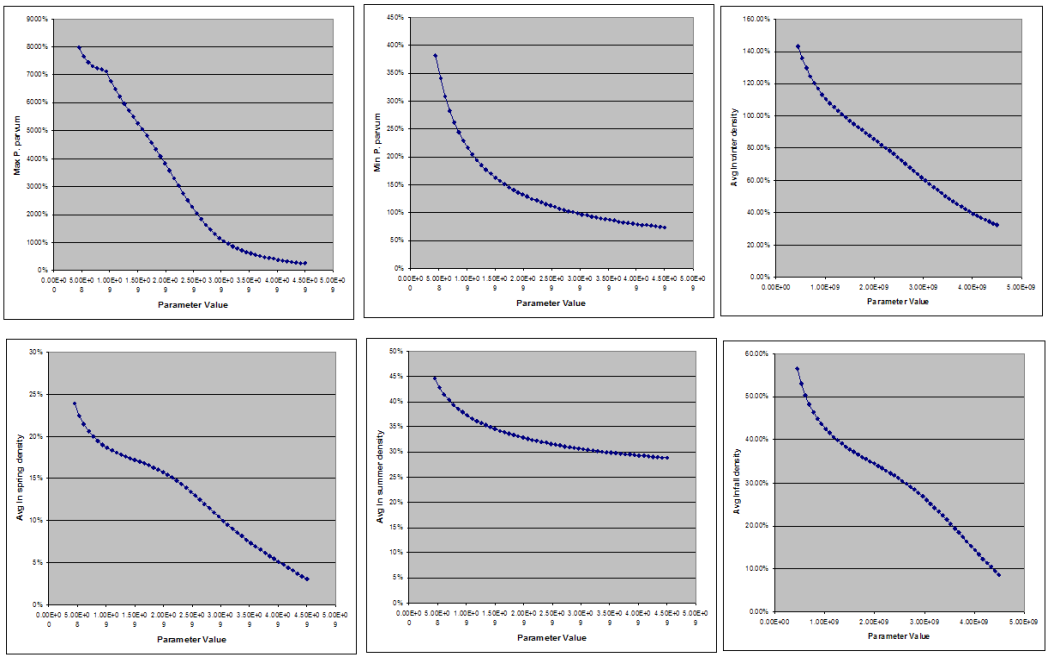

Figure 5.3.2

Based on this result, the first calibration adjustment was to raise K_Z to 4.5 × 10^9 μm^3 / liter, which is plausible because it is within the range of 1.3 – 20.5 × 10^9 μm^3 / liter documented by Hansen et al. (1997). This change altered the error metrics as follows:

Metric	Value
M_1	245%
M_2	74%
M_3	32%
M_4	4%
M_5	29%
M_6	8%

The population density of *P. parvum* is under-predicted, especially through the winter. Spring and fall densities are fairly well predicted. Zooplankton biovolume is again over-predicted substantially (about 6×). Some aspects of the dynamics are intriguing. A summer minimum of *P. parvum* results from the combination of high zooplankton and high cyanobacteria, leading to high grazing, resource competition and allelopathy affecting *P. parvum*. Relatively high density of *P. parvum* in autumn, winter, and spring results from reduced zooplankton and cyanobacteria densities, with reduced grazing and competition for *P. parvum*. This is caused by the lower growth rates of zooplankton and

cyanobacteria at low temperature, and by the production of toxin by *P. parvum* during cooler weather which further reduces grazing.

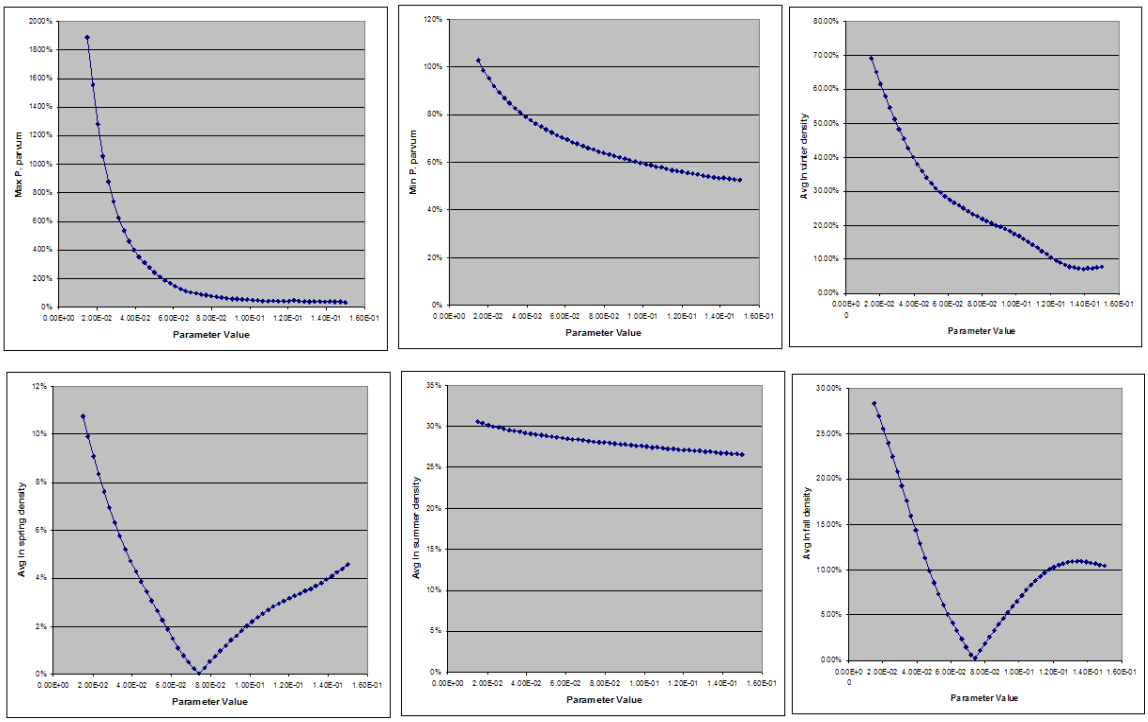

Figure 5.3.3

After adjusting K_Z to 4.5×10^9 μm^3 / liter, sensitivity analysis showed that errors in predicted *P. parvum* density were still highly sensitive to other parameters describing the zooplankton algae interaction (Fig. 5.3.3). Further calibration focused on metrics M_1 and M_3 measuring errors in maximum population density and population during winter, because these predictions are critical to managing blooms of *P. parvum* in Texas. Changing several parameters would reduce both error metrics, but most of these would lead to values regarded as biologically unlikely. Raising zooplankton mortality to 0.14 d^{-1} minimized M_3 and reduced M_1, and is a plausible value for this parameter. This change would also likely reduce the over-prediction of zooplankton biovolume.

Making this change produced these error metrics:

Metric	Value
M_1	40%
M_2	53%
M_3	7%
M_4	3%
M_5	27%
M_6	11%

Zooplankton abundance was still over-predicted (3× on average). Under-prediction of *P. parvum* density in summer and over-prediction in autumn remain deficiencies of the model. At this stage, the next priority was to reduce the error in predicting maximum abundance (metric M_1) from 40% while keeping other errors below 15% (metrics M_3, M_4, M_6). Several parameter changes accomplished these goals, so changes were also screened for their ability to reduce errors in predicting minimum and average summer abundance (metrics M_2 and M_5).

Parameter	Change	M_1	Reduced M_2 and M_5?
N_{in}	1000 → 1800	2%	Yes (large decrease)
K_{Rp}	0.009 → 0.008	21%	No
q_{Rp}	$1.39 \times 10^{-9} \rightarrow 0.42 \times 10^{-9}$	15%	No
q_{Sp}	$32 \times 10^{-9} \rightarrow 20 \times 10^{-9}$	0%	No
V_p	300 → 835	0%	No
w_p	0.5 → 0.366	7%	No
K_{Rc}	0.166 → 0.184	15%	No
Q_{Rc}	$2.86 \times 10^{-9} \rightarrow 7.03 \times 10^{-9}$	4%	No
Q_{Sc}	$32 \times 10^{-9} \rightarrow 27.3 \times 10^{-9}$	9%	No
V_c	35 → 37	25%	No
w_c	0.49 → 0.967	0%	No
$m_Z(20)$	0.14 → 0.239	4%	No
Q_{10}	2.8 → 3.41	13%	No
e_Z	0.3 → 0.349	0%	No
$\iota_{\max}(20)$	2.4 → 1.76	0%	No
K_Z	$4.5 \times 10^{9} \rightarrow 5.97 \times 10^{9}$	3%	Yes (moderate decrease)
Q_R	$6.1 \times 10^{-11} \rightarrow 5.5 \times 10^{-11}$	27%	No
Q_S	$1.2 \times 10^{-9} \rightarrow 1.4 \times 10^{-9}$	21%	No
ε_C	$1.25 \times 10^{-8} \rightarrow 1.05 \times 10^{-8}$	13%	No
k_C	0.5 → 0.582	14%	Yes (small decrease)
K_C^I	0.1 → 0.116	12%	Yes (small decrease)
ξ	1.0 → 3.0	21%	No
ε_P	$1.0 \times 10^{-8} \rightarrow 1.22 \times 10^{-8}$	9%	No
k_P	0.5 → 0.393	1%	No
K_P^I	0.5 → 0.393	24%	No
η	2.0 → 0.6	11%	No

Some changes that completely eliminated error in predicted maximum abundance were rejected because they offered no improvement in predicted minimum or average summer abundances, or because they were biologically implausible. Two changes that reduced error in predicted maximum abundance to ≤ 3% also improved predictions of minimum abundance and average summer density. The largest improvement came from increasing the inflowing concentration of algae to 1800 cells / ml. This adjustment was rejected because N_{in} is a nuisance parameter introduced to prevent competitive exclusion rather than a fundamental biophysical parameter based on first principles or experimental

observation. The goal of this model calibration was to see whether biological plausible parameters would enable prediction, so instead further adjustment of the half-saturation constant for zooplankton grazing (K_Z) was made, increasing it to 5.97×10^9 μm^3 / liter.

Making this change produced these error metrics:

Metric	Value
M_1	3%
M_2	47%
M_3	4%
M_4	6%
M_5	25%
M_6	8%

Zooplankton abundance was still over-predicted (3× on average). Although the maximum and average winter densities are reasonably well predicted (Fig. 5.3.4), timing of the bloom's rise and peak are not perfectly represented. Under-prediction of *P. parvum* density in summer and over-prediction in autumn remain deficiencies of the model. A first peak is predicted in autumn, followed by a decline then a higher peak in late winter about six weeks after the observed peak.

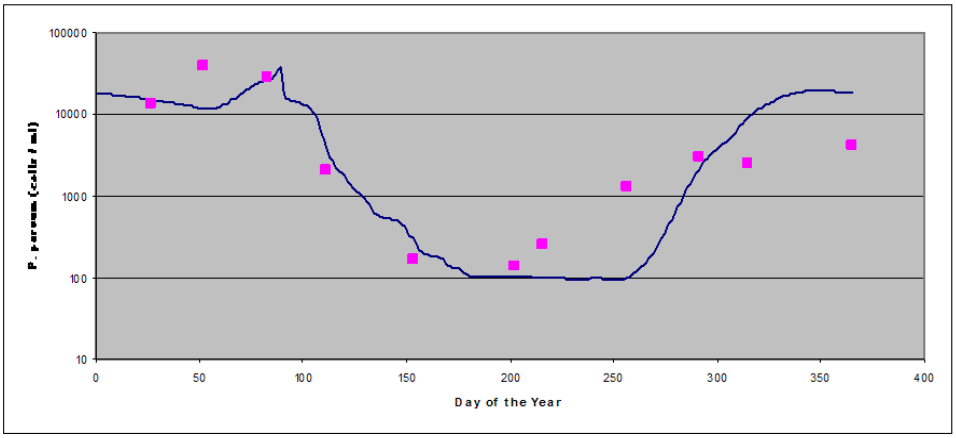

Figure 5.3.4

At this stage, the model better simulates *P. parvum* dynamics using the calibration data than any model our group has developed. For this reason we conducted an initial validation experiment. At the time of this experiment, *P. parvum* observations and necessary input data are available from observations on Lake Granbury from the end of the calibration data set in August 2007 to August 2009, a time period when large blooms did not occur, although a modest bloom peaked at a little over 10^4 cells / ml in the winter of 2008-2009. The data available for this validation exercise did not include the larger bloom that occurred in the winter of 2009-2010. The model did not succeed in predicting *P. parvum* dynamics over the two-year period of observations beyond the calibration

period (Fig. 5.3.5). It predicted a modest bloom of 10,000 – 15,000 cells / ml in the winter of 2007-2008, when observed population were < 5,000 cells / ml. The model failed to predict the bloom of about 10,000 cells / ml in the winter of 2008-2009, and instead predicted only a small increase from a summer minimum. Finally the model predicted that a very large bloom would occur in late summer to autumn of 2009, which did not occur.

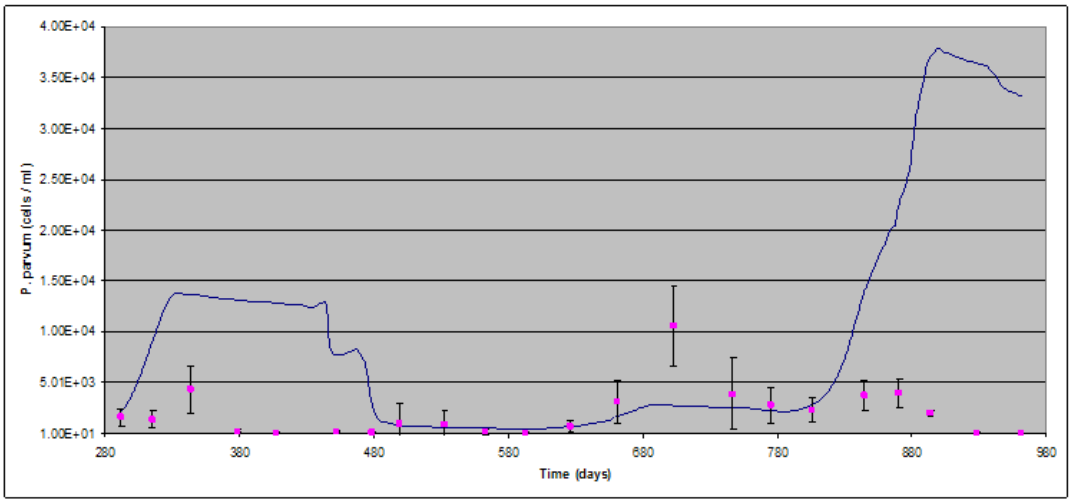

Figure 5.3.5

5.4 Building *P. parvum* mixotrophy effects into numerical model from laboratory experiments

5.4.1 Laboratory Experiments

Prymnesium parvum grows phototrophically in defined mineral media supplemented with small amounts of vitamins (Baker et al. 2007), though it also obtains nutrients through consumption of bacteria (Nygaard & Tobiesen 1993) and eukaryotic microorganisms (Tillman 2003). To date, studies of mixotrophy in *P. parvum* document short-term consumption, while the long-term consequences for population dynamics remain uncertain. The culture experiments reported here focused on mixotrophic consumption of bacteria under phosphorus-limitation in the presence of adequate light for photosynthesis. Cultures received varying amounts of glucose. Given that bacteria are likely to be better competitors for limiting phosphorus than *P. parvum*, three distinct outcomes are theoretically possible depending on the contribution of mixotrophic nutrition to population dynamics of the flagellate. If the contribution of mixotrophy negligible, then *P. parvum* should decline and even be excluded through competition with bacteria. If *P. parvum* is primarily a heterotrophic predator of bacteria, then its density should increase with enrichment of its prey (Pengerud et al. 1987). Finally, mixotrophy could be a nutritional supplement enabling *P. parvum* to persist but not necessarily to thrive under nutrient-limited, competitive conditions (Nygaard & Tobiesen 1993).

Stock cultures of *P. parvum* (strain UTEX LB ZZ181) were grown in artificial sea water diluted to 5.8 psu salinity and enriched with nitrate, phosphate, trace metals, and vitamins (Baker et al. 2007). Stock cultures were maintained at 20 °C and on a 12:12 photoperiod with photon flux of about 150 µmol m^{-2} s^{-1}. Stock cultures were not axenic and these incidental contaminants served to inoculate experimental cultures with bacterial populations. The experiment exposed *P. parvum* to organic carbon (glucose) in the presence of these bacteria, and phosphorus was reduced to 0.5 µM to facilitate competition for this nutrient. The basal salts concentration was reduced to a salinity of 4 psu, and glucose was supplied at 0, 50, 100 and 250 µM, producing molar C:P supply ratios of 0, 100, 200, and 500. At each C:P supply ratio, triplicate cultures of 240 ml working volume were grown in 500 ml conical flasks under the same illumination and temperature as stock cultures. Experimental cultures were inoculated with *P. parvum* populations of 10^4 cells/ml and bacterial populations of 10^5 cells/ml, and were diluted every other day for 30 d with 100 ml of sterile medium to produce an average dilution rate of 0.27 d^{-1}. Samples of populations were taken every 4 d until day 24 and every 2 d thereafter. *P. parvum* and bacteria were preserved with Lugol's solution and formalin, respectively. To enumerate *P. parvum*, aliquots of 5 or 10 ml were sedimented and counted with an inverted microscope (Utermöhl 1958). To enumerate bacteria, aliquots of 200 µl were stained with acridine orange and filtered onto black polycarbonate filters for epifluorescence microscopy (Hobbie et al. 1977).

In cultures receiving no glucose, *P. parvum* increased to population densities of about 5×10^4 cells/ml by day 12 (Fig. 5.4.1A), while in cultures receiving glucose, *P. parvum* either remained at about 10^4 cells/ml throughout the experiment (C:P supply ratios of 100 and 200), or declined to about 5000 cells/ml (C:P supply ratio of 500). Although cultures might not have reached a steady state, differences in relation to C:P supply ratios were evident by about day 20. For statistical analysis, we averaged data for each culture over days 24 – 30 (Table 5.4.1). The null hypothesis of no difference in mean *P. parvum* density in relation to C:P supply ratio was rejected (ANOVA, $F_{3,8} = 52.7$, $p < 0.001$), and cultures with no glucose had significantly higher density than others (Tukey's HSD, $p < 0.05$). For cultures receiving glucose, mean *P. parvum* density did differ significantly in relation to C:P supply ratio.

Table 5.4.1. Average data over days 24-30, showing mean and standard deviation for three replicate cultures.

C:P Supply Ratio	Total *P. parvum* (10^3 cells / ml)	Bacteria (10^6 cells / ml)	Proportion *P. parvum* in swarms	Mean size of swarms (cells)
0	55 ± 9.5	0.95 ± 0.12	0	0
100	9.9 ± 3.7	1.4 ± 0.055	0.89 ± 0.12	5.0 ± 1.0
200	12 ± 2.8	1.2 ± 0.066	0.86 ± 0.09	4.7 ± 0.90
500	4.9 ± 3.0	0.93 ± 0.2	0.70 ± 0.03	4.1 ± 0.26

Bacteria increased to population densities of about 10^6 cells/ml in all cultures by day 12 (Fig. 5.4.1B). For data averaged over days 24 – 30, the null hypothesis of no difference in mean bacterial density in relation to C:P supply ratio was rejected (ANOVA, $F_{3,8} =$

12.1, p = 0.002), and cultures with a C:P supply ratio of 100 had significantly higher density than those with C:P supply ratios of 0 or 500 (Tukey's HSD, p < 0.05).

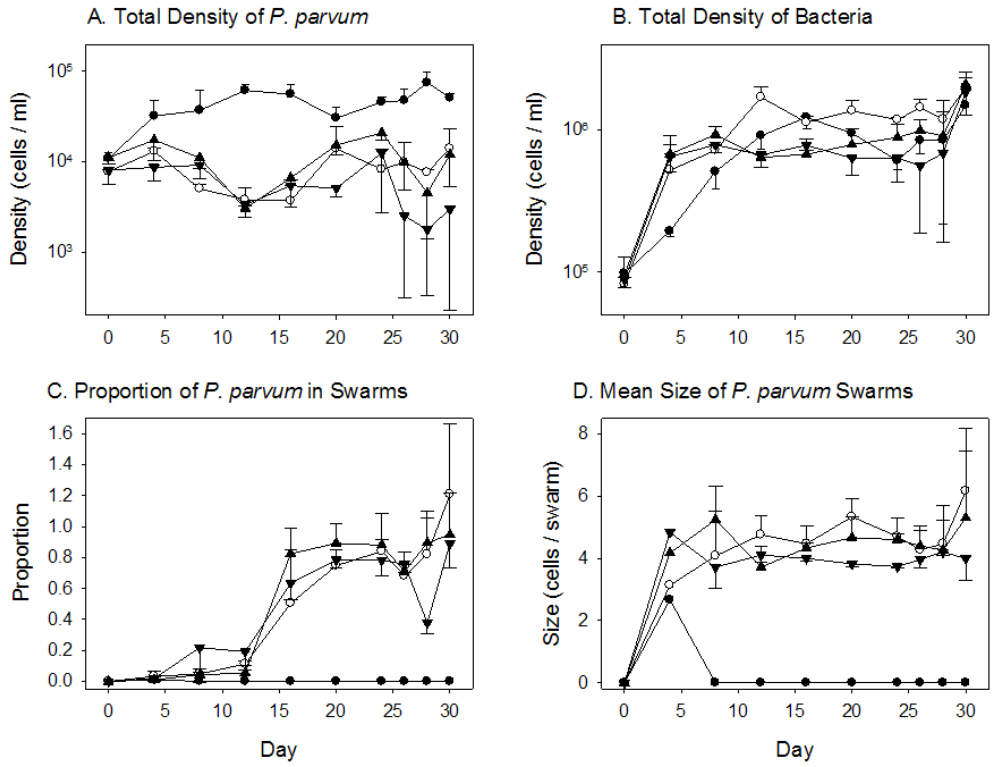

Figure 5.4.1. Time series of population densities and characteristics of multicellular swarms. Symbols show means of three replicate cultures, with error bars showing standard deviations (except for day 4 in panel D, for which variances were exceptionally large): ● – C:P = 0; ○ – C:P = 100; ▲ – C:P = 200; ▼ – C:P = 500.

During the course of the experiment, multicellular aggregations ("swarms") of *P. parvum* were noticed, resembling the aggregations of individuals feeding heterotrophically that were observed by Tillman (2003). In microscope enumerations, we counted the total number of *P. parvum* individuals (in swarms or unicellular) and the number of multicellular swarms. We also counted the number of individuals per swarm for ten randomly selected swarms per sample. From these data, the proportion of the *P. parvum* population in swarms was calculated (Fig. 5.4.1C). By day 20, 60-100% of the total *P. parvum* population occurred in swarms, but only in cultures receiving glucose. For cultures receiving no glucose, swarms were not observed after day 4. The number of *P. parvum* cells per swarm ranged 2 – 23, but the average swarm size was close to 4 for all cultures in which swarms occurred (Fig. 5.4.1D, Table 5.4.1). *P. parvum* achieved high population densities in cultures with no glucose, where it grew phototrophically. In cultures receiving glucose, *P. parvum* persisted, but at densities 80-90% lower than populations growing phototrophically. In these cultures, most cells of *P. parvum* were in multicellular aggregations interpreted as feeding swarms. Such swarms have been

observed when *P. parvum* preys on large eukaryotic microorganisms (Tillman 2003). Cells of *P. parvum* aggregate around the prey and induce lysis, remaining aggregated while ingesting the materials thus released. *P. parvum* also ingests smaller-celled prey whole, such as nanoplanktonic diatoms and bacteria (Martin-Cereceda et al. 2003). We suggest that swarming, prey consumption, and possibly the production of lytic toxins constitute a syndrome of phenotypes induced by circumstances under which mixotrophy is advantageous.

Under this interpretation, mixotrophy by *P. parvum* enables population persistence under stressful conditions, such as nutrient depletion (Nygaard & Tobiesen 1993). In these experiments, providing glucose under conditions of low phosphorus supply was intended to produce competition for the latter nutrient. In similar experiments with purely phototrophic algae, C:P supply ratios of 100 – 300 have been sufficient to produce exclusion of algae by competitively superior bacteria (Pengerud et al. 1987; Grover 2000; Codeço & Grover 2001). Thus *P. parvum* benefited sufficiently from mixotrophy to persist under conditions where pure phototrophy is not a viable strategy. In similar experiments with purely heterotrophic flagellates, increasing C:P supply ratios through the same range enhances flagellate population density (Pengerud et al. 1987). Thus *P. parvum* did not benefit sufficiently from mixotrophy to thrive under conditions where pure heterotrophy is a favorable strategy. Under the conditions of this experiment, mixotrophy by *P. parvum* contributed to population persistence, but did not permit populations to thrive. Under other conditions, the benefits of mixotrophy to *P. parvum* could be larger. Bacteria were the only prey available to *P. parvum* in this experiment, but *P. parvum* can also attack larger eukaryotic microorganisms (Tillman 2003). In natural habitats with diverse microbial communities, predation on larger microorganisms might provide greater benefits to mixotrophic populations of *P. parvum* (Skovgaard et al. 2003).

5.4.2 Modeling

Using laboratory cultures, Baker et al. (2007, 2009) determined that *P. parvum* displays rapid growth at relatively warm temperatures. This property was incorporated into mathematical models for *P. parvum* growth in Texas (Grover et. al 2010). These models were based on conventional approaches for modeling in water quality studies (Chapra 1997), and designed to predict algal dynamics given input data on commonly measured limnological conditions. The models included up to five algal populations with two limiting resources, and allelopathic effects. However, the models all assumed that *P. parvum* grows strictly as an autotroph. None of the models provided satisfying predictions of *P. parvum* dynamics when using input data from a Texas reservoir, since all of them predicted a winter decline precisely at the time when annual maxima were observed.

The existing models treat a lake as a chemostat, whose dilution rate is estimated from hydrological data. Limiting resources are nitrogen and phosphorus, whose supply is estimated from observations of total nitrogen and phosphorus. Growth rates depend on temperature, light and salinity, while grazing mortality is estimated from observations of

zooplankton abundance. One model represents only the population of *P. parvum*, while others represent one or four competing populations of other algae. The model that represents only the population of *P. parvum* was designated PP0. Observational data from Lake Granbury were collected from 10 stations arranged along the length of the lake, and were spatially averaged to obtain input data and observations of *P. parvum* dynamics for evaluating model predictions.

Based on laboratory experiments indicating that mixotrophy provides a nutritional supplement to the reproductive growth of *P. parvum*, we construct a model which adds mixotrophy to a much simplified version of the PP0 model. Mixotrophy was treated as an additive effect to the autotrophic growth previously modeled for *P. parvum*. This likely gives the *P. parvum* population more of an advantage than would be expected in a natural system, where diminishing returns to mixotrophic nutrition might be expected, but we attempted to determine whether adding mixotrophy to the prior model would produce results more accurately predicting observed population dynamics, rather than trying to create a perfectly accurate and general model. The model developed here only examines one limiting resource, here taken to be phosphorus, since Lake Granbury has a fairly high N:P ratio (Grover et al. 2010, Roelke et al. 2010) In order to allow for mixotrophy, the model includes in a simple way, a dynamic population of bacteria as a prey species for *P. parvum*.

The modeling exercise presented here attempts to ascertain whether incorporating mixotrophy can correct the principal flaw of previous models – their tendency to predict a winter decline of *P. parvum* when instead a maximum is observed. To do this, several features of the model are designed to give *P. parvum* a strong contribution of mixotrophy to population growth, especially in winter. The parameters describing ingestion of bacterial prey are set to values that are high compared to some published observations, and ingestion is assumed to be up-regulated in response to low P availability and low light. The goal was to determine first whether mixotrophy could boost the predicted winter growth of *P. parvum*, giving it every possibility to do so, and then if so, to evaluate whether the resulting model was plausible in other aspects.

The model consists of three ordinary differential equations. Notation is summarized in Table 5.4.2. The model tracks the densities of *P. parvum* and their edible bacterial prey along with the concentration of a limiting inorganic resource here taken to be phosphorus.

$$\frac{dN}{dt} = D(N_{in} - N) + \mu N - mN \tag{5.4.1}$$

$$\mu = \frac{\mu_{max} R}{K_R + R} + \frac{\iota_{max} B}{(K_B + B) Y_{RB}} e Y_{RP} \tag{5.4.2}$$

The change in density of *P. parvum* (N_P, cells / liter) through time has three terms (Eq. 5.4.1). The first term is a standard chemostat supply term with dilution (D) times the difference between an inflow of *P. parvum* cells (N_{in}) and the current *P. parvum* density. This term allows for immigration of *P. parvum* in the inflow, though we have primarily

analyzed cases where such immigration does not occur ($N_{in} = 0$). Setting N_{in} to a low value prevents transient extinction of *P. parvum* in cases where seasonal variations are large, but such extinction did not generally occur for the conditions examined here. The second term in Eq. 5.4.1 is the change in density due to growth. The P-limited growth rate of *P. parvum* (Eq. 5.4.2) is the sum of rates based on two sources of P. One source is uptake of dissolved P (at concentration *R*, µmol / liter) and the other is ingestion of bacterial prey (at density *B*, cells / liter). Growth in relation to dissolved P is a Monod function with μ_{max} being the maximal growth rate and K_R the half-saturation constant. The growth rate based on ingestion of bacteria is also a Monod function with ι_{max} as the maximal ingestion rate of bacterial cells per day per *P. parvum* and K_B the half-saturation constant for the bacteria. Dividing this ingestion function by the yield for bacteria (Y_{RB}) gives us the amount of P obtained per bacterial cell ingested. This is then multiplied by the yield of *P. parvum* cells per amount of P (Y_{RP}) and an efficiency (*e*) that is the proportion of P from ingested bacteria that is converted into *P. parvum*. The final term in Eq. 5.4.1 is the loss due to mortality at a per capita rate *m*.

$$\frac{dB}{dt} = a(B_{max} - B) - N_P \frac{\iota_{max} B}{K_B + B} - DB \qquad (5.4.3)$$

The change in edible bacterial density (*B*) through time (Eq.5.4.3) also has three terms. The first term is like a standard chemostat supply term with *a* being a turnover, or growth rate of edible bacteria times the difference between a maximal bacterial density (B_{max}), similar to a carrying capacity, and the current density (*B*). This simple form was adopted to avoid complicated dynamics and possible numerical problems that could arise with a more realistic description of bacterial growth. The second and third terms are decreases due to ingestion from *P. parvum* and dilution.

$$\frac{dR}{dt} = D(R_{in} - R) - \frac{\mu_{max} R}{(K_R + R) Y_{RP}} N_P + \frac{r m_P N_P}{Y_{RP}} + N_P (1 - e) \frac{\iota_{max} B}{(K_B + B) Y_{RB}} \qquad (5.4.4)$$

The change in the concentration of P (Eq. 5.4.4) has four terms. The first is a standard chemostat supply term with the dilution rate (*D*) times the difference between supplied P (R_{in}) and current P (*R*). The next term is the loss due to the uptake of P and its conversion to cells during growth of *P. parvum*. The third term is the return of P due to the mortality of *P. parvum*. This term has a recycling efficiency (*r*) that determines the proportion of P that is returned to the dissolved state. The final term is the return to the dissolved state of the proportion of P from ingested bacteria that is not converted to *P. parvum*.

Table 4.2 Notation.

Symbol	Description	Value	Units
N	Density of *P. parvum*	variable	cells/liter
B	Density of edible bacteria	variable	cells/liter
R	Phosphate	variable	µmolP/liter
D	Dilution rate	input	/day
R_{in}	Phosphate supply	input	µmolP/liter
r	Recycling efficiency of *P. parvum*	input	dimensionless
B_{max}	Maximum density of edible bacteria	f(B_0(t))	cells/liter
a	Turnover rate of bacteria	f(T)	/day
μ_{max}	Maximum *P. parvum* growth rate	f(T,I,σ)	/day
μ	Growth rate of *P. parvum*	f(T,σ,I,R,S)	/day
ι_{max}	Maximum ingestion rate	f(T,σ,I,R,S)	bacteria cells /day/Prym. cell
K_R	Half-saturation constant for phosphorus	0.009	µmolP/liter
m	Mortality of *P. parvum*	0.1	/day
e	Conversion efficiency of *P. parvum*	0.5	dimensionless
N_{in}	Supply of *P. parvum*	0	cells/liter
Y_{RB}	Yield of bacteria from P	4.03×10^8	cells/µmolP
K_B	Half-saturation constant for ingestion of bacteria	5×10^8	cells/liter
Y_{RP}	Yield coefficient for P in *P. parvum*	7.2×10^8	cells/µmolP

Parameters with constant values are listed in Table 5.4.2 with their values. Several parameters are shared with a previously published model and were assigned the same values (Grover et al., 2010). Parameters listed with the word 'input' are read from an array of daily values for Lake Granbury (constructed from observations as described in Grover et al., 2010). Other quantities in Table 5.4.2 are functions, which in turn depend on input and on additional parameters.

The first of these functions is the maximum density of edible bacteria (B_{max}). This was taken as an input parameter based on total bacterial densities observed during the sampling events described in Grover et al. (2010). To obtain values for every day of the year, linear interpolation was used between sampling dates over one year. It was then assumed arbitrarily that since possibly not all bacteria are edible to *P. parvum*, $B_{\max}$ would be ½ of the observed, interpolated total density. The turnover rate of bacteria (a) was assumed to be equal to the empirical temperature-dependent population growth rate found in other Texas reservoirs (Chrzanowski and Grover, 2001), given by the expression $\max(0, 0.032T - 0.1611)$. The maximal *P. parvum* growth rate based on P

(Eq. 5.4.5) is taken directly from the previous models (Grover et al., 2010, based on Baker et al. 2009). It is a function of temperature (T), light (I), and salinity (σ).

$$\mu_{\max}(\sigma,I,T) = \max\left\{0, \beta_0 + \beta_1(\sigma-\sigma_{\text{ref}}) + \beta_2 e^{\left[0.7\left(\frac{T-T_{\text{ref}}}{T_{\text{ref}}}\right)\right]} + \beta_3(I-I_{\text{ref}}) + \beta_4(\sigma-\sigma_{\text{ref}})^2 + \beta_5 e^{\left[1.4\left(\frac{T-T_{\text{ref}}}{T_{\text{ref}}}\right)\right]} + \beta_6(I-I_{\text{ref}})^2 + \beta_7(\sigma-\sigma_{\text{ref}})e^{\left[0.7\left(\frac{T-T_{\text{ref}}}{T_{\text{ref}}}\right)\right]}\right\} \quad (5.4.5)$$

The parameters β_i were set to the values used in the previous models of *P. parvum* (Grover et al. 2010).

The maximum ingestion rate ($i_{\max}$) under optimal conditions was assumed to be 100 bacterial cells consumed per *P. parvum* cell per day (Nygaard and Tobiessen, 1993; Legrand et al., 2001). This rate was reduced by a product of three functions (f_i) taking values between 0 and 1 to account for reduced ingestion under various conditions (Eq. 5.4.6). The maximum bacterial ingestion rate is a function of temperature, light, and salinity like the autotrophic growth.

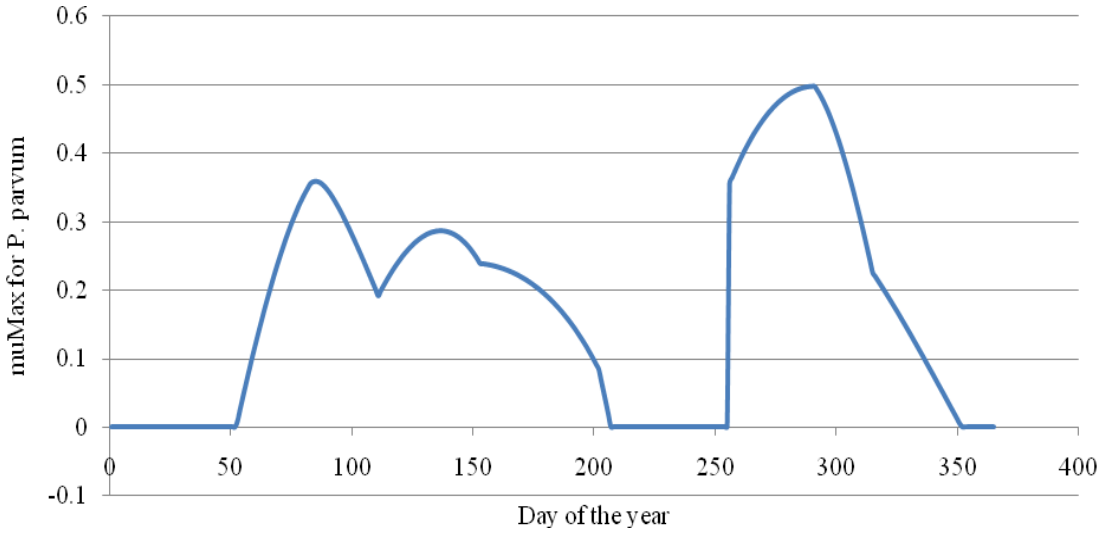

Figure 5.4.2 Environmentally dependent maximum growth rate for *P. parvum* by day of the year, for autotrophic growth.

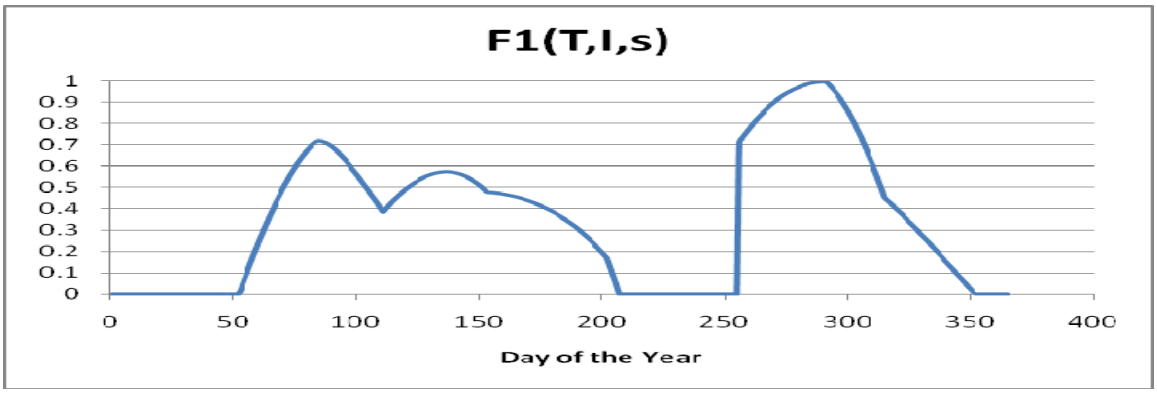

Figure 5.4.3. Function that modifies maximal ingestion rate due to temperature, light, and salinity by day of the year.

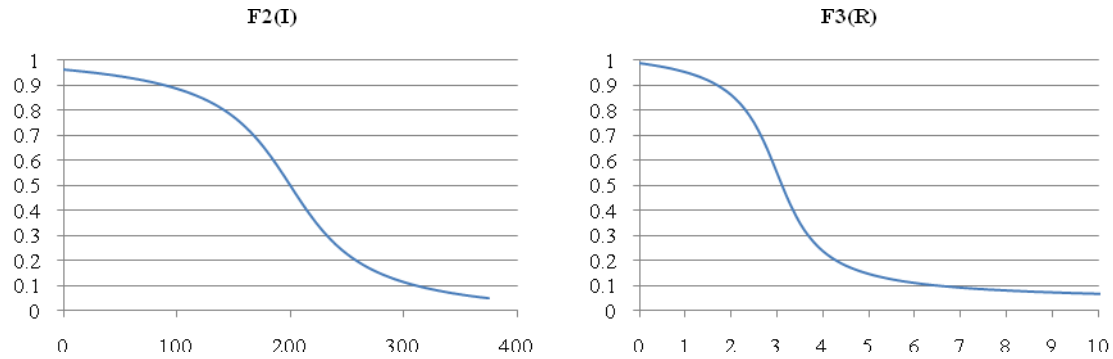

Figure 5.4.4. Functions that modify maximum ingestion rate A) due to irradiance and B) due to P

$$i_{max} = 100 \times f_1(T, I, \sigma) \times f_2(I) \times f_3(R) \tag{5.4.6}$$

The first of these functions ($f_1(T, I, \sigma)$) is a rescaling of the maximum growth rate function (Eq. 5.4.5, Fig. 5.4.2) into the range of 0 to 1 (Fig. 5.4.3). The second function ($f_2(I)$) decreases with irradiance (Fig. 5.4.4A).

$$f_2(I) = -0.35 \arctan(0.02(I - 200)) + 0.5 \tag{5.4.7}$$

This function reduces mixotrophy, growth based on ingestion of bacteria, as irradiance increases through a range of 100 – 400 μE m^{-2} s^{-1}. In simulations, the array of daily irradiances from Grover et al. (2010) was used to determine the value of this function. The third function ($f_3(R)$) is a decreasing function of P (Fig. 5.4.4B)

$$f_3(R) = -0.33 \arctan(1.4(R - 3)) + 0.55 \tag{5.4.8}$$

This function reduces mixotrophy when dissolved P is high, assuming that *P. parvum* regulates mixotrophy in a manner similar to the closely related haptophyte *Chrysochromulina polylepis* (Stibor and Sommer, 2003). The number of bacterial cells consumed by *P. parvum* each day is graphed in Fig. 5.4.5.

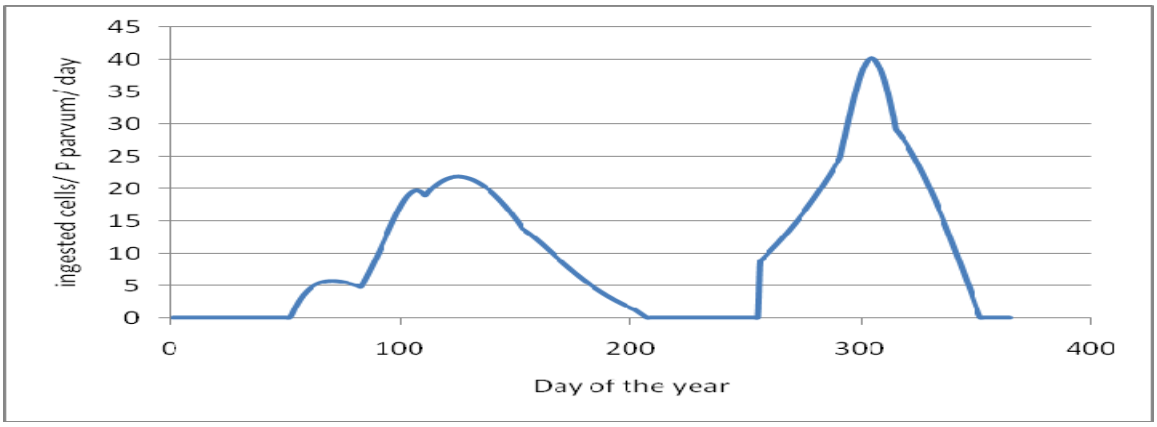

Figure 5.4.5. Maximum ingested cells by *P. parvum* per day using the initially parameterized ingestion rate.

One final modification was made to the model. The *P parvum* population declines in the summer. There have been arguments that mixotrophy is a response to adverse conditions. Assuming that *P. parvum* is mostly autotrophic, mixotrophic feeding may be a response to a decrease in nutrients when there is not enough light to carry out enough photosynthesis. Therefore, the ingestion of bacteria was made to be dependent on light level (Eq. 5.4.9). This causes *P. parvum* to ingest fewer bacteria in the bright summer and more bacteria in the dark winter. To give the mixotrophy an advantage, a multiplier was created for a maximum ingestion amount that was arbitrarily chosen to be 100 bacterial cells per day per *P. parvum* cell, at the higher end of estimates in the literature cited elsewhere.

$$i_{max} = 100 \times (1 - \frac{I_{day}}{I_{\max}}) \qquad (5.4.9)$$

The multiplier was made relative to the maximum light level for the year by dividing the light level for each day by the maximum light level for the year. This is then subtracted from one. This makes the multiplier zero at the maximum light level for the year and closer to one for the lowest light level for the year. The maximum ingestion rate and light levels for the year are graphed in Fig. 5.4.6.

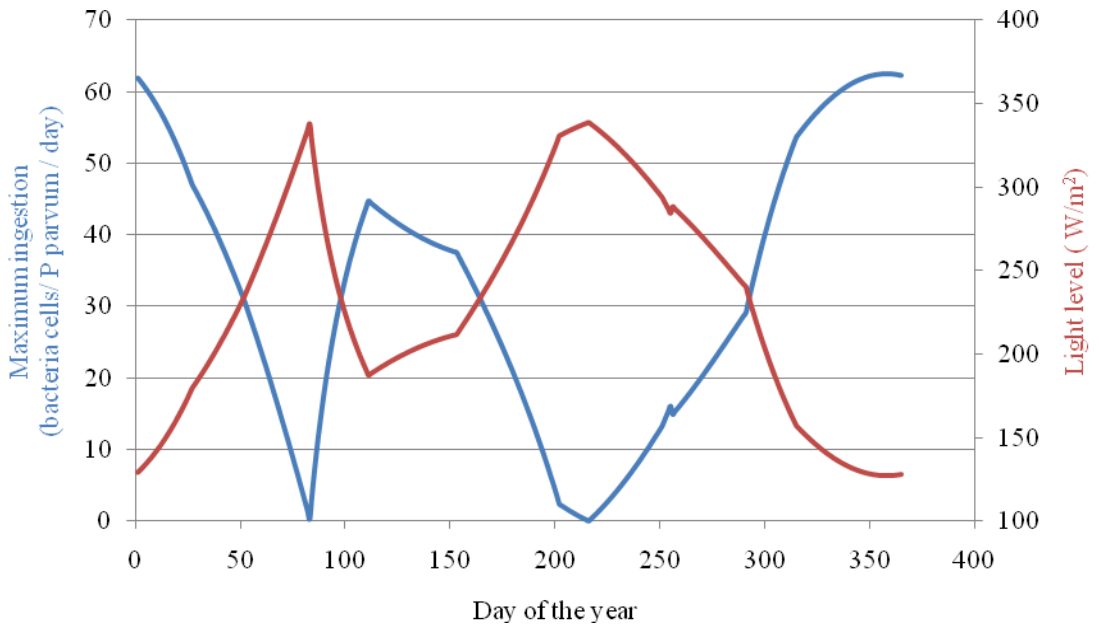

Figure 5.4.6. Maximum ingested cells by *P. parvum* per day using the modified ingestion rate.

Though this model was written with the idea that values from the input array would change every day for time-variable simulations, the first analyses addressed steady states using average values from the input array over one year as constant parameters. Solutions for the steady state were found both numerically and analytically. The analytic solutions were calculated using Mathematica's Solve function while the numeric solutions were found using MATLAB's numerical solvers for ordinary differential equations. Results from MATLAB's ode45 solver indicated convergence to a steady state to within 4 or 5 decimal places (with fluctuations in less significant digits indicating potential stiffness or other problems). Analytical solutions and numerical integration to achieve steady state agree well (Table 5.4.3).

Table 4.3. Analytical and numerical steady state solutions.

Variable	Analytical	Numerical
N (cells / liter)	1.67617×10^{10}	1.676174×10^{10}
B (cells / liter)	1.17543×10^{6}	1.175×10^{6}
R (µmol P / liter)	0.00312755	0.00312

The same two methods were used to explore the values of the parameters that affect the growth of *P. parvum* and the density of bacteria (i_{max}, K_B, e, Y_{RB}, a, and B_{max}). (Sensitivity analyses for other parameters, which were carried over from previous models, were reported in Grover et al., 2010). The Matlab solver ode23s was used for these simulations to cope with stiffness that arose for some parameter values. There were also some parameter values for which Mathematica algorithms could not find solutions. When there were analytical and numerical solutions, they agreed well.

Daily environmental data (temperature, light, salinity, irradiance, and phosphorus) was fed into the solver each day for one year. This same data was then used for five years, and the results are presented as the values obtained for the fifth year. The model was run with bacteria alone, *P. parvum* alone, and *P parvum* with bacteria. Equation 5.4.2 describes the growth rate of *P. parvum* as the sum of an autotrophic part and a heterotrophic part. Seasonality in the autotrophic component of growth is controlled by the function $\mu_{\max}$. This is the function described by Baker et al. (2009) and is governed by temperature, light, and salinity. These quantities vary seasonally and corresponding variations of growth rate throughout the year are shown in Fig. 5.4.2. Autotrophic growth is reduced to zero by low temperature in winter, and by low salinity in summer. Seasonality in the mixotrophic component of growth similarly arises from the initial description of maximum ingestion rate because it shares a similar dependence on temperature and salinity. The seasonal variation of the maximum ingestion rate is shown in Fig. 5.5.5. Note that in this case mixotrophic growth, like autotrophic growth, goes to zero in winter due to a strong effect of low temperature portrayed by Eq. 5.4.5.

As the maximal ingestion rate ($i_{\max}$) increases, the density of the bacteria decreases while the *P. parvum* population receives a small and diminishing benefit (Fig. 5.4.7). As the half-saturation constant for ingestion of bacteria (K_B) increases, *P. parvum* decreases linearly but slightly, while the bacteria increase linearly about ten-fold (Fig. 5.4.8). As the yield coefficient relating bacteria to phosphorus (Y_{RB}) increases, the density of the bacteria increases and the *P. parvum* density decreases by about 100-fold (Fig. 5.4.9). Note that the yield coefficient is an inverse measure of the P content of bacteria, thus an inverse measure of their contribution to growth of *P. parvum* by mixotrophy. The density of *P. parvum* shows an increase as the turnover rate of bacteria (a) increases and the bacteria show a very slight increase (Fig. 5.4.10). There is an increase in the density of bacteria as maximal density (B_{max}) first increases, but this quickly becomes constant with further increases, while the *P. parvum* density increases more steadily (Fig. 5.4.11). Variations in the efficiency of mixotrophic growth (e) do not affect the steady state *P. parvum* and bacteria populations, but the dissolved P concentration (R) decreased as efficiency increased (Fig. 5.4.12). With the exception of Y_{RB}, all of the parameter variations produced little change in the steady state concentration of dissolved P, but as Y_{RB} increases, dissolved P increases (Fig. 5.4.13).

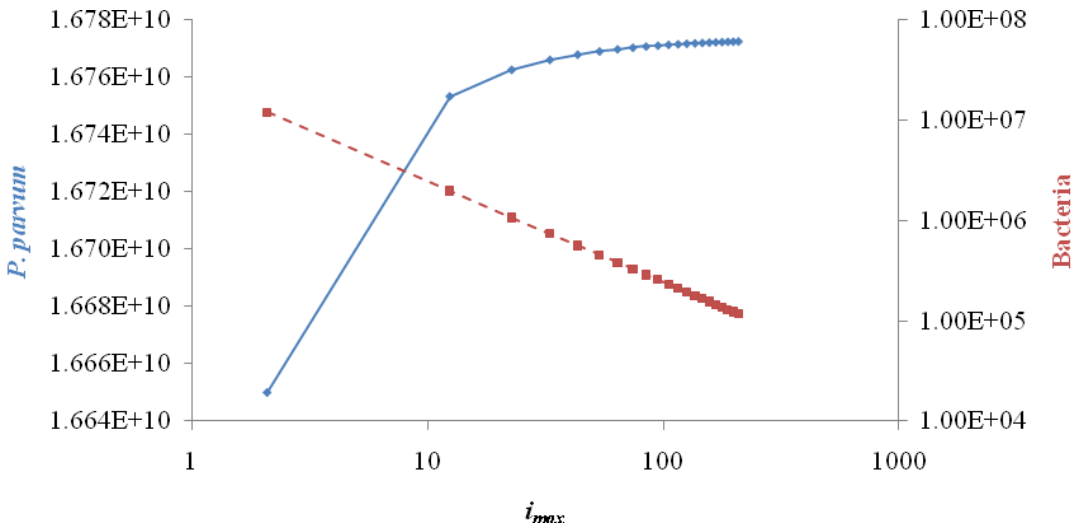

Figure 5.4.7. *P. parvum* (solid) and Bacteria (dashed) densities in response to the maximum ingestion rate (i_{max}). Note that *P. parvum* is linearly scaled while i_{max} and Bacteria are log scaled.

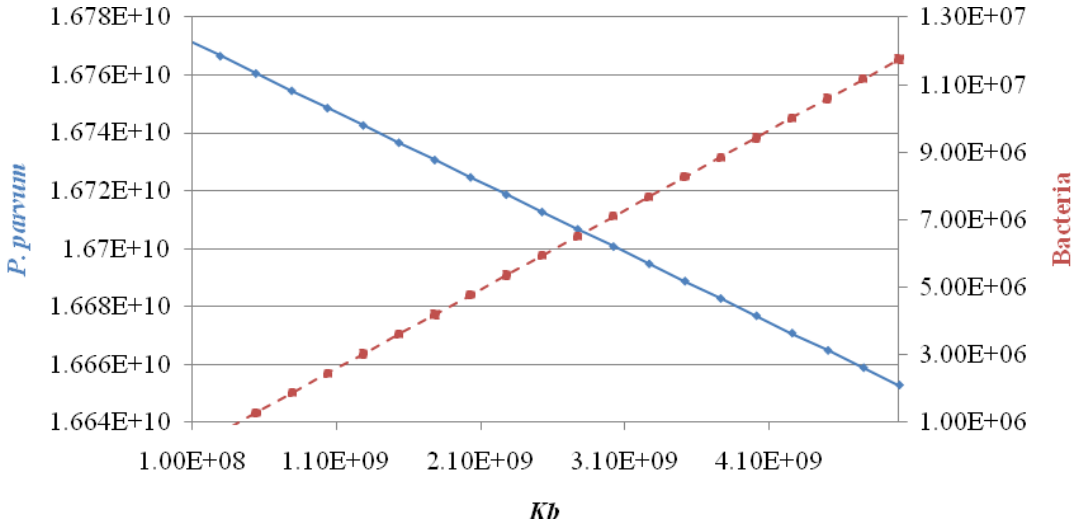

Figure 5.4.8. *P. parvum* (solid) and Bacteria (dashed) densities in response to the half saturation constant for ingestion of bacteria (K_b). Note that all axes are linearly scaled.

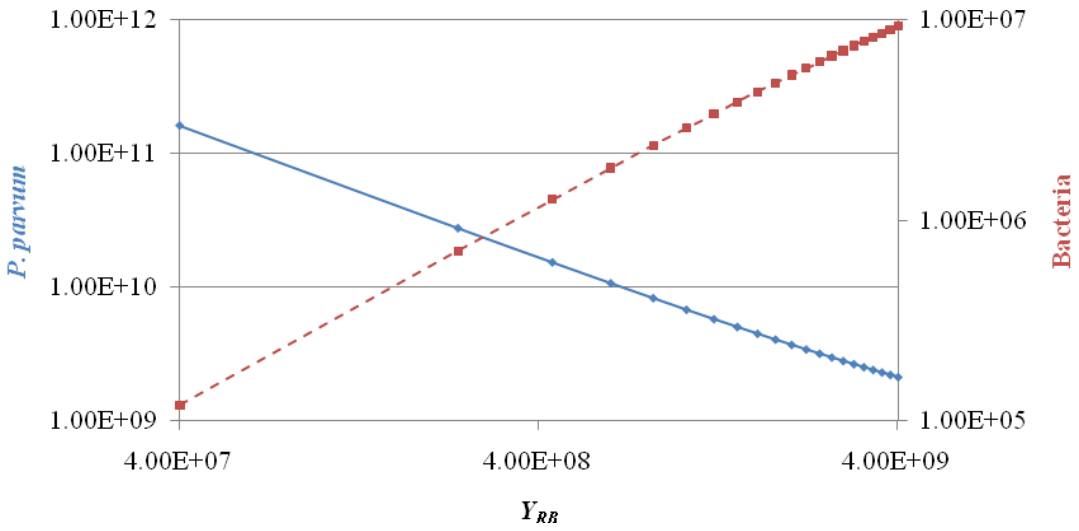

Figure 5.4.9. *P. parvum* (solid) and bacteria (dashed) densities in response to the yield coefficient of bacteria from P (Y_{RB}). Note that all of the axes are log scaled.

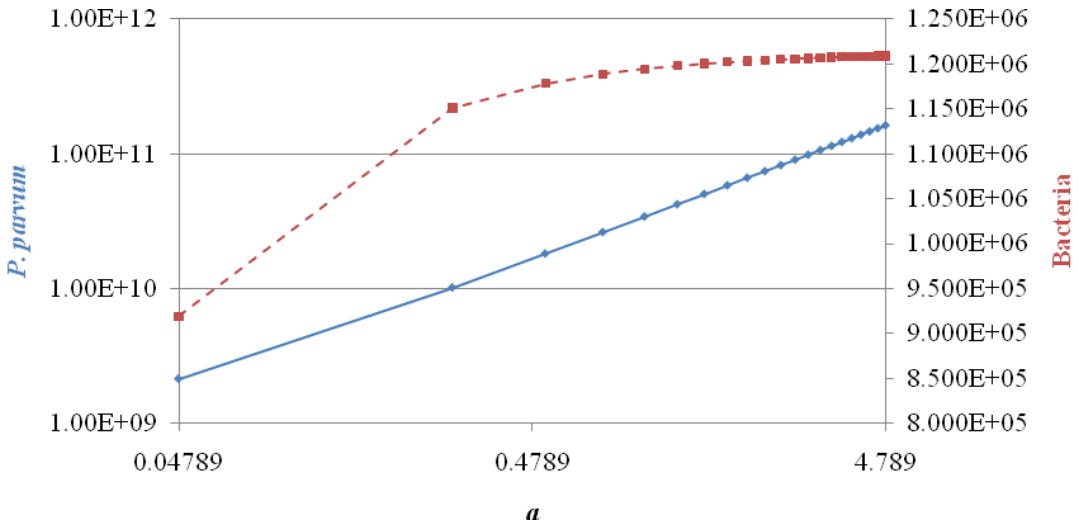

Figure 5.4.10. *P. parvum* (solid) and bacteria (dashed) densities in response to turnover rate for bacteria (*a*). Note that the *P. parvum* density (solid line) and the turnover rate are on log scales, while the bacteria (dashed line) are on a linear scale.

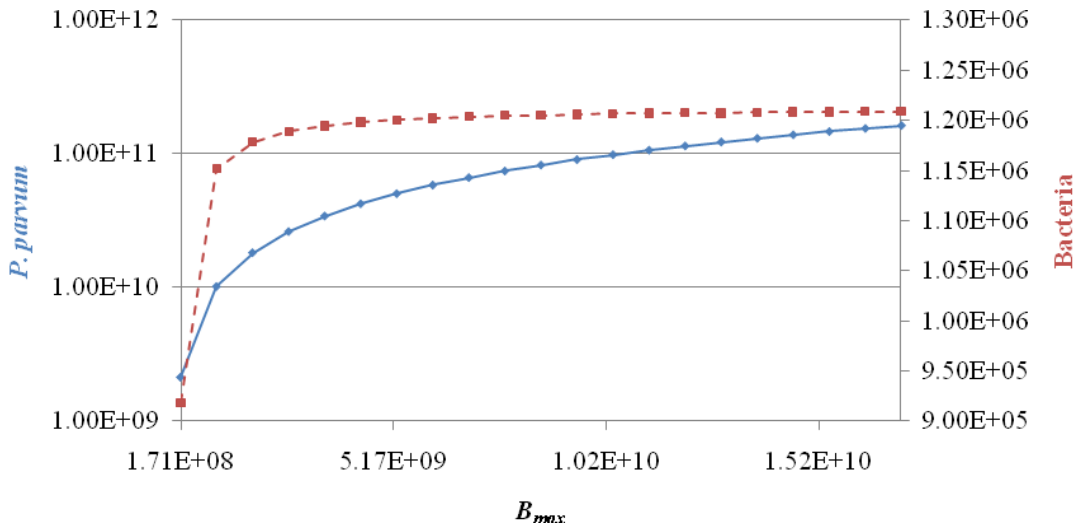

Figure 5.4.11. *P parvum* (solid) and bacteria (dashed) densities in response to the maximum density of edible bacteria (B_{max}). Note that the *P. parvum* densities (solid line) are on a log scale, but *Bmax* and the bacteria (dashed line) are on a linear scale.

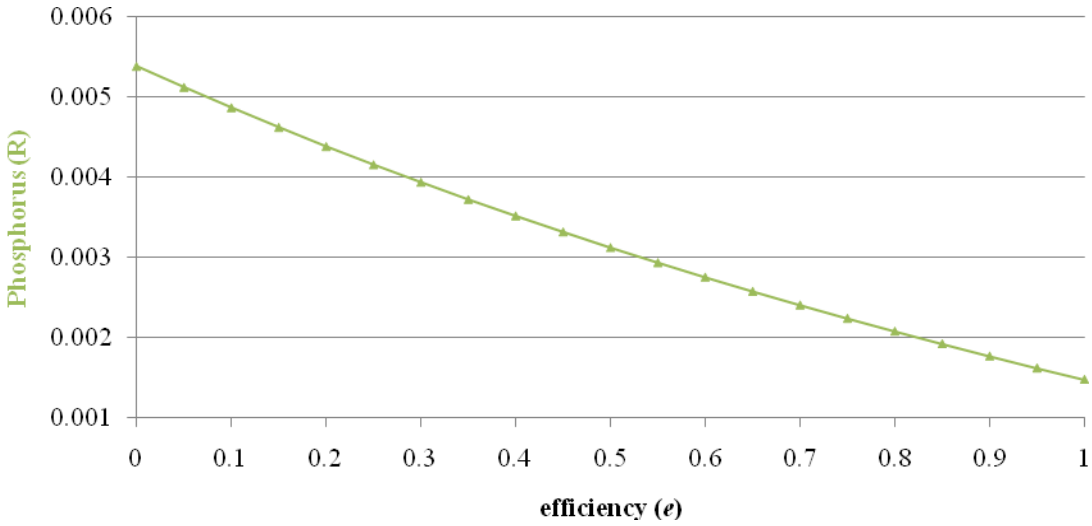

Figure 5.4.12. Dissolved P concentration in response to efficiency of mixrotophic growth (*e*).

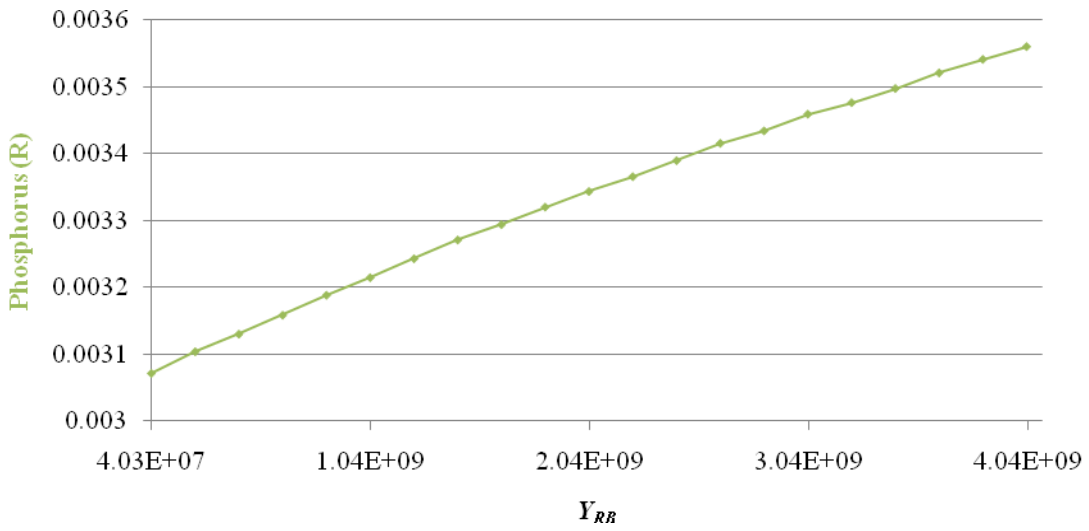

Figure 5.4.13. Dissolved P in response to the yield of bacteria from P.

When seasonal simulations are run using input data based on observations from Lake Granbury, with the bacteria growing alone and no *P. parvum* present, the bacteria have a fairly constant predicted population density through the year. When *P. parvum* are present, the bacteria show large reductions in densities in the summer and early winter (Fig. 5.4.14). The *P. parvum* density for the fifth year of running the model for five years is shown in Fig. 5.4.15. The *P. parvum* densities showed large sharp decreases in density during days 350-50 and 200-250. After these sharp declines, the densities rapidly increase to show higher and lightly changing population densities in the summer and early winter. Without the bacteria, the densities of the P. parvum through the year showed a greater range in values (Fig. 5.4.15). The length of the declines increased with declining densities from about days 290-60 and 175-250. Recoveries from minima also took longer. Finally, overall densities were always lower when the *P. parvum* were without bacteria than when they were present.

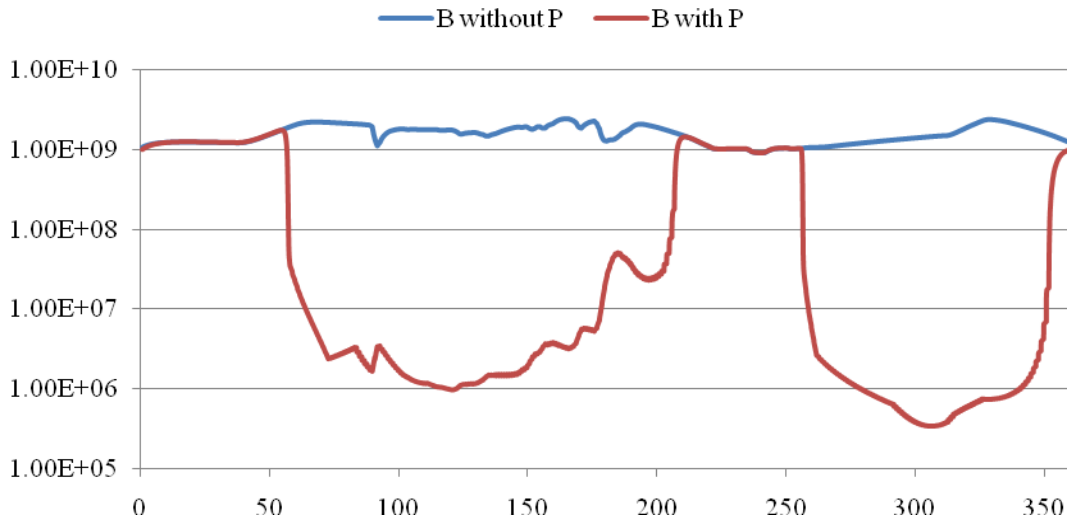

Figure 5.4.14. Simulated densities of bacteria with and without *P. parvum* over the course of a year.

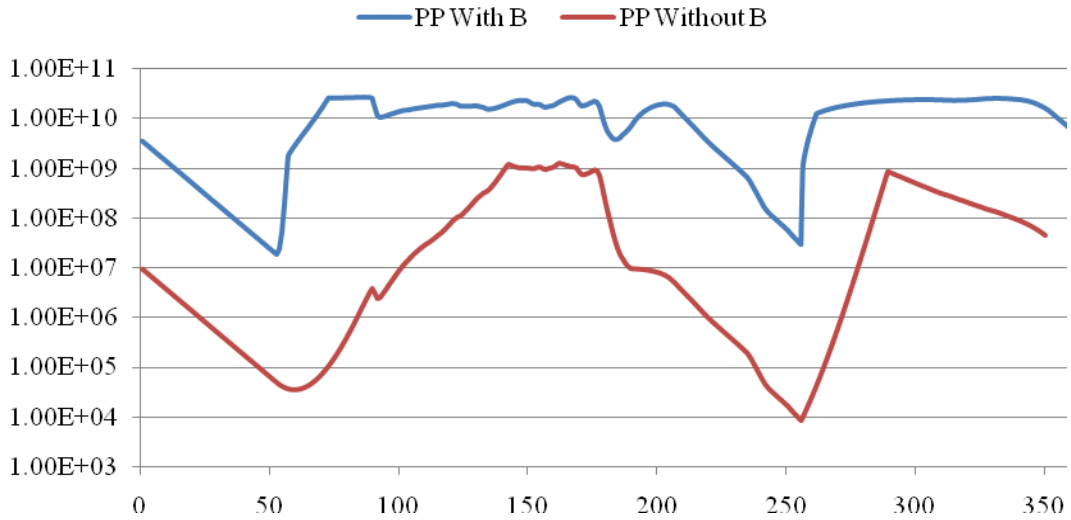

Figure 5.4.15. Simulated *P parvum* densities with and without bacteria, over the course of a year.

Using the modified description of maximum ingestion rate to produce strong mixotrophic growth in winter, leads to a seasonal pattern with strong mixotrophic growth in winter as intended, but also strong growth during a period in spring when irradiance was low due to turbid water associated with rainy weather (Fig. 5.4.16). However, both descriptions of mixotrophy predict reduced mixotrophic growth in late summer – due to low salinity in the original description and due to high light in the alternative description. The alternative, strongly light-dependent description of the maximal ingestion rate decreases the extent of these winter and summer minima. However, there is still an annual

minimum during winter, so that even with a deliberately overestimated consumption rate, the winter minimum does not disappear.

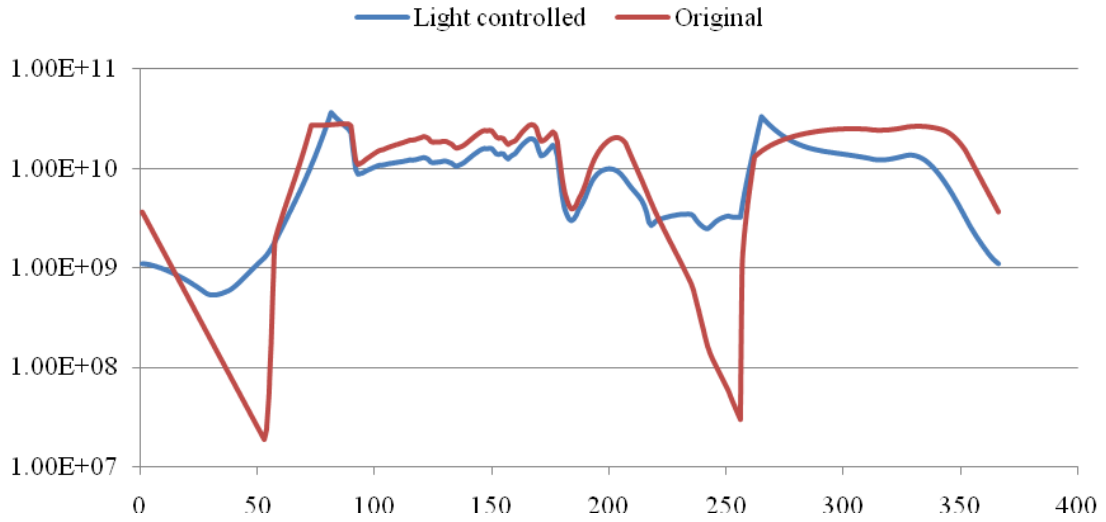

Figure 5.4.16. Comparison of simulated *P. parvum* densities using the modified light controlled ingestion and the originally formulated light-independent ingestion rate.

Some further changes to some of the other parameters were pursued to see if they could appreciably change the predicted seasonal dynamics of the *P. parvum* population. There were four parameters, yield coefficient of bacteria from P (Y_{Rb}), turnover rate for the bacteria (a), half-saturation constant for ingestion of bacteria (K_b), efficiency of mixotrophic growth (e), that were varied from 1/10 of their original value to ten times their original value. The results were summarized in Table 5.4.4. Although parameter changes could substantially alter the population densities predicted for *P. parvum*, they did not change the seasonal pattern much. For all the parameter values explored, an annual minimum was predicted to occur in winter.

Table 5.4.4. Results.

Parameter that increases	Changes to P. parvum density
yield coefficient of bacteria from P (Y_{Rb})	Decreased
turnover rate for the bacteria (a)	Increased
half-saturation constant for ingestion of bacteria (K_b)	Little change
efficiency of mixotrophic growth (e)	Little change

This study examined the consequences of adding mixotrophy to a model for *Prymnesium parvum*, a harmful algal species that forms blooms in Texas in the winter. The model used here was based on a previous model (Grover et al. 2010) that has *P. parvum* growing phototrophically and alone, without competitors. The previous model predicted

a winter decline when natural populations in Texas show winter blooms. The model examined here has *P. parvum* growing as a mixotroph, using both phototrophic and heterotrophic nutritional modes, with a dynamic prey population of bacteria and one limiting resource (phosphorus). The mixotrophy for P. *parvum* in this model had bacterivory as providing additive nutrition, in addition to that of phototrophy. This possibly gives *P. parvum* as modeled here an unrealistic advantage from mixotrophy, in an attempt to overcome the winter loss predicted by the previous model. Numerical simulations were done for steady state and seasonally forced systems. The densities of the organisms and the effects of changing parameters were examined.

The steady state analysis of sensitivity to parameters varied only those specifically introduced to model mixotrophic growth, and varied them one-at-a-time with other parameters set to default values. The population density of *P. parvum* was not sensitive to the three parameters describing mixotrophic ingestion and growth rates, $i_{\max}$, K_B, and e. As is often the case in chemostat models, these growth rate parameters probably do more to determine the rate of approach to steady state than the ultimate value reached, which is often controlled more by resource supply. The three parameters governing the rate of supply of bacteria (a, $B_{\max}$) and the nutrient available from them (Y_{RB}) strongly affected the steady state density of *P. parvum*. Of these three parameters, there is empirical information to constrain a and Y_{BR}.

However, $B_{\max}$ is essentially unknown. It corresponds to the maximum density of edible bacteria that would occur in the habitat without mixotrophic ingestion. Under many conditions in aquatic habitats, total bacterial density can be reasonably estimated from observations, but the fraction of the total bacteria that is edible to *P. parvum* is unknown. In addition, *P. parvum* may be able to ingest particulate matter released by lysis of cells targeted by its toxins (as observed for ciliates by Tillman 2003). So the mixotrophic resource base available to *P. parvum* may extend beyond bacteria. To some extent, this can be accounted by increasing the value of $B_{\max}$. But a thorough empirical description of resources available to mixotrophic *P. parvum* is not yet available.

The growth rate of *P. parvum* is zero for days 350-50 and 200-250. This is when previous mathematical models such as PP0 predict large decreases in *P. parvum* densities, in the winter and fall (Fig. 5.4.18). These large sharp decreases in density make the model not very useful for predicting *P. parvum* in Texas. The new version of model PP0 with mixotrophy results in higher densities than the original PP0 model. Given that this model treats mixotrophy as an additive to the original growth this is not surprising. However, the model is plagued with the same difficulty as the PP0 model, the steep drops in density during the winter while the natural population has an increase in the winter.

The hypothesis for this model was that the incorporation of mixotrophy to the existing PP0 model as an additive effect of bacterivory would eliminate winter declines in *P. parvum* density predicted by the current model, and thus generate more realistic predictions of natural populations. In several ways, mixotrophy was modeled with unrealistic advantages for growth of *P. parvum*, especially in winter. Mixotrophy was

additive to phototrophic growth, and the ingestion of bacteria was at the high end of values indicated from the literature. This did indeed boost the density of the mixotrophs, but did not eliminate the decline in density during winter (Fig. 5.4.18). The ingestion of bacteria by the *P. parvum* was also made to be reciprocal to light level so that the mixotrophs would ingest more bacteria in the dark of winter. This did raise the minima of predicted population density, but did not eliminate them (Fig. 5.4.18).

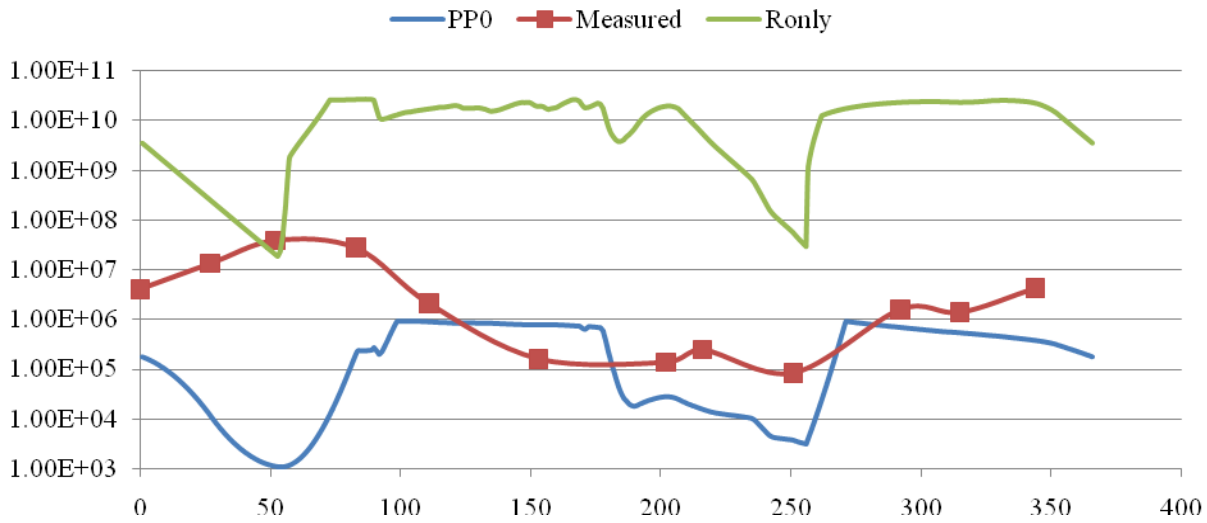

Figure 5.4.18. Comparison of simulated and measured values for *P. parvum* densities through the year, for a model without mixotrophy (PP0) and a corresponding model with mixotrophy (Ronly).

This model incorporating mixotrophy is thus unable to account for the winter increase in the *P. parvum* population in Texas. Even with extraordinary parameter changes, it cannot avoid the predicted winter decline in density of *P. parvum*. The model is based on growth responses to temperature and salinity generated from Baker et al. (2007, 2009). So far, the only way to change the predictions of the PP0 and related models is to change these growth responses (Grover et al. 2010). Though the problem of modeling *P. parvum* blooms in Texas was not solved with this study of mixotrophy, we have eliminated one of the simpler routes to incorporating this process into predicting *P. parvum* blooms in Texas. Possibly, a more sophisticated description of mixotrophy would prove more helpful. Alternatively, other processes may be more influential on bloom formation than the growth physiology of *P. parvum*. There has been some success with mathematical modeling that stresses spatial dynamics and hydrology as factors in bloom formation (Grover et al. 2010), and field observations support a strong role for hydrology (Roelke et al. 2010a, b). There has also been some success with models that include zooplankton grazing on *P. parvum* that is inhibited by toxin production (unpublished work included later in this report).

5.5 Expanding "box" model into a 1-dimensional model

In this part of the project, a one-dimensional model was constructed to study spatial variations of harmful algae such as *P. parvum* and their toxins, in riverine reservoirs. Inland waters present a spectrum of flowing-water habitats that are inhabited to varying degrees by planktonic algae. In small, low-order streams with rapid currents, no true plankton develops and suspended algae arise transiently from the benthos. As order increases, and especially in broad rivers and riverine reservoirs, development of plankton becomes more likely. Nevertheless, the ecology of planktonic algae in flow-dominated systems has been somewhat neglected, and raises many paradoxes (Reynolds, 1990).

Among these is a basic question of persistence. Strong flow washes out populations of suspended algae (Moustaka-Gouni *et al*., 2006; Roelke *et al*., 2010a), and continual strong flow can overwhelm the reproductive capacity of planktonic algae (Reynolds, 1990). A possible resolution of the persistence paradox lies in the complexity of the channel. There are many features along shorelines and on the bed that retard flow, producing slack regions and backwaters. These slow-flowing regions constitute a hydraulic storage zone that affects the downstream transport of suspended and dissolved constituents (Bencala and Walters, 1983; Martinez and Wise, 2003). Within such zones, the reproductive capacity of algae may suffice to permit population growth, even to bloom proportions.

Indeed, recent decades have seen the emergence of harmful algal blooms in high order rivers and riverine reservoirs. For example, the haptophyte flagellate *Prymnesium parvum* was first documented to cause fish kills in the southwestern U.S. in a stretch of the Pecos River in Texas (James and De La Cruz, 1989). Since that event in 1985, blooms of *P. parvum* have occurred in several reservoirs along multiple rivers in Texas (Roelke *et al.*, 2010a, 2010b; Southard et al., 2010). Blooms of several types of harmful algae have occurred in several other river, reservoir and estuary systems (Krogman *et al.*, 1986; Davis and Koop, 2006).

The occurrence of harmful algal blooms in riverine ecosystems demonstrates a viable phytoplankton community. In addition to a basic question of persistence in the presence of flow, other questions arise concerning the spatial variation of algal abundance and toxicity during bloom and flow events. Manipulation of flow is possible in some river systems, and has been suggested as a potential technique for managing and mitigating harmful algal blooms (Maier *et al*., 2001; Roelke *et al.*, 2010a; Mitrovic *et al.*, 2010). This possibility motivates the theoretical exploration of harmful algal dynamics in flowing conditions undertaken here. Another motivation lies in the fact that coves along the shoreline of riverine reservoirs might represent habitats where dynamics of harmful algae differ from the main reservoir. Such differences could perhaps also be exploited to mitigate harmful blooms and their effects.

This study addressed two basic questions: What is the longitudinal distribution of algal abundance and toxicity under various flows, in a riverine reservoir? And what differences arise between a fringing cove and a main lake? For the first question, an idealized

riverine reservoir was conceived in which a main channel with advective transport and dispersion was coupled to a hydraulic storage zone, representing an ensemble of fringing coves on the shoreline. Similar models are well developed for studying contaminant dynamics in flowing water systems, and were recently extended by the addition of algal populations (Grover *et al.*, 2009). As conceived here, this model of a riverine reservoir is best suited for understanding longitudinal patterns arising along the axis of flow. The second question addresses differences from the main reservoir arising in a single cove, rather than an ensemble. For this purpose, a simpler, two-compartment model of algal dynamics was constructed, in which one compartment is a small cove connected to a larger lake.

For both of these idealized habitats, models of algal and toxin dynamics were constructed, which deliberately simplified many of the complexities that pertain to harmful algae, with the goal of highlighting the role of flow. There is a long history of modeling to study water quality problems relating to algae, especially eutrophication (Chapra, 1997). Some models treat space very simply and assume that there are one to three well mixed zones, permitting considerable elaboration of biological and chemical kinetics (e.g. Park and Clough, 2004). Other models explicitly address one to three spatial dimensions, with sophisticated treatment of hydrodynamics at specific sites, though they sometimes less easily accommodate biological realism (Martin and McCutcheon, 1999). What is developed here occupies a middle ground. Biological processes essential to understanding harmful algae are incorporated, including population dynamics and toxin production and decay. The models are spatially explicit, but one-dimensional with simple habitat geometry and transport processes. A number of potential complications are neglected, including vertical stratification, light limitation, and higher trophic levels. Such simplifications permit focusing on the role of one or a few key processes such as longitudinal flow and mode of toxin production.

In this study, steady state analyses of the models constructed were complemented by examining event-driven dynamics using documented, extreme flow events from a riverine reservoir to force model output. Although the model structures are idealized, they support elaboration with details necessary for modeling specific systems, and although parameters are based on riverine reservoirs in Texas, USA, where harmful blooms have occurred, they could readily be changed to represent conditions found in other riverine systems worldwide.

5.5.1 Physical settings

We developed spatially explicit models that approach the dynamic interactions of a main lake and its coves with two different idealizations. The first is a continuum approach using an advection-dispersion-reaction system to resolve transport and biochemical reaction kinetics along the main stem of a riverine reservoir. In this approach, an ensemble of fringing coves is represented as a hydraulic storage zone. The second approach focuses on a single cove that is coupled to a larger, main lake.

The continuum approach has one spatial dimension, the longitudinal axis (x) of a riverine reservoir from the headwaters ($x = 0$) to the dam ($x = L$) (Fig. 5.5.1, see Table 5.5.1 for notation). In the main, flowing channel of the reservoir, advection occurs at a rate ν (m / d) and dispersion with coefficient δ (m^2 / d), which are constants unless otherwise specified. The main channel is connected to an ensemble of fringing coves treated as a hydraulic storage zone (Bencala and Walters, 1983), in which there is no longitudinal transport. At any point x along the length of the reservoir, there is exchange by Fickian diffusion between the main channel and storage zone at a rate α (d^{-1}). When the partial differential equations of the model are discretized for computation, the continuous storage zone becomes a series of coves of equal length. The cross-section of the channel is partitioned into area A representing the main channel, and A_S representing the storage zone. Both cross-sections are assumed to be invariant with length. Within both the main channel and the storage zone, algae grow and consume the limiting nutrient, while producing a toxin. Flow enters the headwaters at a rate F (m^3 / d), carrying the limiting nutrient for algal growth at a concentration R_{in} (μmol / L), and a balancing flow exits at the dam, removing algae, nutrients, and algal toxin. To simplify the model, constant reservoir volume V is assumed and the total system dilution rate is defined as $D = F / V$. To maintain water balance, the advection velocity ν must then equal DL, where L is the reservoir length.

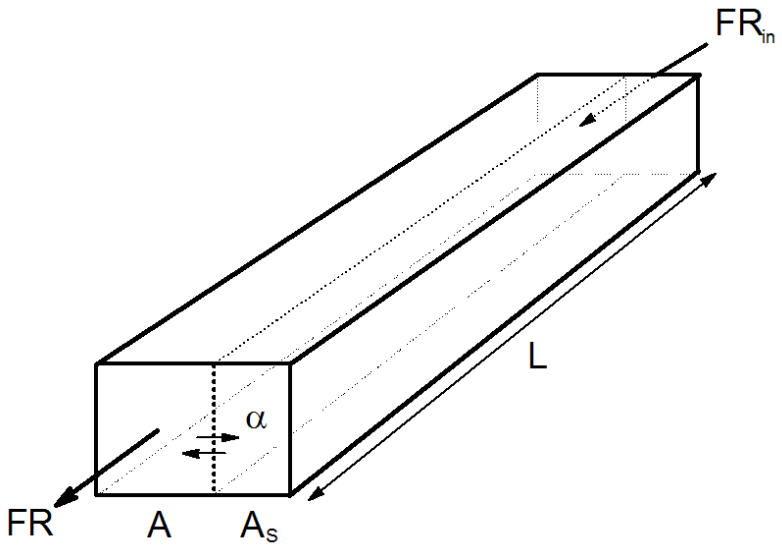

Figure 5.5.1. One-dimensional representation of a riverine reservoir with a hydraulic storage zone composed of fringing coves and shoreline features.

The second modeling approach focuses on a single cove, rather than a distributed ensemble, which undergoes Fickian exchange with a main lake (Fig. 5.5.2). A fraction ψ of the total system volume V occurs in the cove, and a fraction ϕ of the total inflow F goes into the cove. The same total flow F exits from the main lake. The limiting nutrient for algal growth enters the main lake at a concentration R_1^{in} and enters the cove at a concentration R_2^{in}. Water exchanges between the main lake and cove at a rate E' (m^3 / d) and a net flow of ϕF also goes from the cove to the main lake to maintain constant

volume. Flows of algae and algal toxin follow those of the nutrient. To simplify the model, constant volume was assumed, the system dilution rate was defined as $D = F / V$, and the system exchange rate (d^{-1}) was defined as $E = E' / V$.

Table 5.5.1. Notation.

Symbol	Meaning	Units
t	time coordinate	d
x	space coordinate	m
$R(x,t)$	nutrient concentration in main channel	µmol / L
$N(x,t)$	algal abundance in main channel	cells / mL
$C(x,t)$	toxin concentration in main channel	µg / L
$R_S(x,t)$	nutrient concentration in storage zone	µmol / L
$N_S(x,t)$	algal abundance in storage zone	cells / mL
$C_S(x,t)$	toxin concentration in storage zone	µg / L
$R_1(t)$, $R_2(t)$	nutrient concentrations in main lake (1) and cove (2)	µmol / L
$N_1(t)$, $N_2(t)$	algal abundances in main lake (1) and cove (2)	cells / mL
$C_1(t)$, $C_2(t)$	toxin concentrations in main lake (1) and cove (2)	µg / L
L	reservoir length	m
ν	advection rate	m / d
δ	dispersion coefficient	m^2 / d
F	flow rate (discharge)	m^3 / d
α	exchange rate between main channel and storage zone	d^{-1}
A	cross-sectional area of main channel	m^2
A_S	cross-sectional area of storage zone	m^2
V	reservoir volume	m^3
D	dilution rate	d^{-1}
R_{in}	nutrient supply to reservoir	µmol / L
ψ	fraction of reservoir volume in cove	none
ϕ	fraction of inflow entering cove	none
R_1^{in}, R_2^{in}	nutrient supply to main lake (1) and cove (2)	µmol / L
E'	volumetric exchange rate between main lake and cove	m^3 / d
E	first order exchange rate between main lake and cove	d^{-1}
μ_{max}	maximal growth rate of algae	d^{-1}
K	half-saturation constant for algal growth	µmol / L
m	mortality rate of algae	d^{-1}
ε	toxin production coefficient	µg / cell or none
k	first order decay rate of toxin	d^{-1}
q_N	nutrient quota of algae	µmol / cell
q_C	nutrient quota of toxin	µmol / µg
T	temperature	°C
Pe	Péclet number	none

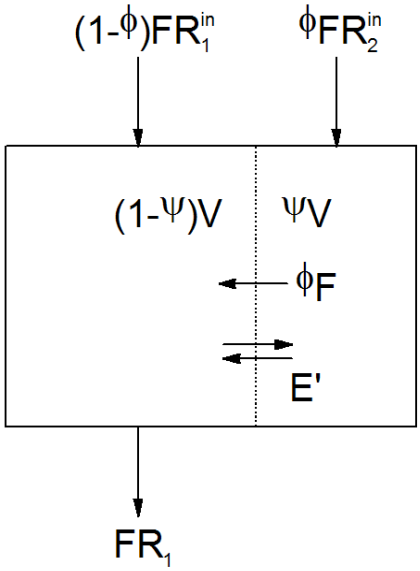

Figure 5.5.2. Representation of a coupled cove – main lake system. Zone 1 on the left is the main lake, and zone 2 on the right is the cove.

5.5.2 Biological and chemical assumptions

For both modeling approaches, the same sets of assumptions were applied for algal population dynamics, and toxin production and decay. Algal growth is a Monod function of the limiting nutrient concentration (R) at a given location:

$$\mu(R) = \frac{\mu_{\max} R}{K + R} \qquad (5.5.1)$$

with maximal growth rate $\mu_{\max}$ (d^{-1}) and half-saturation constant K (µM). Constant algal mortality is assumed at a rate m (d^{-1}). As algae grow they consume nutrient with constant quota q_N (µmol / cell) and, for simplicity, the nutrient content of algae that die is instantaneously and locally recycled.

Three modes of production for dissolved toxins were explored. The first assumes that the rate of toxin production p (µg toxin L^{-1} d^{-1}) is proportional to the degree of algal nutrient limitation and to algal abundance, N (cells / L):

$$\varepsilon p(R,N) = \varepsilon\left(\mu_{\max} - \mu(R)\right)N = \varepsilon\left(\frac{\mu_{\max} K}{K + R}\right)N \qquad (5.5.2)$$

where ε (µg toxin / cell) is a constant coefficient. We refer to this as the flagellate case, because some toxic flagellates such as *Prymnesium parvum* have been observed to produce toxins more rapidly when stressed by nutrient limitation (Johansson and Granéli,

1999; Granéli and Johansson, 2003; Chakraborty *et al.*, 2008; but see Lekan and Tomas, 2010).

The second mode of toxin production assumes that the rate of production is proportional to algal productivity, i.e. to the product of growth rate and abundance:

$$\varepsilon p(R,N) = \varepsilon \mu(R) N = \varepsilon \left(\frac{\mu_{\max} R}{K+R} \right) N \qquad (5.5.3)$$

This case assumes that toxin is produced in proportion to other cellular products, and is then released to the water at a constant rate. We refer to this as the cylindrospermopsin case, because it appears some producers of this toxin act in such a fashion (Hawkins *et al.*, 2001; Falconer and Humpage, 2006).

For simplicity, toxin degradation is assumed to follow first order kinetics with a decay coefficient k (d^{-1}).

5.5.3 Governing equations

For the riverine reservoir model, the governing equation system is

$$\frac{\partial R}{\partial t} = -DL\frac{\partial R}{\partial x} + \delta \frac{\partial^2 R}{\partial x^2} - \left(\mu(R) - m\right) N q_N + \alpha \left(R_S - R\right) \qquad (5.5.4a)$$

$$\frac{\partial N}{\partial t} = -DL\frac{\partial N}{\partial x} + \delta \frac{\partial^2 N}{\partial x^2} + \left(\mu(R) - m\right) N + \alpha \left(N_S - N\right) \qquad (5.5.4b)$$

$$\frac{\partial C}{\partial t} = -DL\frac{\partial C}{\partial x} + \delta \frac{\partial^2 C}{\partial x^2} + \varepsilon p(R,N) - kC + \alpha \left(C_S - C\right) \qquad (5.5.4c)$$

$$\frac{\partial R_S}{\partial t} = -\left(\mu(R_S) - m\right) N_S q_N - \alpha \frac{A}{A_S}\left(R_S - R\right) \qquad (5.5.4d)$$

$$\frac{\partial N_S}{\partial t} = \left(\mu(R_S) - m\right) N_S - \alpha \frac{A}{A_S}\left(N_S - N\right) \qquad (5.5.4e)$$

$$\frac{\partial C_S}{\partial t} = \varepsilon p(R_S, N_S) - kC - \alpha \frac{A}{A_S}\left(C_S - C\right) \qquad (5.5.4f)$$

with boundary conditions

$$\delta \left.\frac{\partial R}{\partial x}\right|_{x=0} - DLR(0,t) = -DLR_{in} \qquad (5.5.5a)$$

$$\delta \left.\frac{\partial N}{\partial x}\right|_{x=0} - DLN(0,t) = 0 \qquad (5.5.5b)$$

$$\delta \left.\frac{\partial C}{\partial x}\right|_{x=0} - DLC(0,t) = 0 \qquad (5.5.5c)$$

$$\delta \left.\frac{\partial R}{\partial x}\right|_{x=L} = \delta \left.\frac{\partial N}{\partial x}\right|_{x=L} = \delta \left.\frac{\partial C}{\partial x}\right|_{x=L} = 0 \qquad (5.5.5d)$$

where in the main flowing channel $R(x,t)$ is dissolved nutrient concentration at location x and time t, $N(x,t)$ is algal abundance at location x and time t, and $C(x,t)$ is dissolved toxin concentration at location x and time t. The respective quantities in the hydraulic storage zone are denoted with a subscript S. Boundary condition (5.5.5a) specifies an inflow with nutrient concentration R_{in}, conditions (5.5.5b) and (5.5.5c) specify no inflowing algae or toxin, and conditions (5.5.5d) specify that outflow occurs by advection only, as over a dam or weir.

Equation system (5.5.4) is appropriate when the toxin contains little or none of the limiting nutrient, which is true for many flagellate toxins (Murata and Yasumoto, 2000). In contrast, many cyanotoxins contain substantial amounts of nitrogen (Berry *et al.*, 2008), a potential limiting nutrient. For N-limited cyanobacteria producing toxin in proportion to growth (cylindrospermopsin case), nutrient taken up from the medium is partitioned between cell production and toxin production, with ε being a dimensionless coefficient specifying the allocation to toxin production. The nutrient content of the toxin is designated q_C (mol nutrient / g toxin) and toxin degradation is assumed to recycle this content to dissolved nutrient. Dynamic mass balance for the nutrient then leads to these governing equations:

$$\frac{\partial R}{\partial t} = -DL\frac{\partial R}{\partial x} + \delta\frac{\partial^2 R}{\partial x^2} - \left(\mu(R) - m\right)Nq_N + kCq_C + \alpha\left(R_S - R\right) \qquad (5.5.6a)$$

$$\frac{\partial N}{\partial t} = -DL\frac{\partial N}{\partial x} + \delta\frac{\partial^2 N}{\partial x^2} + \left[\left(1-\varepsilon\right)\mu(R) - m\right]N + \alpha\left(N_S - N\right) \qquad (5.5.6b)$$

$$\frac{\partial C}{\partial t} = -DL\frac{\partial C}{\partial x} + \delta\frac{\partial^2 C}{\partial x^2} + \varepsilon\mu(R)Nq_N / q_C - kC + \alpha\left(C_S - C\right) \qquad (5.5.6c)$$

$$\frac{\partial R_S}{\partial t} = -\left(\mu(R_S) - m\right)N_S q_N + kCq_C - \alpha\frac{A}{A_S}\left(R_S - R\right) \qquad (5.5.6d)$$

$$\frac{\partial N_S}{\partial t} = \left[\left(1-\varepsilon\right)\mu(R_S) - m\right]N_S - \alpha\frac{A}{A_S}\left(N_S - N\right) \qquad (5.5.6e)$$

$$\frac{\partial C_S}{\partial t} = \varepsilon\mu(R_S)N_S q_N / q_C - \alpha\frac{A}{A_S}\left(C_S - C\right) \qquad (5.5.6f)$$

Boundary conditions (5.5.5) remain unchanged for equation system (5.5.6).

For the cove – main lake model, the governing equation system is

$$\frac{dR_1}{dt} = \frac{\left(1-\phi\right)D}{1-\psi}R_1^{in} - \frac{D+E}{1-\psi}R_1 + \frac{\phi D+E}{1-\psi}R_2 - \left(\mu(R_1) - m\right)N_1 q_N \qquad (5.5.7a)$$

$$\frac{dR_2}{dt} = \frac{\phi D}{\psi}R_2^{in} + \frac{E}{\psi}R_1 - \frac{\phi D+E}{\psi}R_2 - \left(\mu(R_2) - m\right)N_2 q_N \qquad (5.5.7b)$$

$$\frac{dN_1}{dt} = -\frac{D+E}{1-\psi} N_1 + \frac{\phi D+E}{1-\psi} N_2 - \left(\mu(R_1) - m\right) N_1 \quad (5.5.7c)$$

$$\frac{dN_2}{dt} = \frac{E}{\psi} N_1 - \frac{\phi D+E}{\psi} N_2 - \left(\mu(R_2) - m\right) N_2 \quad (5.5.7d)$$

$$\frac{dC_1}{dt} = -\frac{D+E}{1-\psi} C_1 + \frac{\phi D+E}{1-\psi} C_2 + \varepsilon p(R_1, N_1) - kC_1 \quad (5.5.7e)$$

$$\frac{dC_2}{dt} = \frac{E}{\psi} C_1 - \frac{\phi D+E}{\psi} C_2 + \varepsilon p(R_2, N_2) - kC_2 \quad (5.5.7f)$$

where subscripts 1 and 2 denote quantities in the main lake and cove, respectively. Equation system (5.5.7) is appropriate when the toxin contains little or none of the limiting nutrient. For N-limited cyanobacteria producing toxin in proportion to growth (cylindrospermopsin case), dynamic mass balance for the nutrient requires these governing equations:

$$\frac{dR_1}{dt} = \frac{(1-\phi)D}{1-\psi} R_1^{in} - \frac{D+E}{1-\psi} R_1 + \frac{\phi D+E}{1-\psi} R_2 - \left(\mu(R_1) - m\right) N_1 q_N + kC_1 q_C \quad (5.5.8a)$$

$$\frac{dR_2}{dt} = \frac{\phi D}{\psi} R_2^{in} + \frac{E}{\psi} R_1 - \frac{\phi D+E}{\psi} R_2 - \left(\mu(R_2) - m\right) N_2 q_N + kC_2 q_C \quad (5.5.8b)$$

$$\frac{dN_1}{dt} = -\frac{D+E}{1-\psi} N_1 + \frac{\phi D+E}{1-\psi} N_2 - \left[(1-\varepsilon)\mu(R_1) - m\right] N_1 \quad (5.5.8c)$$

$$\frac{dN_2}{dt} = \frac{E}{\psi} N_1 - \frac{\phi D+E}{\psi} N_2 - \left[(1-\varepsilon)\mu(R_2) - m\right] N_2 \quad (5.5.8d)$$

$$\frac{dC_1}{dt} = -\frac{D+E}{1-\psi} C_1 + \frac{\phi D+E}{1-\psi} C_2 + \varepsilon\mu(R_1) N_1 q_N / q_C - kC_1 \quad (5.5.8e)$$

$$\frac{dC_2}{dt} = \frac{E}{\psi} C_1 - \frac{\phi D+E}{\psi} C_2 + \varepsilon\mu(R_2) N_2 q_N / q_C - kC_2 \quad (5.5.8f)$$

5.5.4 Parameterization and numerical analysis

Biological parameters were assigned differing values for flagellates or cyanobacteria (Table 5.5.2). Flagellates were assumed to be P-limited, while N-limitation was also considered for cyanobacteria. Parameter values are similar to those in previous models of flagellates and cyanobacteria in a Texas reservoir (Grover *et al.*, 2010). Algal mortality (m) was assigned a value of 0.1 d^{-1}, similar to the average value estimated for a Texas reservoir (Grover *et al.*, 2010). The first order degradation rate for the algal toxin was assigned a value of 0.5 d^{-1}, corresponding to a half-life of 1.4 d, broadly consistent with observations of cyanotoxin degradation (Cousins *et al.*, 1996; Twist and Codd, 1997). For N-limited cyanobacteria, the parameter q_C was set to 0.001 μmol N / μg C, consistent with the stoichiometry of peptide cyanotoxins (Berry *et al.*, 2008).

Table 5.5.2. Biological parameters for models of harmful, toxin-producing algae.

Parameter	P-limited flagellates	P-limited cyanobacteria	N-limited cyanobacteria
μ_{max} (d^{-1})	0.3	0.6	0.6
K (μmol / L)	0.009	0.1	0.01
q_N (μmol / cell)	1.39×10^{-9}	2.9×10^{-9}	32.5×10^{-9}
ε	1.0×10^{-8} μg / cell	1.25×10^{-8} μg / cell	0.00308

For both the riverine reservoir and cove-main lake models, dilution rate D was set to 0.01 d^{-1}, near the average value for a Texas reservoir (Grover *et al.*, 2010). Assignments for the other physical parameters of the riverine reservoir model, which are likely highly variable, were arbitrary but within environmentally likely ranges: length L = 10000 m; dispersion $\delta = 3 \times 10^5$ m^2 / d; storage zone exchange $\alpha = 0.5$ d^{-1}; and cross-section ratio of main channel to storage zone $A:A_S = 4$. Likewise, assignments for the other physical parameters of the cove-main lake model were arbitrary within environmentally likely ranges: exchange rate $E = 0.3$ d^{-1}; cove volume fraction $\psi = 0.01$; and cove flow fraction $\phi = 0.001$. For the riverine reservoir model, nutrient supply R_{in} was set to 1 μmol / L for P-limited cases, and 20 μmol / L for N-limited cases. For the cove-main lake model, nutrient supply to the main lake R_1^{in} was set to 0.5 μmol / L for P-limited cases, and 10 μmol / L for N-limited cases, while nutrient supply to the cove R_2^{in} was set to 1 μmol / L for P-limited cases, and 20 μmol / L for N-limited cases.

Many of the parameters were varied from these default values in sensitivity analyses focused on steady states. To explore non-steady dynamics under realistically variable flow conditions, daily dilution rates for Lake Granbury, Texas were estimated from 40-year discharge histories of two gauges, as described previously (Grover *et al.*, 2010). The most extreme flow events were characterized by using dilution rate data from the wettest year on record, 1990, to force time-variable simulations of both models. Forcing data for this year were repeated until annually periodic dynamics emerged. To explore the influence of seasonal temperature variations on non-steady dynamics, a sinusoidal model was used to assign daily temperatures (T, °C) in a pattern consistent with observations of Texas reservoirs:

$$T = 20 + 10\sin(2\pi t / 365 + 4.275) \qquad (5.5.9)$$

Then, for every day the algal maximal growth rate as a function of temperature $\mu_{max}(T)$ was adjusted from the values in Table I, here denoted $\mu_{max}(20)$, to indicate values at 20 °C. For flagellates, the adjustment followed a unimodal function similar to that found by Baker *et al.* (2009) for *P. parvum*:

$$\mu_{max}(T) = \mu_{max}(20)\left[-0.1 + 1.07\exp\left(1.86\frac{T-20}{20}\right) - 0.26\exp\left(3.72\frac{T-20}{20}\right)\right] \qquad (5.5.10)$$

For cyanobacteria, the adjustment followed a monotonically increasing function doubling the growth rate for a 10 °C rise in temperature:

$$\mu_{max}(T) = \mu_{max}(20)\exp\left[\frac{\ln 2}{10}(T-20)\right] \qquad (5.5.11)$$

Numerical analyses of the riverine reservoir model used the MacCormack algorithm (Chapra, 1997), with a discretization into 100 nodes of equal length. Numerical analyses of the cove-main lake models used a fourth / fifth order Runge-Kutta algorithm (Press *et al.*, 1986).

5.5.5 Results

Extensive sensitivity analyses of the riverine reservoir model examined how parameter variations influenced the spatial patterns predicted at steady state. With other parameters at default values, physical parameters were varied through large ranges: dilution rate D = 0.001 to 0.05 d^{-1}; dispersion $\delta = 3 \times 10^4$ to 3×10^7 m^2 / d; exchange rate $\alpha = 0.01$ to 10 d-1; and storage ratio $A:A_S = 0.01$ to 100. The development of longitudinal patterns at steady state generally depended on flow conditions, as summarized by the Péclet number

$$\text{Pe} = \frac{DL^2}{\delta} \qquad (5.5.12)$$

with upstream-downstream gradients arising for Pe in a critical range of about 10-100. For higher values of Pe, algal populations were predicted to be washed out by rapid flow, but in this critical range downstream abundance was generally higher than upstream abundance (e.g. Figs. 5.5.3, 5.5.4). Under these critical flow conditions, predicted toxin concentration was higher downstream than upstream for flagellates (e.g. Fig. 5.5.3), but mid-reservoir peaks of toxin concentration were predicted for cylindrospermopsin producers for the critical Pe range (e.g. Fig. 5.5.4). Qualitatively similar results were found whether the critical range for Pe was accomplished by varying the dilution rate D or the dispersion δ.

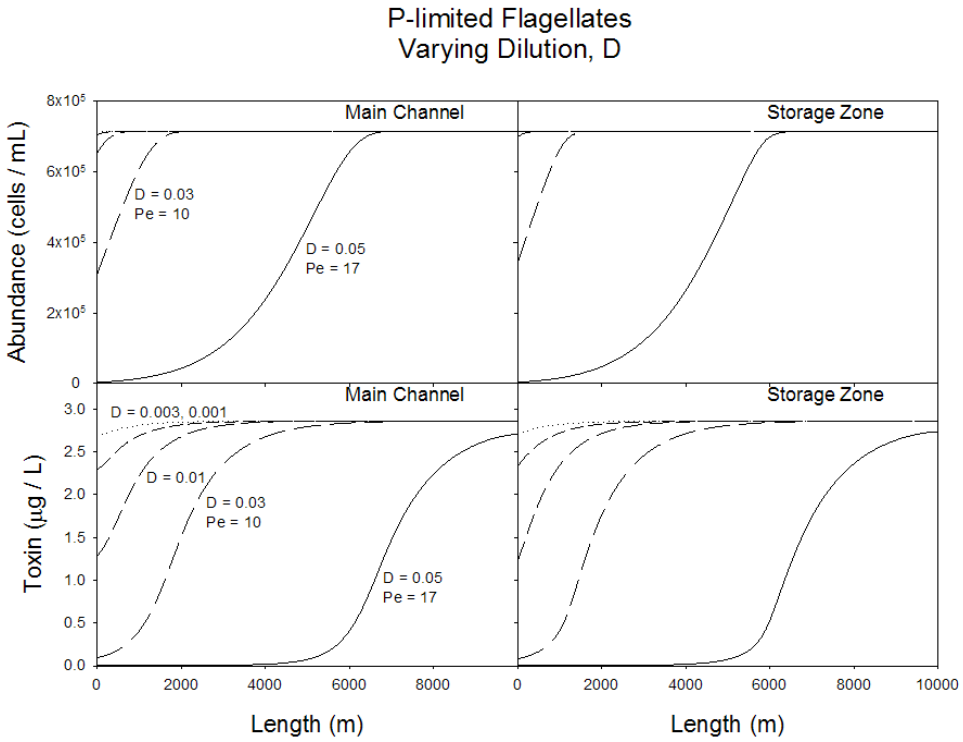

Figure 5.5.3. Abundance and toxin concentration predicted by the riverine reservoir model at steady state for P-limited flagellates.

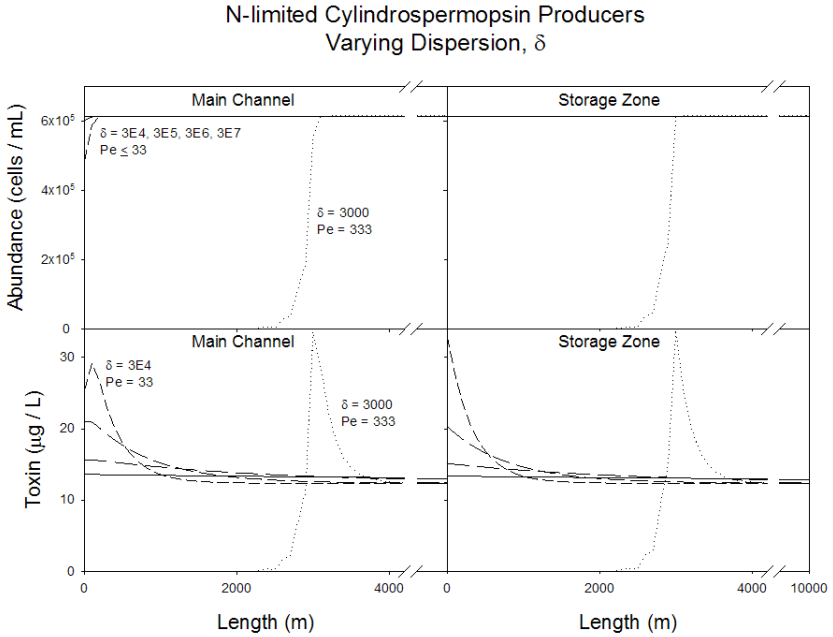

Figure 5.5.4. Abundance and toxin concentration predicted by the riverine reservoir model at steady state for N-limited cylindrospermopsin producers.

In general, the steady state differences between the storage zone and adjacent locations in the main channel were predicted to be small, for both algal abundance and toxin concentration. Under critical flow conditions producing upstream-downstream gradients, abundance and toxin concentration in upstream locations were up to about two-fold higher in the storage zone than the main channel (e.g. Fig. 5.5.5), but only if the exchange between these zones was very slow ($\alpha \leq 0.01$ d^{-1}) or if the main channel was very small in relation to the storage zone ($A{:}A_S \leq 0.1$).

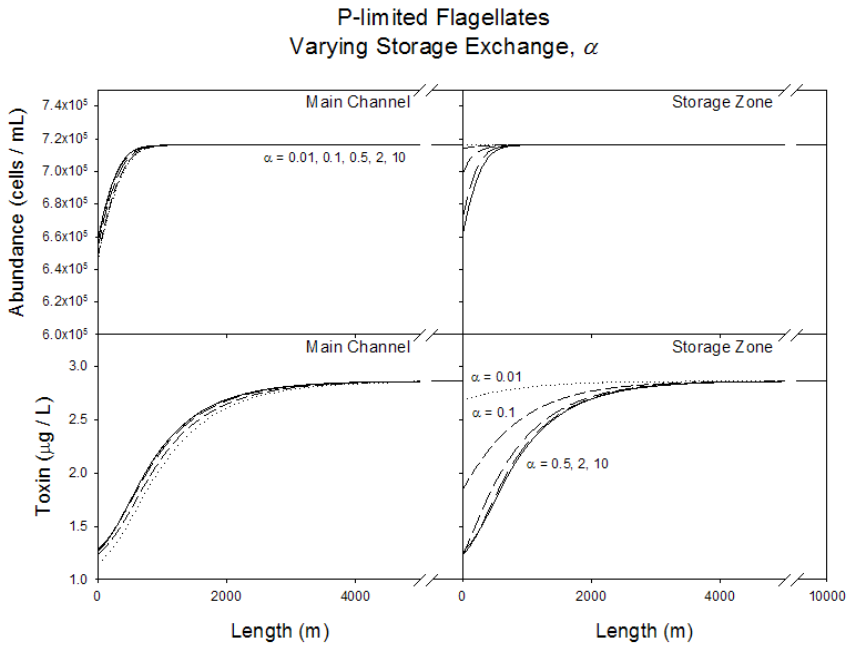

Figure 5.5.5. Abundance and toxin concentration predicted by the riverine reservoir model at steady state for P-limited flagellates.

Examining steady states predicted by the cove-main lake model reinforces the conclusion that large differences between coves and a main lake arise only under restricted circumstances. Algal abundance and toxin concentration were predicted to be up to 40% higher in the cove than the main lake (e.g. Fig. 5.5.6). But differences exceeding about 10% arose only if the cove was relatively isolated from the main lake, with an exchange rate < 0.01 d^{-1}, and had a nutrient supply concentration 10 – 20 times that of the main lake.

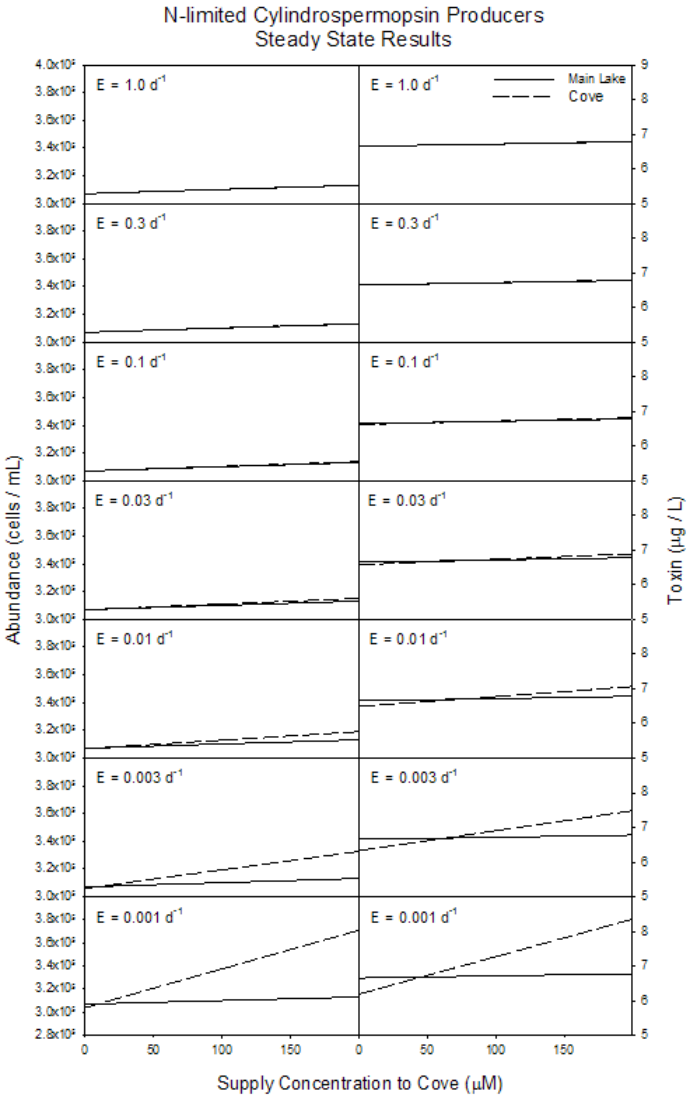

Figure 5.5.6. Abundance and toxin concentration predicted by the cove-main lake model at steady state for N-limited cylindrospermopsin producers for varying exchange rates (E) and nutrient supply concentrations to the cove (R_2^{in}).

For both models, sensitivity analyses also explored steady state predictions in response to changes in toxin production (ε) and decay (k) coefficients. Increasing the production coefficient or decreasing the decay coefficient always increased predicted toxin concentrations (with opposite results for opposite changes). However, even very large changes in these coefficients did not affect predicted spatial distributions, so results are not shown.

Extreme flow events were predicted to have a strong influence on dynamics of harmful algae and their toxins, with washout occurring for dilution rates exceeding about 0.1 d^{-1}. Small residual algal populations permitted recovery from such events, but low abundance and lack of toxicity could persist several months past washout. For example, using dilution rates from a high flow year in Lake Granbury, Texas, P-limited flagellates

suppressed by floods in late April did not recover their previous abundance until late November, and toxin concentration did not recover until December (Fig. 5.5.7). Adding temperature-dependent growth kinetics to the simulation shortened the predicted time to recover to August, because late summer – early autumn temperatures are similar to the modeled optimum for flagellate growth. Temperatures at this time increased the potential growth rate in relation to realized, nutrient-limited growth rate, and enhanced predicted toxin production by flagellates (Fig. 5.5.7, compare top and bottom panels). Spatially averaged abundance and toxin concentrations predicted for cyanobacteria were very similar to those shown for flagellates: spring flooding suppressed abundance and toxicity for weeks to months, which were otherwise predicted to be high, and enhanced by high temperatures assumed to favor cyanobacterial growth (results not shown).

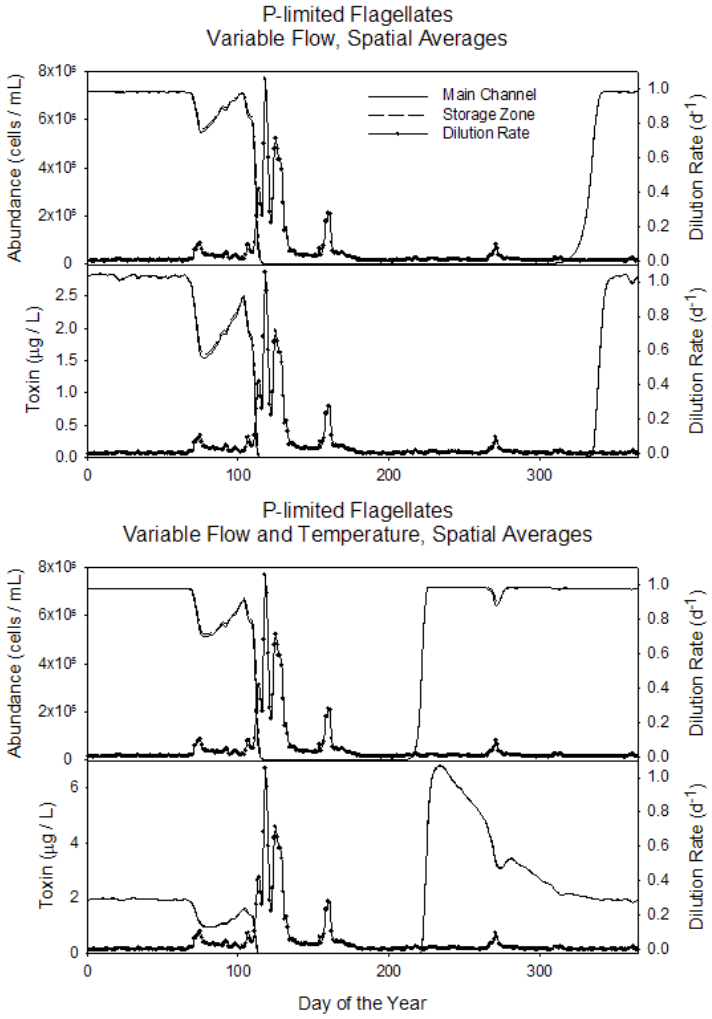

Figure 5.5.7. Spatially-averaged algal abundance and toxin concentration predicted by the riverine reservoir model in response to variable flow.

During periods of time with flows much lower than those high enough to wash out algal populations, the riverine reservoir model predicted that longitudinal distributions of abundance and toxin concentration would be near-uniform (e.g. Fig. 5.5.8). However,

flows approaching those causing washout had Pe numbers in the critical range for producing longitudinal variations. In all cases, predicted transient distributions of algal abundance in the main channel and the storage zone during such critical flows resembled steady state distributions, with low abundance upstream and higher abundance downstream (e.g. Fig. 5.5.8, around day 80). Predicted toxin concentrations showed similar longitudinal distributions in response to flow variation for P-limited flagellates (e.g. Fig. 5.5.9). However, predicted toxin concentrations for cylindrospermopsin producers showed maxima in the upstream reaches for variable, but critical flow conditions (e.g. Fig. 5.5.10).

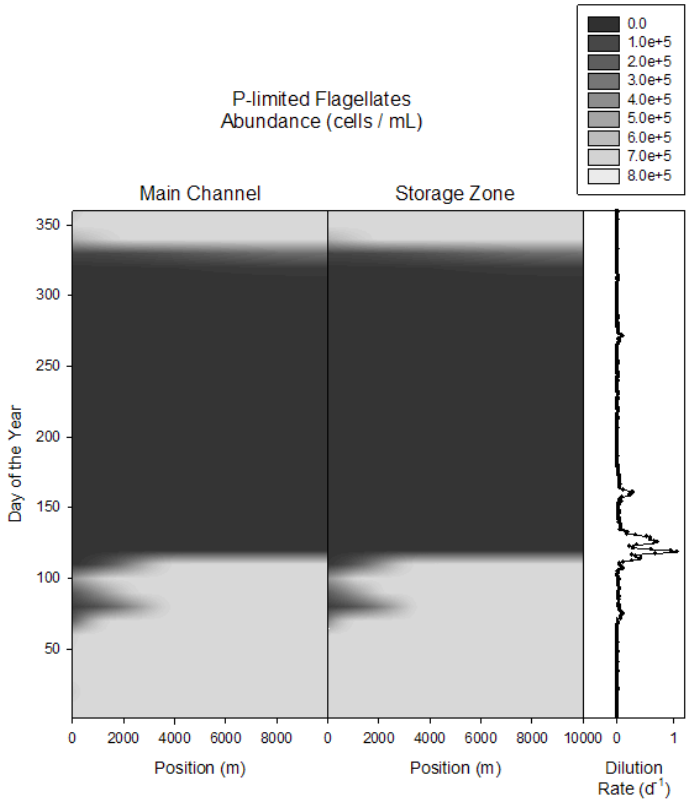

Figure 5.5.8. Spatial distributions of algal abundance predicted by the riverine reservoir model in response to variable flow.

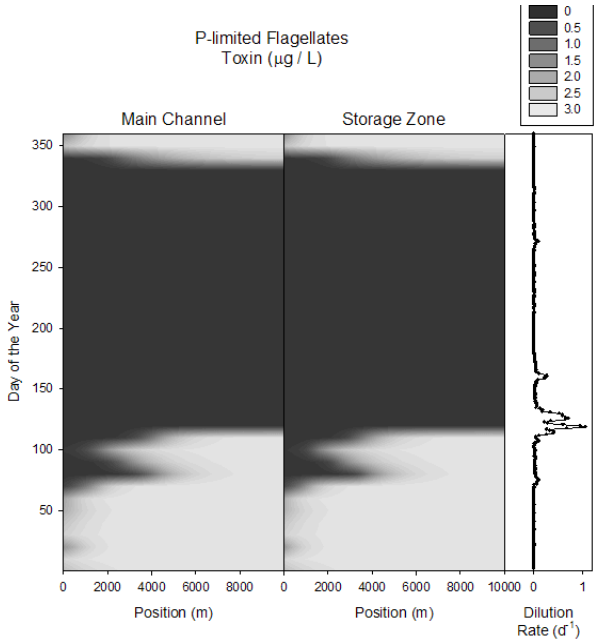

Figure 5.5.9. Spatial distributions of toxin concentration predicted by the riverine reservoir model in response to variable flow.

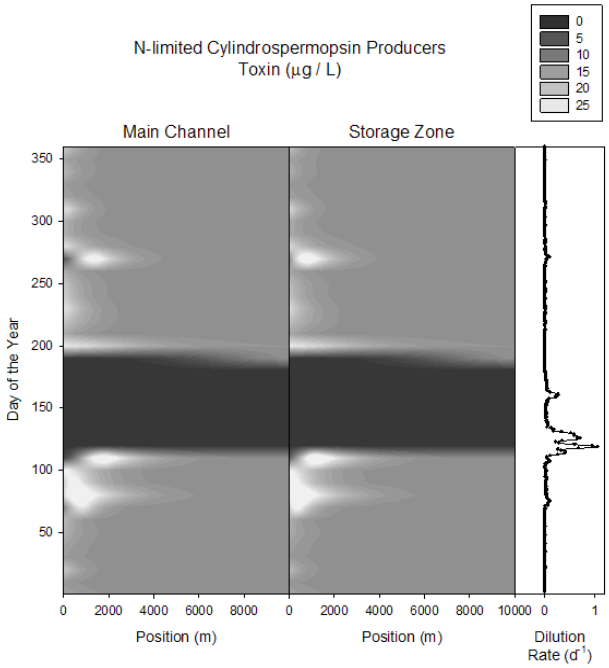

Figure 5.5.10. Spatial distributions of toxin concentration predicted by the riverine reservoir model in response to variable flow.

In all variable flow simulations, algal abundance and toxin concentrations were predicted to be similar in the main channel and storage zone at most times (e.g. Figs. 5.5.7 – 5.5.10). However, during high flows approaching or exceeding those producing washout,

large transient differences were predicted in upstream reaches, with the storage zone having several-fold larger algal abundance and toxin concentration than the main channel (e.g. Fig. 5.5.11).

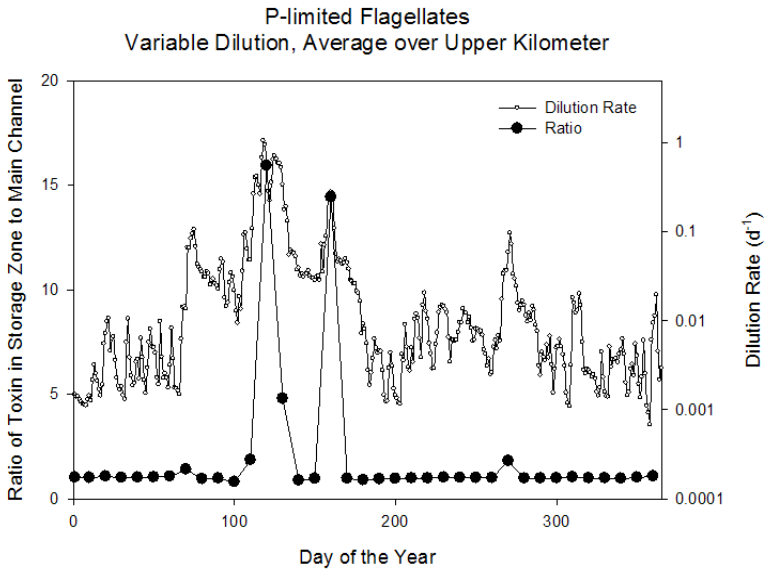

Figure 5.5.11. Comparison of toxin concentrations predicted by the riverine reservoir model for the storage zone and the main channel in response to variable flow.

Under most conditions explored, the cove-main lake model also predicted that a fringing cove would have similar algal abundance and toxin concentration to the main lake. Exceptions occurred on a transient basis in response to high flow, but only for coves that were relatively isolated from the main lake (with exchange rates $\leq$ about 0.01 d^{-1}), receiving much higher nutrient supply (e.g. Fig. 5.5.12). The cove-main lake model was also less susceptible than the riverine reservoir model to washout and prolonged low algal populations during high flow events (e.g. compare Fig. 5.5.12 to Fig. 5.5.7).

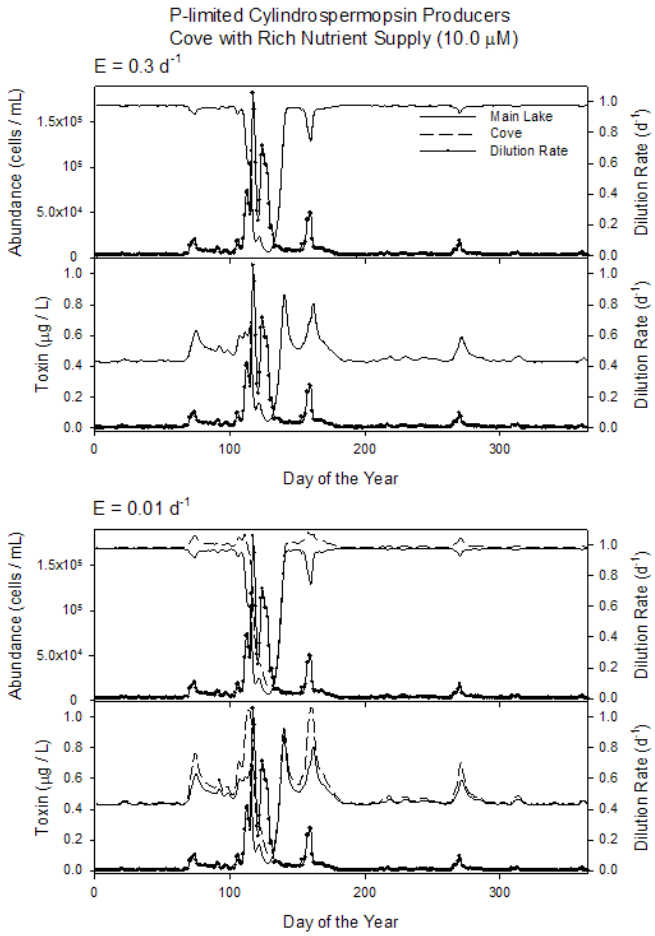

Figure 5.5.12. Algal abundance and toxin concentration predicted by the cove-main lake model in response to variable flow.

5.5.6 Discussion

This study examines the impact of flow on persistence of harmful planktonic algae, their accumulation to high abundance during blooms, and the development of toxicity in riverine habitats. Flow has long been recognized as important for planktonic dynamics in such habitats, and it has been suggested that hydraulic storage zones might be important in persistence and accumulation of phytoplankton in general (Reynolds, 1990). Formal modeling of that possibility is more recent, but has confirmed that hydraulic storage zones, such as those in the riverine reservoir model presented here, do contribute to persistence of planktonic algae (Grover *et al.*, 2009). The strong effect of flow on population dynamics of harmful algae has been confirmed by recent observations in riverine reservoirs (Roelke *et al.*, 2010a, this volume). Flow events of the magnitude used in simulations presented here are strong enough to terminate blooms, and both observations and the modeling done here suggest that harmful algae remain sparse for weeks to months after such events.

This study also focused on the spatial patterns that develop in response to flow variation: longitudinal variations along the axis of flow, and differences between main channels where flow is strong and the fringing coves that compose the hydraulic storage zone. Steady state models suggest some important principles. Longitudinal patterns are most likely to develop in a critical range of flows (identified by Pe ≈ 10 – 100) just below those strong enough to wash out planktonic algae. Persistent differences between coves and the main channel are most likely to develop when coves have strong hydraulic isolation and high nutrient loading, and are located in upstream reaches.

The signatures of these steady state patterns were partially maintained in dynamic simulations of variable flow. Strong longitudinal variations arose when flow events were in the critical range, and differences between coves and the main channel were often small. The most important qualification is that transient differences between coves and the main channel could be large in the aftermath of strong flow events. When high flows affect an established, toxic bloom, coves act as expected for hydraulic storage zones: algal abundance and toxin concentration remain high while washout occurs in the main channel. This retention of harmful algae and toxins is predicted to persist for tens of days during extended, high-flow events. Organisms moving to the slower waters of the hydraulic storage zone to avoid downstream transport in the main channel could suffer extended toxicity.

The spatial patterns predicted by this study should be testable with data that are often collected in riverine reservoirs. For example, Roelke *et al.* (2010a) documented the washout of a toxic bloom by a strong flow event. However, the spatial and temporal resolution of many monitoring programs might be too coarse to detect some of the predicted patterns. Transient patterns produced by the models presented here often lasted less than one month, but could persist for 7 – 10 days, and thus might be detected by weekly sampling. Ideally, spatial coverage would be synoptic. In cases where blooms are largely monospecific, continuous spatial sampling of *in vivo* chlorophyll (e.g. Roelke *et al.*, 2010a) would suffice to document the distribution of harmful algae.
In some reservoirs and other riverine habitats where toxic blooms have occurred, there might be opportunities to suppress blooms by controlled flow management (Maier *et al.*, 2001; Mitrovic *et al.*, 2003; 2010; Roelke *et al.*, 2010a). Flow in many river systems is regulated, often to suppress flooding, which can have negative ecological consequences (Dewson *et al.*, 2007). Controlled flooding from upstream reservoirs could have benefits beyond suppressing harmful algae, such as restoring riparian vegetation (Stromberg *et al.*, 2007), and thus contribute to multiple objectives in the management of river ecosystems.

For large reservoirs prone to toxic, fish-killing blooms, such as those of *P. parvum*, smaller areas such as coves might be treated to suppress blooms or mitigate toxicity and provide a refuge for fish (Roelke *et al.*, 2010c; Rodgers *et al.*, 2010). The models examined here suggest that hydraulic isolation of coves will enhance such efforts. Coves often have short hydraulic residence times and relatively rapid exchange with the main lake body (Monismith *et al.*, 1990; James *et al.*, 1994). Treatment to mitigate toxic blooms could be ineffective unless a cove has an unusual degree of hydraulic isolation, or such isolation is effected with structures that impede flow.

Ecosystem management of harmful algae through enhanced flow or mitigation treatments within coves will carry costs and risks. It will be helpful to support any such effort with modeling. Ideally, models to support such management would be more sophisticated and tailored to specific sites than the generalized theoretical models presented here. These models were deliberately simplified to have a minimally realistic portrayal of biological and physical processes, and explored in ways that emphasized the potential impact of flow. Necessary elaborations to support management decisions could include more complete physical description, such as variable channel geometry, spatially-varying advection and dispersion coefficients, and biological realism in the form of competitors, grazers and pathogens of harmful algae.

The simple models explored here neglect vertical variations and light limitation is not considered. Shallow, riverine reservoirs often have average irradiance above the likely limiting levels for algae (e.g. Grover *et al.*, 2010), though deeper reservoirs can display light limitation (Grover and Chrzanowski, 2004). Sediment loads associated with high flow events often reduce irradiance in such reservoirs, which could enhance the predicted suppression of harmful algae. Given the neglect of vertical variation and light limitation in the models studied here, they apply best to shallow systems that do not stratify. In deeper riverine systems, flow interacts with stratification to affect dynamics of algal blooms (Sherman *et al.*, 1998). Moreover, production and degradation of dissolved toxins are more complex than the simple idealizations considered here (e.g. Baker *et al.*, 2007; Preußel *et al.*, 2009). This study and others (Maier *et al.*, 2001; Roelke *et al.*, 2010a) suggest that flow manipulations can assist management of harmful algae in riverine systems, and provide a motivation for continued development of mathematical models.

5.6 References

American Public Health Association, American Water Works Association, and Water Environment Foundation. (1998). *Standard Methods for the Examination of Water and Wastewater, 20th ed*. American Public Health Association, Washington, DC, USA.

Antoniou, M. (2008). LC/MS/MS structure elucidation of reaction intermediates formed during the TiO_2 photocatalysis of microcystin-LR. *Toxicon* 51: 1103-1118.

Armstrong, F.A., and Sterns, C.R. (1967). The measurement of upwelling and subsequent biological processes by means of the Technicon Autoanalyzer and associated equipment. *Deep-Sea Res I* 14:381-389.

Baker, J.W., Grover, J.P., Brooks, B.W., Ureña-Boeck, F., Roelke, D.L., Errera, R., and Kiesling, R.L. (2007). Growth and toxicity of Prymnesium parvum (Haptophyta) as a function of salinity, light and temperature. *J. Phycol.*, 43, 219-227.

Baker, J.W., Grover, J.P., Ramachandrannair, R., Black, C., Valenti Jr., T.W., Brooks, B.W., and Roelke, D.L. (2009). Growth at the edge of the niche: an experimental study of the harmful alga Prymnesium parvum. *Limnol. Oceanogr.*, 54, 1679–1687.

Barkoh, A., Smith, D.G., and Schlechte, J.W. (2003). An effective minimum concentration of un-ionized ammonia nitrogen for controlling Prymnesium parvum. *N. Am. J. Aquacult.*, 65, 220-225.

Barreiro, A., Guisande, C., Maneiro, I., Lien, T.P., Legrand, C., Tamminen, T., Lehtinen, S., Uronen, P., and Granéli, E. (2005). Relative importance of the different negative effects of the toxic haptophyte *Prymnesium parvum* on Rhodomonas salina and Brachionus plicatilis. *Aquat Microb Ecol* 38:259-267.

Bencala, K.E., and Walters, R.A. (1983). Simulation of solute transport in a mountain pool-and-riffle stream: a transient storage model. *Water Resour. Res.*, **19**, 718-724.

Berges, J.A., Franklin, D.J., and Harrison, P.J. (2001). Evolution of an artificial seawater medium: improvements in enriched seawater, artificial water over the last two decades. *J. Phycol*., 37**:** 1138-1145.

Berry, J.P., Gantar, M., Perez, M.H., *et al.* (2008). Cyanobacterial toxins as allelochemicals with potential applications as algaecides, herbicides and insecticides. *Marine Drugs*, **6**, 117-146.

Brooks, B.W., James, S.V., Valenti Jr., T.W., Urena-Boeck, F., Serrano, C., Berninger, J.P., Schwierzke, L., Mydlarz, L.D., Grover, J.P., and Roelke, D.L. (2010). Comparative toxicity of Prymnesium parvum in inland waters. *J. Am. Water Res. Assoc.* 46, 45-62.

Buskey, E.J., Wysor, B., and Hyatt, C. (1998). The role of hypersalinity in the persistence of the Texas 'brown tide' bloom in the Laguna Madre. *J. Plankton Res.*, 20, 1553–1565.

Cai, Y., and McCarl, B.A. (2009). Agricultural & Applied Economics Association Annual Meeting, Milwaukee, Wisconsin, July 26-29.

Carmichael, W.W. (2001). *Assessment of Blue-Green Algal Toxins in Raw and Finished DrinkingWater*. AWWA Research Foundation, Denver, CO.

Chakraborty, S., Roy, S., and Chattopadhyay, J. (2008). Nutrient-limited toxin production and the dynamics of two phytoplankton in culture media: a mathematical model. *Ecol. Model.*, **213**, 191-201.

Chang, F.H., Uddstrom, M.J., Pinkerton, M.H., and Richardson, K.A., (2008). Characterizing the 2002 toxic Karenia concordia (Dinophyceae) outbreak and its development using satellite imagery on the north-eastern coast of New Zealand. *Harmful Algae*, 7, 532-544.

Chapra, S.C. (1997). *Surface Water-Quality Modeling*. McGraw-Hill, N.Y.

Chen, W., Song, L., Ou, D. *et al*. (2005). Chronic toxicity and responses of several important enzymes in *Daphnia magna* on exposure to sublethal microcystin-LR. *Environ*. *Toxicol*. 20: 323-330.

Chorus, I., and Bartram, J. (eds.) (1999). *Toxic Cyanobacteria in Water, A Guide to their public health consequences, monitoring and management*. WHO, Spon Press, London.

Cousins, I.T., Bealing, D.J., James, H.A., *et al.* (1996). Biodegradation of microcystin-LR by indigenous mixed bacterial populations. *Water Res.*, **30**, 481-485.

Davis, J.R., and Koop, K. (2006). Eutrophication in Australian rivers, reservoirs and estuaries – a southern hemisphere perspective on the science and its implications. *Hydrobiologia*, **559**, 23-76.

De Maagd, P.G.J., Hendricks, A.J., Seinen, W., *et al*. (1999). pH dependent hydrophobic of the cyanobacteria toxin microcystin-LR. *Water Res*., 33, 677-680.

DeMott, W.R., Zhang, Q.X., and Carmichael, W.W. (1991). Effects of toxic cyanobacteria and purified toxins on the survival and feeding of a copepod and three species of Daphnia. *Limnol*. *Oceanog*., 36 (7), 1346-1357.

Dewson, Z.S., James, A.B.W., and Death, R.G. (2007). A review of the consequences of decreased flow for instream habitat and macroinvertebrates. *J. N. Am. Benthol. Soc.*, **26**, 401-415.

Dobbins, L.L., Brain, R.A., and Brooks, B.W. (2008). Comparison of the sensitivities of common in vitro and in vivo assays of estrogenic activity: Application of chemical toxicity distributions. *Environ. Toxicol. Chem.*, 28: 2608-2616.

Dobbins, L.L., Usenko, S., Brain, R.A., and Brooks, B.W. (2009). Probabilistic ecological hazard assessment of parabens using *Daphnia magna* and *Pimephales promelas*. *Environ. Toxicol. Chem.*, 28: 2744-2753.

Errera, R.M., Roelke, D.L., Kiesling, R., Brooks, B.W., Grover, J.P., Schwierzke, L., Ureña-Boeck, F., Baker, J.W., and Pinckney, J.L. (2008). The effect of imbalanced nutrients and immigration on Prymnesium parvum community dominance and toxicity: Results from in-lake microcosm experiments, Texas, US. *Aquat. Microb. Ecol.*, 52, 33-44.

Falconer, I.R., and Humpage, A.R. (2006). Cyanobacterial (blue-green algal) toxins in water supplies: cylindrospermopsins. *Environ. Toxicol.*, **21**, 299-304

Fistarol, G.O., Legrand, C., and Granéli, E. (2003). Allelopathic effect of Prymnesium parvum on a natural plankton community. *Mar. Ecol. Prog. Ser.*, 255, 115-125.

Fistarol, G.O., Legrand, C., and Granéli, E. (2005). Allelopathic effect on a nutrient-limited phytoplankton species. *Aquat. Microb. Ecol.*, 41, 153-161.

Fristachi, A., Rice, G., Steevens, J., *et al*. (2007). A preliminary exposure assessment of microcystins from consumption of drinking water in the United States. *Lake Reserv. Man*., 23, 203-210.

Graham, J.L., and Jones, J.R. (2007). Microcystin distribution in physical size class separations of natural plankton communities. *Lake Reserv*. *Man*., 23, 161-168.

Granéli, E., and Johansson, N. (2003). Effects of the toxic haptophyte Prymnesium parvum on the survival and feeding of a ciliate: the influence of different nutrient conditions. *Mar. Ecol. Prog. Ser.*, 254, 49-56.

Granéli, E., and Hansen, P.J. (2006). Allelopathy in harmful algae: A mechanism to compete for resources? Ecology of Harmful Algae, E. Granéli and J.T. Turner (eds.), Springer, *Berlin Heidelberg*, pp. 189-202.

Granéli, E., and Salomon, P.S. (2010). Factors influencing allelopathy and toxicity in Prymnesium parvum. *J. Am. Water Res. Assoc.*, 46, 108-120.

Grover, J.P. (1989). Phosphorus-dependent growth kinetics of 11 species of freshwater algae. *Limnol. Oceanogr.*, 34, 341-348.

Grover, J.P., Sterner, R.W., Robinson, J.L. (1999). Algal growth in warm-temperate reservoirs: nutrient-dependent kinetics of individual taxa and seasonal patterns of dominance. *Arch. Hydrobiol.*, 145, 1-23.

Grover, J.P., Baker, J.W., Ureña-Boeck, F., Brooks, B.W., Errera, R., Roelke, D.L., and Kiesling, R.L. (2007). Laboratory tests of ammonium and barley straw extract as agents to suppress abundance of the harmful alga Prymnesium parvum and its toxicity to fish. *Water Res.*, 41, 2503-2512.

Grover, J.P., and Chrzanowski, T.H. (2004). Limiting resources, disturbance, and diversity in phytoplankton communities. *Ecol. Monogr.* **74,** 533-551.

Grover, J.P., Hsu, S.-B., and Wang, F.-B. (2009). Competition and coexistence in flowing habitats with a hydraulic storage zone. *Math. Biosci.*, 222, 42-52.

Grover J.P., Baker, J.W., Roelke, D.L., and Brooks, B.W. (2010). Mathematical models of population dynamics of *Prymnesium parvum* in inland waters. *J. Am. Water Res. Assoc.*, 46, 92-107.

Grover, J.P., Crane, K.W., Baker, J.W., Brooks, B.W., and Roelke, D.L. (2010). Spatial variation of harmful algae and their toxins in flowing-water habitats: a theoretical exploration. *J. Plankton Res.*, In Press.

Guillard, R.R.L. (1975). Culture of phytoplankton for feeding marine invertebrates. In Smith, W.L. and Chanley, M.H. (eds), *Culture of Marine Invertebrate Animals*. Plenum Press, New York, pp. 29-60.

Hamilton, M.A., Russo, R.C., and Thurston, R.V. (1977). Trimmed Spearman-Karber method for estimating median lethal concentrations in toxicity bioassays. *Environ Sci Tech* 117:714-719; correction 12:417(1978).

Hambright, K.D., Zamor, R.M., Easton, J.D., Glenn, K.L., Remmel, E.J., Easton, A.C. (2010). Temporal and spatial variability of an invasive toxigenic protist in a North American subtropical reservoir. *Harmful Algae*. In Press. doi:10.1016/j.hal.2010.04.006.

Hansen, P.J., Bjørnsen, P.K., and Hansen, B.W. (2010). Zooplankton grazing and growth: scaling within the 2-2,000-µm body size range. *Limnol. Oceanogr.* 42: 687-704.

Harada, K., and Tsuji, K. (1998). Persistence and decomposition of hepatotoxic microcystins produced by cyanobacteria in natural environment. *J. Toxicol.-Tox. Rev.*, 17: 385-403.

Hawkins, P.R., Putt, E., Falconer, I., *et al.* (2001). Phenotypical variation in a toxic strain of the phytoplankter, *Cylindrospermopsis raciborskii* (Nostocales, Cyanophyceae) during batch culture. *Environ. Toxicol.*, 16, 460-476.

Hobbie, J.E., Daley, R.J., and Jasper, S. (1977). Use of nuclepore filters for counting bacteria by fluorescence microscopy. *Applied and Environmental Microbiology*, 33: 5: 1225-1228.
Hoppe, H. (2003). Phosphatase activity in the sea. *Hydrobiologia* 493: 187-200.
Jacoby, J.M., Collier, D.C., Welch, E.B., Hardy, F.J., and Crayton, M. (2000). Environmental factors associated with a toxic bloom of Microcystis aeruginosa. *Can. J. Fish. Aquat. Sci.*, 57, 231-240.
Jacoby, J.M., and Kann, J. (2007). The occurrence and response to toxic cyanobacteria in the Pacific Northwest, North America. *Lake Res*. *Man*. 23: 123-143.
James, W.F., Barko, J.W., and Eakin, H.L. (1994). Convective water exchanges during differential cooling and heating: implications for dissolved constituent transport. *Hydrobiologia*, **294**, 167-176.
James, T.L., and De La Cruz, A. (1989). *Prymnesium parvum* Carter (Chrysophyceae) as a suspect of mass mortalities of fish and shellfish communities in western Texas. *Texas J. Sci.*, 41, 429–430.
James, S.V., Valenti, T.W., Prosser, K.N., *et al.* (2010, In press). Sunlight amelioration of *Prymnesium parvum* acute toxicity to fish. *J. Plankton Res.*
James, S.V., Valenti, T.W., Roelke, D.L., Grover, J.P., and Brooks, B.W. (2010, In press). Probabilistic ecological assessment of microcystin-LR allelopathy to *Prymnesium parvum*. *J. Plankton Res.*
Johansson, N., and Granéli, E. (1999). Influence of different nutrient conditions on cell density, chemical composition and toxicity of *Prymnesium parvum* (Haptophyta) in semi-continuous cultures. *J. Exp. Mar. Biol. Ecol.* 239: 243-258.
Jones, G.J., and Orr, P.T. (1994). Release and degradation of microcystins following algicide treatment of a *Microcystis aeruginosa* bloom in a recreational lake, as determined by HPLC and protein phosphatase inhibition assay. *Water Res*., 28(4), 871-876.
Jonsson, P.R., Pavla, H., and Toth, G. (2009). Formation of harmful algal blooms cannot be explained by allelopathic interactions. *PNAS*, 106(27), 11177-11182.
Kearns, K.D., and Hunter, M.D. (2001). Toxin-producing *Anabaena flos-aquae* induces settling of *Chlamydomonas reinhardtii*, a competing motile alga. *Microb*. *Ecol*., 42**:** 80-86.
Ketchum, B.H. (1951). The flushing of tidal estuaries. *Sewage and Industrial Wastes*, 23: 198-209.
Ketchum, B.H. (1954). The relation between circulation and planktonic populations in estuaries. *Ecology*, 35: 191-200.
Kiviranta, J., Sivonen, K., Niemela, S.I., *et al*. (1991). Detection of toxicity of cyanobacteria by *Artemia salina* bioassay. *Environ*. *Tox*. *Water Qual*., 6, 423-436.
Kirk, J.T.O. (1984). *Light and Photosynthesis in Aquatic Ecosystems, 2nd edition*. Cambridge University Press, Cambridge, UK.
Kodama, M., Doucette, G.J., Green, D.H. (2006). Relationships between bacteria and harmful algae, pp. 243-258. In E. Graneli and J.T. Turner (Eds.) *Ecology of Harmful Algae*. Springer-Verlag, Berlin.
Kotak, B.G., Zurawell, R.W., Prepas, E.E., *et al*. (1996). Microcystin-LR concentration in aquatic food web compartments from lakes of varying trophic status. *Canadian J. Fish Aquat*. *Sci*., 53(9), 1974-1985.

Kotak, B.G., and Zurawell, R.W. (2007). Cyanobacterial toxins in Canadian freshwaters: A review. *Lake Res*. *Man*., 23,109-122.

Krogman, D.W., Butalla, R., and Sprinkle, J. (1986). Blooms of cyanobacteria on the Potomac River. *Plant Physiol.*, 80, 667-671.

Larsen, A., and Bryant, S. (1998). Growth rate and toxicity of *Prymnesium parvum* and *Prymnesium patelliferum* (Haptophyta) in response to changes in salinity, light, and temperature. *Sarsia*., 83, 409-418.

Leibold, M.A., Miller, T.E. (2004). From metapopulations to metacommunities. Ecology, Genetics, and Evolution of Metapopulations, I. Hanski and O.E. Gaggiotti (eds.), Elsevier, Boston. pp. 133-150.

Lekan, D., and Tomas, C.R. (2010). The brevetoxin and brevenal composition of three *Karenia brevis* clones at different salinities and nutrient conditions. *Harmful Algae*, **9**, 39-47.

Lindehoff, E., Granéli, E., and Granéli, W. (2009). Effect of tertiary sewage effluent additions on *Prymnesium parvum* cell toxicity and stable isotope ratios. *Harmful Algae*, 8, 247-253.

Liu, Y., Song, L., Li, X., *et al*. (2002). The toxic effects of microcystin-LR on embryo-larval and juvenile development of loach, *Misguruns mizolepis Gunthe*. *Toxicon*, 40: 395-399.

Lopez, C.B., Jewett, E.B., Dortch, Q., *et al*. (2008). Scientific assessment of freshwater harmful algal blooms. *Interagency Working Group on Harmful Algal Blooms, Hypoxia, and Human Health of the Joint Subcommittee on Ocean Science and Technology*. Washington, DC.

Lutz-Carrillo, D.J., Southard, G.M., and Fries, L.T. (2010). Global genetic relationships among isolates of golden alga (Prymnesium parvum). *J. Am. Water Res. Assoc.*, 46, 24-32.

Mackey, M., Mackey, D., Higgins, H., and Wright, S. (1997). CHEMTAX—a program for estimating class abundances from chemical markers: application to HPLC measurements of phytoplankton. *Mar Ecol Prog Ser* 144: 265-83.

MacKintosh, C., Beattie, K., Klumpp, S., *et al*. (1990). Cyanobacterial microcystin-LR is a potent and specific inhibitor of protein phosphatases 1 and 2A from both mammals and higher plants. *FEBS Lett*., 264, 187-192.

Madden, C.J., and Day, Jr., J.W. (1992). An instrument system for high speed mapping of chlorophyll-a and physico-chemical variables in surface waters. *Estuaries* 15:421-427.

Manning, S.R., and La Claire, J. (2010). Prymnesins: Toxic metabolites of the golden alga, *Prymnesium parvum* Carter (Haptophyta). *Mar. Drugs*, 8, 678-704**.**

Maier, G. R., Burch, M. D., and Bormans, M. (2001). Flow management strategies to control blooms of the cyanobacterium, *Anabaena circinalis*, in the river Murray at Morgan, South Australia. *Regul. Rivers: Res. Mgmt.*, 17, 637-650.

Martin, J.L., and McCutcheon, S.C. (1999). *Hydrodynamics and Transport for Water Quality Modeling*. Lewis Publishers, Boca Raton, Florida, USA.

Martin-Cereceda, M., Novarino, G., and Young, J.R. (2003). Grazing by *Prymnesium parvum* on small diatoms. *Aquat. Microb. Ecol*. 33: 191-199

Martinez, C.J., and Wise, W.R. (2003). Analysis of constructed treatment wetland hydraulics with the transient storage model OTIS. *Ecol. Engin.* 20, 211-222.

McCune, B., and Mefford, M.J. (1999). *PC-ORD, Multivariate Analysis of Ecological Data*. Version 5.0, MjM Software Design.
McCune, B., and Grace, J.B. (2002). *Analysis of Ecological Communities, 1st ed*. MjM Software Design.
McDermott, C.M., Feola, R., and Plude, J. (1995). Detection of cyanobacterial toxins (microcystins) in waters of northeastern Wisconsin by a new immunoassay technique. *Toxicon*, 33, 1433-1442.
Metcalf, J.S., Lindasay, J., Beattie, K.A., *et al*. (2002). Toxicity of cylindrospermopsin to the brine shrimp *Artemia salina*: comparisons with protein synthesis inhibitors and microcystins. *Toxicon*, 40, 1115-1120.
Michaloudi, E., Moustaka-Gouni, M., Gkelis, S., and Pantelidakis, K. (2009). Plankton community structure during an ecosystem disruptive algal bloom of *Prymnesium parvum*. *J. Plankt. Res.*, 31, 301-309.
Mitrovic, S.M., Allis, O., Furey, A., *et al*. (2005). Bioaccumulation and harmful effects of microcystin-LR in the aquatic plants *Lemna minor* and *Wolffia arrhiza* and the filamentous alga *Chladophora fracta*. *Ecotox*. *Environ*. *Safe*., 61, 345-352.
Mitrovic, S.M., Chessman, B.C., Davie, A., Avery, E.L., and Ryan, N. (2008). Development of blooms of *Cyclotella meneghiniana* and Nitzschia spp. (*Bacillariophyceae*) in a shallow river and estimation of effective suppression flows. *Hydrobiologia*, 596, 173–185
Mitrovic, S.M., Hardwick, L., Oliver, R., *et al.* (2010). Use of flow management to control saxitoxin producing cyanobacterial blooms in the Lower Darling River, Australia. *J. Plankton Res.* (submitted).
Mitrovic, S.M., Oliver, R.L., Rees, C., *et al.* (2003). Critical flow velocities for the growth and dominance of *Anabaena circinalis* in some turbid freshwater rivers. *Freshwater Biol.* 48, 164-174.
Monismith, S.G., Imberger, J., and Morrison, M.L. (1990). Convective motions in the sidearm of a small reservoir. *Limnol. Oceanogr.*, 35, 1676-1702.
Moustaka-Gouni, M., Vardaka, E., Michaloudi, E., Kormas, K.A., Tryfon, E., Mihalatou, H., Gkelis, S., and Lanaras, T. (2006). Plankton food web structure in a eutrophic polymictic lake with a history of toxic cyanobacterial blooms. *Limnol. Oceanogr.*, 51, 715-727.
Murata, M., and Yasumoto, T. (2000). The structure elucidation and biological activities of high molecular weight algal toxins: maitotoxins, prymnesins and zooxanthellatoxins. *Nat Prod. Rep.*, 17, 293-314.
Murphy, T.P., Irvine, K., Guo, J., *et al*. (2003). New microcystin concerns in the lower Great Lakes. *Water Qual*. *Res*. *J. Canada*, 38(1), 127-140.
Nygaard, K., and Tobiesen, A. (1993). Bacterivory in algae: a survival strategy during nutrient limitation. *Limnol. Oceanogr.* 38: 273-279.
Oh, S.J., Matsuyama, Y., Nagai, S., Itakura, S., Yoon, Y.H., and Yang, H.S. (2009). Comparative study on the PSP component and toxicity produced by Alexandrium tamiyavanichii (Dinophyceae) strains occurring in Japanese coastal water. *Harmful Algae*, 8, 362-368.
Ou, D., Song, L., Gan, N., *et al*. (2005). Effects of microcystins on and toxin degradation by *Poterioochromonas* sp. *Environ*. *Toxicol*., **20**:373-380.

Park, R.A., and Clough, J.S. (2004). *AQUATOX (release 2) Modeling Environmental Fate and Ecological Effects in Aquatic Ecosystems*. Volume 2: Technical Documentation. EPA-823-R-04-002. U.S. Environmental Protection Agency, Washington, D.C.

Pengerud, B., Skjoldal, E.F., and Thingstad, T.F. (1987). The reciprocal interaction between degradation of glucose and ecosystem structure: studies in mixed chemostat cultures of marine bacteria, algae, and bacterivorous nanoflagellates. *Mar. Ecol. Prog. Ser.* 35: 111-117.

Pflugmacher, S. (2002). Possible allelopathic effects of cyanotoxins, with reference to microcystin-LR, in aquatic ecosystems. *Environ*. *Toxicol*., **17**: 407-413.

Pinckney, J.L., Paerl, H.W., Harrington, M.B., and Howe, K.E. (1998). Annual cycles of phytoplankton community structure and bloom dynamics in the Neuse River Estuary, North Carolina. *Mar Biol* 131:371-82.

Posthuma, L., Suter II, G.W., and Traas, T.P. (2002). *Species Sensitivity Distributions in Ecotoxicology*. Lewis Publishers, Boca Raton, Florida.

Prakash, S., Lawton, L.A., and Edwards, C. (2009). Stability of toxigenic Microcystis blooms. *Harmful Algae*, 8, 377-384.

Press, W.H., Flannery, B.P., Teukolsky, S.A., *et al.* (1986). *Numerical Recipes*. Cambridge University Press, Cambridge.

Preußel, K., Wessel, G., Fastner, J., *et al.* (2009). Response of cylindrospermopsin production and release in *Aphanizomenon flos-aquae* (Cyanobacteria) to varying light and temperature conditions. *Harmful Algae*, **8**, 645-650.

Reinikainen, M., Lindvall, F., Meriluoto, J.A.O., *et al*. (2002). Effects of dissolved cyanobacterial toxins on the survival and egg hatching of estuarine calanoid copepods. *Marine Biol*., **140:** 577-583.

Reynolds, C.S. (1990). Potamoplankton: paradigms, paradoxes and prognoses. In Round, F E. (ed.), *Algae and Aquatic Environment*. Biopress, Bristol, UK, pp. 285-311.

Rodgers, J.H., Johnson, B.M., and Bishop, W.M. (2010). Comparison of three algaecides for controlling the density of *Prymnesium parvum*. *J. Am. Water Resources Assoc.*, **46**, 153-160.

Roelfsema, C.M., Phinn, S.R., Dennison, W.C., Dekker, A.G., Brando, V.E. (2006). Monitoring toxic cyanobacteria Lyngbya majuscula (Gomont) in Moreton Bay, Australia by integrating satellite image data and field mapping. *Harmful Algae*, 5, 45-56.

Roelke, D.L., Augustine, S., and Buyukates, Y. (2003). Fundamental predictability in multispecies competition: The influence of large disturbance. *The American Naturalist*, 162: 615-623.

Roelke D.L., Errera, R., Kiesling, R., Brooks, B.W., Grover, J.P., Schwierzke, L., Ureña-Boeck, F., Baker, J., and Pinckney, J.L. (2007a). Effects of nutrient enrichment on *Prymnesium parvum* population dynamics and toxicity: Results from field experiments, Lake Possum Kingdom, USA. *Aquatic Microbial Ecology*, 46:125-140.

Roelke D.L., Zohary, T., Hambright, K.D., and Montoya, J.V. (2007b). Alternative states in the phytoplankton of Lake Kinneret, Israel (Sea of Galilee). *Freshw. Biol.,* 52, 399-411.

Roelke D.L., and Eldridge, P.M. (2008). Mixing of supersaturated assemblages and the precipitous loss of species. *The American Naturalist*, 171:162-175.

Roelke D.L., and Eldridge, P.M. (2009). Losers in the 'Rock-Paper-Scissors' game: The role of non-hierarchical competition and chaos as biodiversity sustaining agents in aquatic systems. *Ecological Modelling*. In Press.

Roelke, D.L., Gable, G.M., Valenti Jr., T.W., Grover, J.P., Brooks, B.W., and Pinckney, J.L. (2010a). Hydraulic flushing as a *Prymnesium parvum* bloom-terminating mechanism in a subtropical lake. *Harmful Algae*, 9, 323–332.

Roelke, D. L., Grover, J.P., Brooks, B.W., *et al.* (2010b). A decade of fish-killing blooms in Texas: roles of hydraulic flushing and salinity. *J. Plankton Res.* In Press.

Roelke, D.L., Schwierzke, L., Brooks, B.W., *et al.* (2010c). Factors influencing *Prymnesium parvum* population dynamics during bloom initiation: results from in-lake mesocosm experiments. *J. Am. Water Resources Assoc.*, **46**, 76-91.

Salomon, P.S., and Imai, I. (2006). Pathogens of Harmful Microalgae. pp. 271-282. In E. Graneli and J.T. Turner (Eds.) *Ecology of Harmful Algae*. Springer-Verlag, Berlin.

Schwierzke, L., Roelke, D.L., Brooks, B.W., Grover, J.P., Valenti, Jr., T.W., Lahousse, M., Miller, C.J., and Pinckney, J.L. (2010). *Prymnesium parvum* population dynamics during bloom development: a role assessment of grazers and virus. *J. Am. Water Res. Assoc.* 46, 63-75.

Schwierzke-Wade, L., Roelke, D.L., Brooks, B.W., and Grover, J.P. (In Review). *Prymnesium parvum* bloom decline following an inflow and nutrient-loading event: Roles of dilution and grazing. *J. Plankt. Res.*, In Review.

Shatwell, T., Kohler, J., and Nicklisch, A. (2008). Warming promotes cold-adapted phytoplankton in temperate lakes and opens a loophole for Oscillatoriales in spring. *Global Change Biol.*, 14, 2194–2200.

Sherman, B.S., Webster, I.T., Jones, G.J., *et al.* (1998). Transitions between *Aulacoseira* and *Anabaena* dominance in turbid river weir pool. *Limnol. Oceanogr.*, **43**, 1902-1915.

Sivonen, K., and Jones, G. (1999). Cyanobacterial toxins. In: Chorus, I. and Bartram, J. (eds). *Toxic cyanobacteria in water*. Spon Press, London, pp. 41-111.

Skovgaard, A., and Hansen, P.J. (2003). Food uptake in the harmful alga Prymnesium parvum mediated by excreted toxins. *Limnol. Oceanogr.,* 48, 1161-1166.

Skovgaard, A., Legrand, C., Hansen, P.J., and Granéli, E. (2003). Effects of nutrient limitation on food uptake in the toxic haptophyte *Prymnesium parvum*. *Aquat. Microb. Ecol.* 31: 259-265.

Smith, J.L., Boyer, G.L., Mills, E., *et al*. (2007). Toxicity of microcystin-LR, a cyanobacterial toxin, to multiple life stages of the burrowing mayfly, *Hexagenia*, and possible implications for recruitment. *Environ*. *Toxicol*., 23: 499-506.

Solomon, K., Giesy, J., and Jones, P. (2000). Probabilistic risk assessment of agrochemicals in the environment. *Crop Prot*., 19: 649-655.

Sopanen, S., Koski, M., Kuuppo, P., Uronen, P., Legrand, C., Tamminen, T. (2006). Toxic haptophyte *Prymnesium parvum* affects grazing, survival, egestion and egg production of the calanoid copepods Eurytemora affinis and Acartia bifilosa. *Mar. Ecol. Prog. Ser.,* 327, 223-232.

Sopanen, S., Koski, M., Uronen, P., Kuuppo, P., Lehtinen, S., Legrand, C., and Tamminen, T. (2008). *Prymnesium parvum* exotoxins affect the grazing and viability of the calanoid copepod Eurytemora affinis. *Mar. Ecol. Prog. Ser.,* 361, 191-202.

Southard, G.M., Fries, L.T., and Barkoh, A. (2010). *Prymnesium parvum*: The Texas experience. *J. Am. Water Res. Assoc.*, 46, 14-23.
Stephan, C.E. (2006). Use of species sensitivity distributions in the derivation of water quality criteria for aquatic life by the U.S. Environmental Protection Agency. In: Posthuma, L., G.W. Suter II, T.P. Traas. *Species Sensitivity Distributions in Ecotoxicology.* Lewis Publishers, Boca Raton, Florida., pp. 211-220.
Stromberg, J.C., Beauchamp, V.B., Dixon, M.D., *et al.* (2007). Importance of low-flow and high-flow characteristics to restoration of riparian vegetation along rivers in the arid south-western United States. *Freshwater Biol.*, **52**, 651-679.
Sunda, W.G., Graneli, E., and Gobler, C.J. (2006). Positive feedback and the development and persistence of ecosystem disruptive algal blooms. *J. Phycol.*, 42, 963-974.
Tillmann, U. (2003). Kill and eat your predator: a winning strategy of the planktonic flagellate Prymnesium parvum. *Aquat. Microbial. Ecol.*, 32, 73-84.
Tillmann, U., John, U., and Cembella, A. (2007). On the allelochemical potency of the marine dinoflagellate Alexandrium ostenfeldii against heterotrophic and autotrophic protists. *J. Plank. Res.*, 29:527-543.
Touchette, B.W., Burkholder, J.M., Allen, E.H., *et al*. (2007). Eutrophication and cyanobacteria blooms in run-of-river impoundments in North Carolina, U.S.A. *Lake Res*. *Man*. 23: 179-192.
Turner, J.T. (2006). Harmful algae interactions with marine planktonic grazers. *Ecology of Harmful Algae*, E. Granéli and J.T. Turner (eds.), Springer, Berlin Heidelberg, pp. 259-270.
Twist, H., and Codd, G.A. (1997). Degradation of the cyanobacterial hepatotoxin, nodularin, under light and dark conditions. *FEMS Microbiol. Lett.*, **151**, 83-88.
U.S. Environmental Protection Agency. (1994). *10-day Chronic Toxicity Test Using Daphnia magna or Daphnia pulex*. EPA SOP#2028. Environmental Response Team, U.S. Environmental Protection Agency, Washington, DC.
U.S. Environmental Protection Agency. (2002). Methods for measuring the acute toxicity of effluents and receiving waters to freshwater and marine organisms. EPA-821-R-02-012. United States Environmental Protection Agency, Washington, DC.
Uronen, P., Lehtinen, S., Legrand, C., Kuuppo, P., Tamminen, T. (2005). Haemolytic activity and allelopathy of the haptophyte Prymnesium parvum in nutrient-limited and balanced growth conditions. *Mar Ecol Prog Ser,* 299:137-148.
Utermöhl, H. (1958). Zur Vervollkominnung der quantitativen phytoplankton methodik. *Mitteilumgen Internationale Verejnigung für Theoretische und Angewandte Limnologie*, 9:1-38.
Valenti, T.W., James, S.V., Lahousse, M., Schug, K.A., Grover, J.P., Roelke, D.L., Brooks, B.W. (2010). A potential mechanistic explanation for pH-dependant ambient aquatic toxicity of *Prymnesium parvum* Carter. *Toxicon* 55:990-998.
Van Heukelem, L., Lewitus, A.J., Kana, T.M., and Craft, N.E. (1994). Improved separations of phytoplankton pigments using temperature-controlled high performance liquid chromatography. *Mar Ecol Prog Ser* 114:303-13.
Ward, C.J., and Codd, G.A. (1999). Comparative toxicity of four microcystins of different hydrophobicities to the protozoan, *Tetrahymena pyriformis*. *J. Appl. Microb.* **86:** 874-82.

Watson, S.B. (2003). Cyanobacterial and eukaryotic algal odour compounds: Signals or by-products? *Phycologia*, 42: 332-350.
Watson, S.B., Caldwell, G., and Pohnert, G. (2009). Fatty acids and oxylipins as semiochemicals. In: Arts, M.T., M.T. Brett, and M.J. Kainz (Eds). *Lipids in Aquatic Ecosystems*. Springer, New York. p. 65-91.
Wetzel, R.G., and Likens, G.E. (1991) *Limnological Analysis*. Springer-Verlag, New York.
Wetzel, R.G. (2001). *Limnology, 3rd edition*. Academic Press, San Diego, California, US.
Williams, C.D., Aubel, M.T., Chapman, A.D., *et al*. (2007). Identification of cyanobacterial toxins in Florida's freshwater systems. *Lake Res*. *Man*. 23:144-152.
Williams, E.S., Panko, J., and Paustenbach, D.J. (2009). The European Union's REACH regulation: a review of its history and requirements. *Critical Rev*. *Tox*. **39:** 553-575.
Wright, S., Thomas, D., Marchant, H., Higgins, H., Mackey, M., and Mackey, D. (1996) Analysis of phytoplankton of the Australian sector of the Southern Ocean: comparisons of microscopy and size frequency data with interpretations of pigment HPLC data using the 'CHEMTAX' matrix factorization program. *Mar Ecol Prog Ser* 144:285-298.
Young, F.M., Metcalf, J.S., Meriluoto, J.A.O., *et al*. (2006). Production of antibodies against microcystin-RR for the assessment of purified microcystins and cyanobacterial environmental samples. *Toxicon* 48**:** 295-306.

6. PRODUCTS DEVELOPED

6.1 Publications (18 peer-reviewed journal articles)

Accepted

Grover, J.P., Crane, K.W., Baker, J.W., Brooks, B.W., and Roelke, D.L. (2010). Spatial variation of harmful algae and their toxins in flowing-water habitats: a theoretical exploration. *Journal of Plankton Research*. In Press.

James, S.V., Valenti, T.W., Roelke, D.L., Grover, J.P., Brooks, B.W. (2010). Probabilistic ecological assessment of microcystin-LR: A case study of allelopathy to *Prymnesium parvum*. *Journal of Plankton Research*. Accepted with revision.

James, S.V., Valenti, T.W., Prosser, K., Grover, J.P., Roelke, D.L., and Brooks, B.W.. (2010). Sunlight amelioration of Prymnesium parvum acute toxicity to fish. *Journal of Plankton Research*. In Press.

Roelke, D.L., Grover, J.P., Brooks, B.W., Glass, J., Buzan, D., Southard, G.M., Fries, L., Gable, G.M., Schwierzke-Wade, L., Byrd, M., and Nelson, J. (2010). A decade of fish-killing *Prymnesium parvum* blooms in Texas: Roles of inflow and salinity. *Journal of Plankton Research*. In Press.

Schwierzke-Wade, L., Roelke, D.L., Brooks, B.W., and Grover, J.P. (2010). *Prymnesium parvum* bloom termination: Role of dilution without flushing. *Journal of Plankton Research*. Accepted with revision.

2010

Brooks, B.W., James, S.V., Valenti Jr., T.W., Urena-Boeck, F., Serrano, C., Berninger, J.P., Schwierzke, L., Mydlarz, L.D., Grover, J.P., and Roelke, D.L. (2010). Comparative toxicity of *Prymnesium parvum* in inland waters. *Journal of American Water Resources Association,* 46: 45-62.

Grover J.P., Baker, J.W., Roelke, D.L., and Brooks, B.W. (2010). Mathematical models of population dynamics of *Prymnesium parvum* in inland waters. *Journal of American Water Resources Association*, 46: 92-107.

Roelke, D.L., Gable, G.M., Valenti, T.W., Grover, J.P., Brooks, B.W., and Pinckney, J.L. (2010). Hydraulic flushing as a *Prymnesium parvum* bloom-terminating mechanism in a subtropical lake. *Harmful Algae,* 9: 323–332.

Roelke, D.L., Schwierzke, L., Brooks, B.W., Grover, J.P., Errera, R.M., Valenti Jr., T.W., and Pinckney, J.L. (2010). Factors influencing *Prymnesium parvum* population dynamics during bloom formation: Results from in-lake mesocosm experiments. *Journal of American Water Resources Association*, 46: 76-91.

Schwierzke, L., Roelke, D.L., Brooks, B.W., Grover, J.P., Valenti, Jr., T.W., Lahousse, M., Miller, C.J., and Pinckney, J.L. (2010). *Prymnesium parvum* population dynamics during bloom development: a role assessment of grazers and virus. *Journal of American Water Resources Association,* 46: 63-75.

Valenti, Jr., T.W., James, S.V., Lahousse, M., Schug, K.A., Roelke, D.L., Grover, J.P., and Brooks, B.W. (2010). A mechanistic explanation for pH-dependent ambient aquatic toxicity of *Prymnesium parvum* Carter. *Toxicon*, 55: 990-998.

Valenti, Jr., T.W., James, S.V., Lahousse, M., Schug, K.A., Roelke, D.L., Grover, J.P., and Brooks, B.W. (2010). Influence of pH on amine toxicity and implications for harmful algal bloom ecology. *Toxicon,* 55: 1038–1043.

2009

Baker, J.W., Grover, J.P., Ramachandrannair, R., Black, C., Valenti, Jr., T.W., Brooks, B.W., and Roelke, D.L. (2009). Growth at the edge of the niche: an experimental study of the harmful alga *Prymnesium parvum*. *Limnology and Oceanography*, 54: 1679–1687.

2008

Errera, R.M., Roelke, D.L., Kiesling, R., Brooks, B.W., Grover, J.P., Schwierzke, L., Ureña-Boeck, F., Baker, J.W., and Pinckney, J.L. (2008). The effect of imbalanced nutrients and immigration on *Prymnesium parvum* community dominance and toxicity: Results from in-lake microcosm experiments, Texas, USA. *Aquatic Microbial Ecology*, 52: 33-44.

Harman, J.G., and Grover, J.P. (2008). Mixotrophy and the persistence of *Prymnesium parvum* when in competition with bacteria. *Internationale Vereinigung für Theoretische und Angewandte Limnologie, Verhandlungen* 30, part 2: 231-234.

2007

Baker, J.W., Grover, J.P., Brooks, B.W., Ureña-Boeck, F., Roelke, D.L., Errera, R.M., and Kiesling, R. (2007). Growth and toxicity of *Prymnesium parvum* (Haptophyta) as a function of salinity, light and temperature. *Journal of Phycology,* 43:219-227.

Grover, J.P., Baker, J.W., Ureña-Boeck, F., Brooks, B.W., Errera, R., Roelke, D.L., and Kiesling, R.L. (2007). Laboratory tests of ammonium and barley straw extract as agents to suppress abundance of the harmful alga *Prymnesium parvum* and its toxicity to fish. *Water Research,* 41: 2503-2512.

Roelke D.L., Errera, R., Kiesling, R., Brooks, B.W., Grover, J.P., Schwierzke, L., Ureña-Boeck, F., Baker, J., and Pinckney, J.L. (2007). Effects of nutrient enrichment on *Prymnesium parvum* population dynamics and toxicity: Results from field experiments, Lake Possum Kingdom, USA. *Aquatic Microbial Ecology*, 46:125-140.

6.2 Presentations (35 total)

2010

Brooks BW, Grover, J.P., and Roelke, D.L. (2010). Prymnesium parvum *in inland waters*. Ohio River Valley Water Sanitation Commission, Cincinnati, OH.

2009

Brooks1, Bryan W., Valenti Jr.1, Theodore W., James1, Susan V., Urena-Boeck1, Fabiola, Mydlarz2, Laura D., Grover2, James P., Schwierzke3, Leslie, and Roelke3, Daniel L. (2009). *Factors influencing ambient toxicity associated with Prymnesium parvum in inland waters*. Texas Parks and Wildlife Department, Golden Algae Research Symposium, Fort Worth, TX January 2009.

Gable, G., Roelke, D., Grover, J., and Brooks, B. (2009). *Spatiotemporal water quality monitoring for Lakes Granbury, Whitney and Waco, Texas*. Texas Parks and Wildlife Department, Golden Algae Research Symposium, Fort Worth, TX January 2009.

Glass, J., Li, H.P., and Roelke, D.L. Prymnesium parvum *cell counts, intensity of fish kills and in-situ water quality monitoring of two winters on three Brazos River lakes - 2006 to 2008*. Texas Parks and Wildlife Department, Golden Algae Research Symposium, Fort Worth, TX January 2009.

Grover, J.P. (2009). *Applications of chemostat theory to harmful algae*. National Center for Theoretical Sciences, National Tsing-Hua University, Hsinchu, Taiwan, January 2009.

Grover, J.P., Crane, K.W., Baker, J.W., Brooks, B.W., and Roelke, D.L. (2009). *Spatial variations of harmful algae and their toxins in flowing water habitats: a theoretical exploration*. Society for Environmental Toxicology, North America 30th Annual Meeting, New Orleans, Louisiana, November 2009.

Hewitt, N., Roelke, D., Grover, J., and Brooks, B. (2009). *Numerical approach to modeling* Prymnesium parvum *population dynamics under varied conditions of nutrient availability: Validation with in-lake mesocosm data*. Texas Parks and Wildlife Department, Golden Algae Research Symposium, Fort Worth, TX January 2009.

Grover1, James P., Baker2, Jason W., Roelke3, Daniel L., and Brooks4, Bryan W. *Mathematical models of population dynamics of* Prymnesium parvum *in inland waters*. Texas Parks and Wildlife Department, Golden Algae Research Symposium, Fort Worth, TX January 2009.

James, S.V., Valenti, T.W., Roelke, D.L., Grover, J.P., and Brooks, B.W. (2009). *Comparative toxicity of* Prymnesium parvum *in inland waters and toxin photodegradation*. Annual Meeting of the South Central Society of Environmental Toxicology and Chemistry, San Marcos, TX.

James, S.V., Valenti, T.W., Roelke, D.L., Grover, J.P., Brooks, B.W. (2009). Prymnesium parvum *dynamics in inland waters: Toxin photodegradation and microcystin allelopathy*. Annual Meeting of the Society of Environmental Toxicology and Chemistry (SETAC), New Orleans, LA November 2009.

Roelke, D.L., Schwierzke2, Leslie, Brooks3, Bryan W., Grover4, James P., Errera2, Reagan M., Valenti Jr.5, Theodore W., and Pinckney6, James L. *Factors influencing* Prymnesium parvum *population dynamics: The potential role of cyanobacterial allelopathy during in-lake experiments at the time of bloom initiation*. Texas Parks and Wildlife Department, Golden Algae Research Symposium, Fort Worth, TX January 2009.

Schwierzke, L., Roelke*1, Daniel L., Brooks2, Bryan W., Grover3, James P., Valenti, Jr. 2, Theodore W., Lahousse2, Mieke, Miller1, Carrie J., and Pinckney4, James L. *The role of grazers and viruses in* Prymnesium parvum *bloom development: In situ experiments from a subtropical lake*. Texas Parks and Wildlife Department, Golden Algae Research Symposium, Fort Worth, TX January 2009.

Valenti, T.W., Lahousse1, Mieke, James1, Susan V., Roelke2, Daniel R., Grover3, James P., Schug3, Kevin A., and Brooks1, Bryan W. (2009). *A potential explanation for pH-dependant potency of* Prymnesium parvum *toxins*. Texas Parks and Wildlife Department, Golden Algae Research Symposium, Fort Worth, TX January 2009.

2008

Hewitt, N., Roelke, D., Grover, J., and Brooks, B. (2008). *Numerical approach to modeling* Prymnesium parvum *population dynamics under varied conditions of nutrient availability: Validation with in-lake mesocosm data*. Ecological Integration Symposium, Graduate Student Research Conference, College Station, Texas, May 2008.

Grover, J., Baker, Jason W., Roelke, Daniel L., and Brooks, Bryan W. (2008). *Mathematical models of population dynamics of* Prymnesium parvum *in inland waters*. OTARG 2008

Grover, J., Roelke, D., Brooks, B., and Kiesling, R. (2008). *Advancing the understanding of* Prymnesium parvum *blooms in Texas*. Texas Parks and Wildlife, Golden Algae Research Workshop, Buda, Texas, March 14, 2008.

James, S., Valenti, T.W., Urena-Boeck, F., Brooks, B.W., Grover, J., and Roelke, D. (2008). *Comparative Sensitivity of Select Aquatic Organisms to the Harmful Algae* Prymnesium parvum. SETAC North America, Tampa, Florida, November 16-20, 2008.

Jones, A., Roelke, D.L., Brooks, B., and Grover J.P. (2008). Golden Algae research update. Granbury Town Hall Meeting, Granbury, Texas, June 10, 2008.

Jones, A., Roelke, D.L., Brooks, B., and Grover, J.P. (2008). *Lake Granbury Water Quality*. Texas A&M AgriLife Research supported by Federal Initiatives. College Station, Texas, 2008.

Roelke, D., Brooks, Bryan, and Grover, James. (2008). Prymnesium parvum *Blooms in Texas Lakes and the Importance of Instream Flows*.Invited seminar, University of Kalmar, Sweden, August 2008.

Roelke, D., Brooks, Bryan, and Grover, James. (2008). Prymnesium parvum *Blooms in Texas Lakes and the Importance of Instream Flows*. Invited seminar, Kinneret Limnological Laboratory, Israel, August 2008.

Roelke, D., Schwierzke, Leslie, Brooks, Bryan, Grover, James, Errera, Reagan, Valenti Jr., Theodore, and Pinckney, James. (2008). *Factors influencing* Prymnesium parvum *population dynamics in subtropical lakes: The potential role of cyanobacterial allelopathy*. OTARG 2008.

Roelke, D., Brooks, B., and Grover, J. (2008). *Golden Algae bloom dynamics and thoughts on management strategies for reservoirs*. Granbury Town Hall Meeting, Granbury, Texas, February 20, 2008.

Roelke, D., Leslie Schwierzke, Bryan Brooks, James Grover, Reagan Errera, Theodore Valenti Jr., James Pinckney. (2008). *Factors influencing* Prymnesium parvum *population dynamics in subtropical lakes: The potential role of cyanobacterial allelopathy*. TAPMS 2008.

Valenti, T.W., Lahousse, M., James, S., Brooks, B.W., Grover, J., Roelke, D. (2008). Factors that influence the potency of toxins released by Prymnesium parvum Carter (Golden Algae). SETAC North America, Tampa, Florida, November 16-20, 2008.

Valenti, T.W., Mieke Lahousse, Susan James, Daniel Roelke, James Grover, and Bryan Brooks. (2008). *Potential factors influencing the pH-dependent aquatic toxicity of* Prymnesium parvum *Carter (golden algae)*. SETAC South Central Regional Chapter Annual Meeting, Houston, Texas, May 15-17, 2008.

Valenti, T.W., Lahousse, M., James, S.V., Roelke, D.R., Grover, L.P., Schug, K.A., and Brooks, B.W. (2008). *Implications of site-specific pH for ecological risk assessments of* Prymnesium parvum (Golden algae). Texas Chapter of American Fisheries Society, Ft Worth TX.

2007

Errera, R.M., Pinckney, J., Roelke, D.L. (2007). *Pigment composition of the Texas strain of* Prymnesium parvum *during log, stationary, and senescent growth phases*. 4th Annual HAB Symposium 2007.

Gable, G., Roelke, D., Grover, J., Brooks, B., Davis, S., Gable, A.-M., Baker, J., Ureña-Boeck, F., and Lahousse, M. (2007). *Water quality,* P. parvum *and fecal coliform monitoring for Lake Granbury, TX*. Texas River and Reservoir Management Society.

Gable, G., Roelke, D., Grover, J., Brooks, B., Davis, S., Gable, A.-M., Baker, J., Ureña-Boeck, F., and Lahousse, M. (2007). *Water quality,* P. parvum *and fecal coliform monitoring for Lake Granbury, TX*. Granbury Town Hall Meeting, Granbury, Texas.

Grover, J., Roelke, D., Brooks, B., Davis, S., Gable, G., Gable, A.-M., Baker, J., Stanely, J., Ureña-Boeck, F., and Lahousse, M. (2007). *Water quality research for Lake Granbury, TX*. Granbury Town Hall Meeting, Granbury, Texas, May 22, 2007.

Roelke, D., Grover, J., Brooks, B., Davis, S., Gable, G., Gable, A.-M., Baker, J., Ureña-Boeck, F., and Lahousse, M. (2007). *Water quality research for Lake Granbury, TX*. Texas Parks and Wildlife, TX Harmful Algal Bloom Workshop, College Station, Texas, March 9, 2007.

Roelke, D., Grover, J., Brooks, B., Davis, S., Gable, G., Gable, A.-M., Baker, J., Ureña-Boeck, F., and Lahousse, M. (2007). *Water quality research for Lake Granbury, TX*. Granbury Town Hall Meeting, Granbury, Texas, February 13, 2007.

Valenti, T., Brooks, B., Lahousse, M., Dobbins, L., Grover, J., Roelke, D.L. (2007). *Influences of pH on ambient toxicity of the harmful alga* Prymnesium parvum *to aquatic life*. Society of Environmental Toxicology and Chemistry. Milwaukee, Wisconsin. November 11 – 15, 2007.

2006

Errera, R.M., Roelke, D.L., Kiesling, R.L., Brooks, B.W., Grover, J.P., Ureña-Boeck, F., and Pinckney, J. (2006). *The role of inorganic nutrients and barley straw extract in the invasion and inhibition of* Prymnesium parvum. Aquatic Sciences Meeting, ASLO. Victoria, Canada. June 4-9.

b. Website

Information from this project, as well as other projects in the watershed, is available online at: http://lakegranbury.tamu.edu. A general project description, a list of collaborators, funding agencies, news stories, technical reports and quarterly progress reports are all available at this site.

c. Collaborators

Texas Water Resources Institute
Texas AgriLife Research
Texas AgriLife Extension Service
Texas Commission on Environmental Quality
Brazos River Authority
USDA Natural Resources Conservation Service
Texas Parks and Wildlife Department
Baylor University
University of Texas at Arlington
Hood County, Texas

d. Technologies/Techniques – N/A

e. Inventions/Patents – N/A

f. Other products – N/A